10th International Congress on

ACOUSTICS

SATELLITE SYMPOSIUM ON ENGINEERING FOR NOISE CONTROL

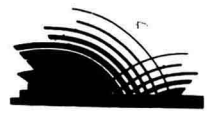

TENTH INTERNATIONAL CONGRESS ON ACOUSTICS

SATELLITE SYMPOSIUM

ON

ENGINEERING FOR NOISE CONTROL

ADELAIDE 7 - 8 JULY 1980

Organised by:
The Australian Acoustical Society (S.A. Division)
The Institution of Engineers, Australia.

ORGANISING COMMITTEE

D.A. Bies
R.W. Boyce
M.K. Bull
K.J. Martin
D.H. Patterson
J.M. Pickles
M.A.G. Pryce
G.R. Wild
M. Zockel

Grateful acknowlegement for financial assistance is made to the following companies;

General Motors-Holdens Limited
Adelaide Brighton Cement Limited
Broken Hill Proprietory Company Limited
Sound Attenuators (Aust.) Pty. Limited

Published by Instant Print Pty. Ltd., 5 Hackney Road, Hackey.

CONTENT

* Keynote speakers

FUNDAMENTAL CONCEPTS OF STRUCTURAL DAMPING FOR NOISE AND VIBRATION CONTROL

ERIC E. UNGAR

Bolt Beranek and Newman Inc.

50 Moulton Street

Cambridge, MA 02238

ABSTRACT

The effects of damping on structural vibrations are discussed and their practical benefits are indicated. The commonly used measures of structural damping are summarized. Several damping mechanisms are described, and the basic rule for adding visoelastic damping to structures so as to obtain highly damped composites is presented.

DEFINITION

"Structural damping" refers to a structure's or structural component's capacity for dissipating energy - or, more precisely, to its capacity for removing from a structural vibration some of the energy associated with that vibration. This removed energy may be converted directly into heat, may be transferred to connected structures or ambient media, or may be transferred to other structural motions than those of immediate concern.

THE EFFECTS OF DAMPING

Damping has two primary effects: (1) It limits the steady-state motions of structures or systems in situations where these motions are controlled by an energy balance; and (2) It increases the rates at which the free (i.e., unforced) vibrations of structures decay. The addition of damping to structures for which neither energy-balance-controlled steady motions nor freely decaying motions are of concern is usually futile.

Consider, for example, a classical lumped-parameter mass-spring-dashpot system driven by a steady sinusoidal force that acts in the mass. For such a system one may readily make the following observations: (1) For excitation frequencies that are considerably lower than the system resonance frequency, the applied force essentially is balanced quasi-statically by the spring force; the mass and dashpot here have virtually no effect. (2) For excitation frequencies that are considerably higher than the system resonance frequency, the applied force essentially is opposed by only the inertia force of the mass; here the spring and dashpot have virtually no effect. (3) For

excitation frequencies near the system resonance frequency, the spring force and the inertia force essentially cancel each other, leaving only the dashpot (i.e., the damping element) to oppose the externally applied force. One may note that changes in the damping do not affect the system response for the first two of the aforementioned conditions, but that for an oscillatory force acting at the system's resonance, the vibration amplitude decreases with increasing damping.

In addition to the case of resonant or near-resonant excitation, there occur several other important steady-state or near-steady-state situations in which the responses of systems or structures are controlled by a balance between the energy input and the energy dissipation. These situations include the cases of (1) broad-band excitation and (2) spatially periodic excitation where the spatial period matches that of freely propagating waves. Because broad-band excitation generally encompasses several structural resonance frequencies, structural responses to broad-band excitation are dominated by the resonant responses of the excited modes, and each resonant modal response is controlled by damping in the manner discussed previously for a single-degree-of-freedom system. Excitation with a spatial distribution that matches that of freely propagating waves - such as occurs in the case of trace-matching, where at a given frequency the acoustic pressures that act on a wall have the same distribution and travel at the same speed along the wall as do flexural waves in the wall - also is essentially a resonance phenomenon, for which the response is controlled by damping.

In addition to controlling the amplitude of resonant vibrations, damping also affects the rate at which vibrations build up when a resonant excitation is applied to an initially quiescent system. Increased damping reduces the rate of build-up, as well as the steady-state amplitude that is eventually reached.

If a structure (or other mechanical system) is deflected from its equilibrium position and then released, the structure vibrates with ever-decreasing amplitude as the result of damping - i.e., as the result of energy being removed from the oscillatory motions. Greater damping corresponds to the dissipation per cycle of a greater fraction of the vibratory energy, thus resulting in more rapid decay of the vibrations. In a somewhat similar manner, increased damping also results in the more rapid decay of freely travelling waves. For

example, if a long beam is subjected to an oscillatory transverse force of constant amplitude and frequency, say near the middle of the beam, then flexural waves travel away from the driving point in both directions; as the result of damping the amplitude of these waves decreases with increasing distance from the driving point - with greater damping leading to lesser amplitudes at a given distance.

The practical consequences of the aforementioned effects of damping generally are the reasons one is interested in systems or devices that increase damping. Reductions in resonant or random responses result in decreased oscillatory stresses and attendant increases in the fatigue lives of structures and in the reliability of mechanical devices, and also in increased mechanical impedance (which tends to improve the effectiveness of vibration isolation.) Reduction of the spatially resonant responses of a wall or panel leads to decreased sound transmission through that structure for frequencies above the coincidence frequency. Increased attenuation of propagating waves results in lesser transmission of vibrations to neighboring structures. More rapid decay of free vibrations reduces the "ringing" sound of structures, thus leading to less noise - particularly from structures excited by repetitive impacts - and also to reduced structural fatigue.

MEASURES OF DAMPING

Damping may be quantified in terms of any of the previously discussed primary effects. The corresponding commonly used measures of damping, defined below, are interrelated as follows:[1,2]

$$\eta = \psi/2\pi = 2.20/f_n T_{60} = \Delta_t/27.3f_n = \delta/\pi = \Delta_\lambda/13.6$$

The loss factor η and damping capacity ψ are defined directly in terms of the cyclic energy dissipation; the damping capacity represents the fraction of the system's vibrational energy that is dissipated per cycle of the vibration, and the loss factor similarly is defined as the fraction of the system's energy that is dissipated per radian of the vibratory motion.

On the other hand, T_{60}, Δ_t, and δ are related to the rate of decay of free vibrations. T_{60} denotes the reverberation time (in seconds), defined (in analogy to the related room-acoustics measure) as the

time within which the vibration level of a system vibrating freely at frequency f_n (Hz) decreases by 60 dB (i.e., the amplitude decreases to 1/1000 of its initial value). A related measure, decay rate Δ_t (dB/sec), represents the rate of reduction of the vibration (acceleration or displacement velocity) level. The logarithmic decrement δ is defined as the natural logarithm of the ratio of a peak excursion of a freely vibrating system to the peak excursion one cycle (period) later. The spatial decay rate Δ_λ (dB/wavelength) represents the reduction in the steady-state vibration level with distance that occurs along a long beam vibrating in flexure.

One may note that none of the measures of damping discussed above depend on *how* the energy is dissipated; within a cycle these measures make no reference to any damping mechanism. On the other hand, some other commonly employed measures of damping are defined on the basis of viscous damping - i.e., damping that results from a retarding force that is proportional to the velocity. The ratio of the magnitude of that force to the velocity is called the viscous damping coefficient and is commonly designated by c.

If a simple mass-spring-dashpot system (where the dashpot provides a viscous retarding force characterized by c) is deflected from equilibrium and released, it typically oscillates with ever decreasing amplitude. However, if c is made large enough, no oscillations occur; instead, the system creeps toward its equilibrium position, never traversing it. The smallest viscous damping coefficient for which this non-oscillatory behavior is obtained - i.e., the viscous damping coefficient that represents the dividing line between oscillatory and non-oscillatory behavior - is called the critical (viscous) damping coefficient c_c. It obeys $c_c = 2\sqrt{km}$, where m denotes the mass and k the spring stiffness. The "damping ratio" c/c_c, also called the fraction of critical damping and often given in terms of "percent of critical damping" is widely used to indicate damping magnitudes.

Two other measures of damping are derived from the steady-state behavior of an ideal linear mass-spring-dashpot system that is driven by a sinusoidal force of constant amplitude. The amplification at resonance, often called "the Q" of the system is defined as the ratio of the amplitude that results at resonance to the amplitude that is obtained if the force acts quasi-statically (i.e., at frequencies considerably below resonance). The proportional bandwidth b takes account of the damping-related broadening of the peak in a plot

of response amplitude versus frequency; this nondimensional bandwith is defined as $\Delta f/f_n$, where Δf denotes the difference between the two frequencies (one above, and one below the resonance frequency f_n) at which the square of the response amplitude is one-half of its maximum value - which maximum occurs at the resonance frequency. For values of damping below critical, the aforementioned measures of damping are related to each other and to the previously discussed loss factor as [1,2]

$$\eta = 2c/c_c = 1/Q = b.$$

DAMPING MECHANISMS

For linear, viscously damped systems, all of the measures of damping discussed previously are independent of amplitude. Amplitude-independence also occurs for other damping mechanisms, and approximate amplitude-independence occurs for almost all systems, provided the damping is small enough. Thus, amplitude-independence cannot be taken as an indication that a system is viscously damped; nevertheless, the damping of systems with unknown energy dissipation mechanisms is often characterized in terms of an equivalent viscous damping coefficient. (In some cases, even an amplitude-dependent viscous damping coefficient is employed.)

Indeed, much analysis is carried out with the (usually tacit) assumption that the damping is viscous - largely because viscous damping leads to linear differential equations that can be solved relatively readily. It is fortunate that for many practical problems - e.g., where only certain response maxima are of concern - the details of the damping mechanism are unimportant, so that one may obtain reasonable response predictions even with inaccurate damping force-vs-velocity representations. However, realistic damping models are required for the analysis of cases where one is interested in details of the response motions.

Unlike mass, which is a single physical phenomenon, and stiffness, which results from a very few physical effects, damping may be caused by a great variety of phenomena. These phenomena include mechanical hysteresis (also called material damping or internal friction), electromagnetic effects (notably eddy currents), friction due to motion relative to fluids or solid surfaces, and energy transport to adjacent structural components or fluids (including by acoustic radiation). This great variety of phenomena that can produce damping

generally makes damping difficult to predict and to eliminate, but enables one to conceive of a variety of means for increasing it.

ADDITION OF DAMPING COMPONENTS (VISCOELASTIC TREATMENTS)

Because the damping of most common structural elements is relatively small (monolithic steel structures typically have loss factors of the order of 10^{-4}, built-up steel or aluminum structures have loss factors of the order of 10^{-3}), whereas rubbery or plastic materials tend to have rather high damping (loss factors between 0.01 and 1.0), the addition of highly damped "viscoelastic" materials to structures so as to achieve a well-damped composite has received considerable attention. A viscoelastic material is one that has some stiffness or energy storage capability (like an elastic solid), and also the capacity for some energy dissipation (like a viscous fluid). Virtually all materials exhibit viscoelastic behavior to some extent.

Although one can conceive of many ways to combine highly damped viscoelastic materials with relatively lightly damped "elastic" materials, not all configurations lead to useful damping improvements. The basic combination rule may be derived by considering how the stored energy associated with a given structural deflection is distributed among the various participating components. One may note that the loss factor η_c of the combined structure is defined in terms of its total energy dissipation (per radian) and its total energy of vibration W_c. One also may observe that the total energy dissipated is the sum of that dissipated by all the components, and that the total energy stored is the sum of the energies stored by all of the components. By applying the definition of loss factor to all the components one may deduce that[1,3]

$$\eta_c = \Sigma\, \eta_i\, (W_i/W_c)\ ;\quad W_c = \Sigma\, W_i$$

where η_i denotes the loss factor of the i-th structural component and W_i represents the energy stored in that component; the summations extend over all components.

This relation states that the loss factor of the composite structure is equal to the weighted average of the loss factors of the components, with the component energy storages constituting the weighting factors. The practical significance of this result may be visualized particularly easily for the special case where all components are assumed to have

negligible damping, except for the one with i = d. For this case the foregoing relation reduces to

$$\eta_c = \eta_d \, W_d/W_c,$$

indicating that here the loss factor η_c of the combination is proportional to the loss factor η_d of the damped component and to the ratio of the energy W_d stored in the damped component to the energy W_c stored in the entire assembly. Thus, in order to achieve a highly damped combination, one not only needs to select a damping component with a high loss factor η_d, but one must also insert that component into the assembly in a way that causes its energy storage to be a significant part of the total energy storage W_c.

Analyses based on the foregoing relation have been used to devise damping treatments consisting of simple coatings ("free", or "extensional" damping layers), treatments using a damping layer covered by a layer of structural material ("constrained" or "shear" damping arrangements), [1,4] damped three-layer and multi-layer sandwich structures, and a variety of more complex damped structures[5], including some that include means that enhance the energy storage in the viscoelastic elements, and thus the system damping.

CONCLUDING REMARKS

Clearly, only a brief introduction to the field of structural damping can be given within the confines of a few pages. The author hopes that he has succeeded in summarizing some of the ideas that are basic to the use of structural damping for the control of vibrations and noise and invites the interested reader to consult the references for further information.

REFERENCES

1. Ungar, E.E., "Damping of Panels," Chapter 14 of *Noise and Vibration Control*, L.L. Beranek, Ed, McGraw-Hill Book Co., Inc., New York, 1971.

2. Cremer, L., Heckl, M., *Structureborne Sound*, Springer-Verlag, New York, 1973.

3. Ungar, E.E., Kerwin, E.M.,Jr., "Loss Factors of Viscoelastic Systems in Terms of Energy Concepts," *J.Acoust.Soc,Am. 34*, 954-957; July 1962.

4. Ross, D., Ungar, E.E., Kerwin, E.M.,Jr., "Damping of Plate Flexural Vibrations by Means of Viscoelastic Laminae," Sec. 3 of *Structural Damping*, J.E. Ruzicka, Ed; American Society of Mechanical Engineers, 1959.

5. Ungar, E.E., "Loss Factors of Viscoelastically Damped Beam Structures," *J.Acous.Soc.Am, 34*, 1082-1089; 1962.

TECHNIQUES FOR NOISE SOURCE IDENTIFICATION IN COMPLEX MACHINES

MALCOLM J. CROCKER
Purdue University,
West LaFayette, Indiana. U.S.A.

MANFRED ZOCKEL
University of Adelaide,
Adelaide, South Australia.

SUMMARY

The identification and ranking of noise sources in complex machines is of prime importance if noise control is to be achieved economically. In this paper currently available methods for the identification and ranking of noise sources are reviewed with emphasis on the advantages and disadvantages of the various techniques. This is followed by some experimental results when lead wrapping, surface velocity and surface intensity methods are used to rank the noise sources of a 260 kW turbocharged diesel engine under various operating conditions. Finally the far field sound pressure levels from selectively exposed surfaces of the engine are ranked when the engine is accelerating. These results indicate that the relative importance of the noise sources may change with different operating conditions.

1. INTRODUCTION

In the majority of cases noise control on machines is currently achieved by the use of enclosures rather than by modification of the source. The cost of noise reduction at the source has been estimated by Richards[1] to be about one-tenth of the cost of enclosures which makes it economically essential to tackle the noise at the source. However, before this can be done the noise source must be identified and in the case where there are several sources, the sound power radiated by these sources should be ranked in order of importance.

There are several techniques available for source identification and the method used in a praticular application will depend on the time, resources and expertise available as well as on the accuracy required. In most cases it is good practice to use more than one technique to ensure greater confidence in the final results. As the complexity of the sources increases it is useful to have some understanding of the propagation of sound from idealised sources, such as monopoles, dipoles, quadrupoles, line sources and vibrating beam and plates. This will not only help in deciding which technique to use but also aid in interpreting the results. In fact, as the techniques become more sophisticated, increasing care must be taken in interpreting the results and a knowledge of random processes and signal processing theory becomes essential.

In this paper both well tried and more recent methods for noise source identification are discussed in terms of their advantages and disadvantages, and in terms of actual experimental results obtained on a diesel engine. Some evidence is presented that the source ranking changes with different operating conditions which tends to increase the complexity of the measuring procedure as well as the noise control problem.

2. METHODS FOR SOURCE IDENTIFICATION

There are several qualitative methods available for the identification of noise sources such as listening, frequency analysis and operating individual components of a machine separately. These methods are described by Crocker[2]. However, for quantitative source identification, which is necessary for source ranking, the following techniques are available.

2.1 Selective wrapping

Some machines can be completely enclosed in tight-fitting, sealed enclosures and then parts of the enclosure can be removed to expose different machine surfaces. It is desirable that the far field sound power radiated by the different surfaces is measured rather than the sound pressure levels at particular points even though the power measurements require special environments such as anechoic or reverberant rooms.

The accuracy of the sound power measurement depends on the relative magnitude between the levels from the exposed source and that measured when the machine is completely enclosed as well as on how the sound field is affected by the changed diffraction pattern around the enclosure. Lead sheeting with some absorptive layer is frequently used as the enclosing material for engines and trucks but the transmission loss at frequencies below 200 - 300 Hz is usually inadequate for accurate measurements. Consequently the technique is restricted to machines which radiate most of their energy in the mid and high frequency ranges. Furthermore the method is time consuming and costly, and care should be taken that the machine does not overheat when completely enclosed.

2.2 Surface Velocity

In the majority of machines the noise is radiated by vibrating surfaces which are excited in either forced or resonant response by one or more primary sources within the machine. In those cases the sound power radiated by the surface can be estimated from the mean square surface velocity $\langle v^2 \rangle$ and the radiation efficiency (σ_{rad}) using the equation

$$W = \rho c A \langle v^2 \rangle \sigma_{rad} \qquad (1)$$

where ρc is the characteristic impedance of the surrounding medium and A is the surface area. The mean square velocity can be obtained by suitably processing the signals from a number of accelerometers attached to the surface. This means the method is time consuming and the accuracy of the power radiated depends critically on the radiation efficiency which is difficult to predict theoretically. At frequencies above the coincidence frequency, which for steel is approximately equal to 12.7 divided by the plate thickness in meters, the radiation efficiency is close to unity and reasonable estimates of sound power radiated by the surface can be obtained. For engine blocks this method has been shown by Chan & Anderton[3] to be useful above the 400 Hz $\frac{1}{3}$ octave band. The main limitation of the surface velocity method is that it cannot be used on rotating or very hot surfaces. It does however provide information about the response of a surface which is essential to the designer if any modification to the structure is necessary.

2.3 Surface Intensity

This method is an extension of the surface velocity technique in that a microphone is used in conjunction with the accelerometer on the surface as shown in Fig. 1(a). The signals from the accelerometer and the microphone are processed using an FFT system to give the acoustic intensity normal to the surface. The intensity expression is given by McGary[4] as

$$I_n = \frac{1}{2\pi} \int_0^f \left[\frac{Q_{pa} \cos \phi + C_{pa} \sin \phi}{f}\right] df \qquad (2)$$

where Q_{pa} and C_{pa} are the imaginary and real parts of the one sided cross-spectral density (G_{pa}) between the pressure and the acceleration signals and ϕ is the phase shift between the two signals due to instrumentation as well as due to the physical displacement (d) of the microphone from the accelerometer. The phase shift due to the instrumentation must be evaluated during the calibration of the system while the phase shift due to the displacement (d) can be calculated for each measurement point. The total power radiated from the surface can finally be obtained using the expression

$$W = \sum_{j=1}^{n} \left(\sum_{i=1}^{N} \left[Q_{pa_{ij}} \cos \phi_j + C_{pa_{ij}} \sin \phi_i \right] A_i \right) \frac{\Delta f}{2\pi f j} \qquad (3)$$

where n is the number of data points in the frequency domain, N is the number of area increments (A_i) on the whole surface and Δf is the frequency resolution ($\Delta f = \frac{f}{n}$).

This method overcomes the uncertainties associated with the radiation efficiency but at the expense of sophisticated equipment and stringent calibration procedures. Other advantages and disadvantages remain the same as for the surface velocity method.

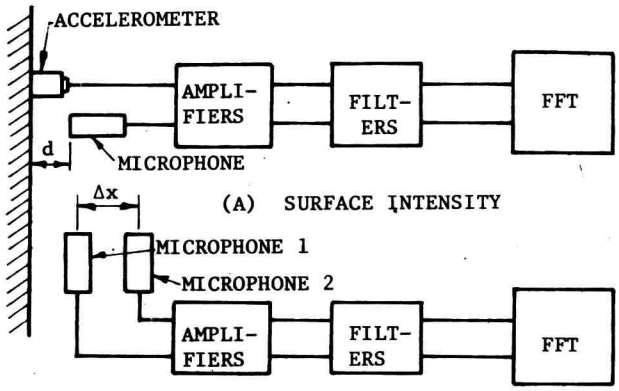

FIG. 1. NEAR FIELD INTENSITY METHODS

2.4 Acoustic Intensity

Although the acoustic intensity meter (watt meter) was first developed by Rayleigh its modern equivalent consists of two microphones, placed near the vibrating surface as shown in Fig. 1(b). The acoustic pressure is taken as the mean pressure obtained from the two microphones

$$\left(\bar{p} = \frac{p_1 + p_2}{2}\right) \tag{4}$$

while the particle velocity normal to the surface is

$$u_n \simeq i \left(\frac{p_2 - p_1}{\rho\omega\Delta x}\right) \tag{5}$$

where ρ is the air density, ω the angular frequency and Δx is the microphone spacing.

The time averaged product of $\bar{p}$ and u_n gives the acoustic intensity ($I_n = \langle \bar{p}\, u_n \rangle$) from which the sound power can be calculated as follows

$$W = \int_A I_n \, dA \tag{6}$$

The phase shift between the two channels is important but difficult to measure accurately. However, using the method suggested by Chung[5] and Fahy[6] all

phase errors can be ignored if a second set of data is taken with the microphones physically switched so that microphone 2 measures the pressure at location 1 and that signal is fed into channel 1 of the FFT analyser. The intensity normal to the surface can then be calculated from

$$I_n = \text{Im}\{[G_{12} \times G_{12}^{S}]^{\frac{1}{2}}\}/\rho\omega\Delta x|H_1||H_2| \qquad (7)$$

where Im means imaginary part, $|H_1|$ and $|H_2|$ are the gain factors of microphone system 1 and 2 respectively, G_{12} is the cross spectrum between p_1 and p_2 and G_{12} is the cross spectrum between p_1 and p_2 switched.

It is possible to space average as well as time average with this technique by sweeping over the surface while the computer takes successive samples for time averaging. The total sound power radiated by individual parts is obtained from equation (6) although the surface area A is now simply a surface area enclosing the source.

Chung[5] has shown the method to be highly accurate and repeatable and much faster than other methods which give quantitative results. In fact source identification and ranking of a whole engine can be accomplished in a single day. Furthermore, as with all near field methods, no special environments are necessary to achieve accurate results.

2.5 Coherence Function

This method has been used for punch press source identification by Koss[7] as well as for diesel engines. By evaluating the multiple coherence function for a multiple input-single output system as explained by Crocker[8] the fraction of the output (usually sound pressure) which is coherent with all the inputs can be obtained. Difficulties arise when several sources are themselves coherent and data handling and computing errors can become large unless the source characteristics are known. This method is still a highly specialised technique which should be used with caution.

3. SOURCE IDENTIFICATION UNDER STEADY OPERATING CONDITIONS

As part of an investigation of the noise sources on engines, a 260 kW, 6 cylinder, 14 litre, turbocharged diesel engine with aftercooler was installed in a 560 m^3 semi-anechoic room. The aim of the test programme was to obtain the source ranking at a number of steady operating conditions using lead wrapping, surface intensity and surface velocity techniques. The details of the experimental set-up are given by Crocker[10]. It is sufficient for the present discussion to say that the intake and exhaust noise were ducted away from the

engine and that the dynamometer was located in an adjoining room with the drive shaft tunnel acoustically sealed.

For the selective enclosure method the engine was completely covered with 0.8 mm thick lead sheeting lined with 25 mm thick foam. Sound power levels were calculated from 30 sound pressure level measurements arranged on a spherical surface of 1.73 m radius. The sound power spectra for the bare and fully wrapped engine, given in Fig. 2, indicate the wrapping was inadequate at $^1/_3$ octave bands below 315 Hz. Eight engine parts were then exposed sequentially and the sound power levels evaluated at three engine operating conditions.

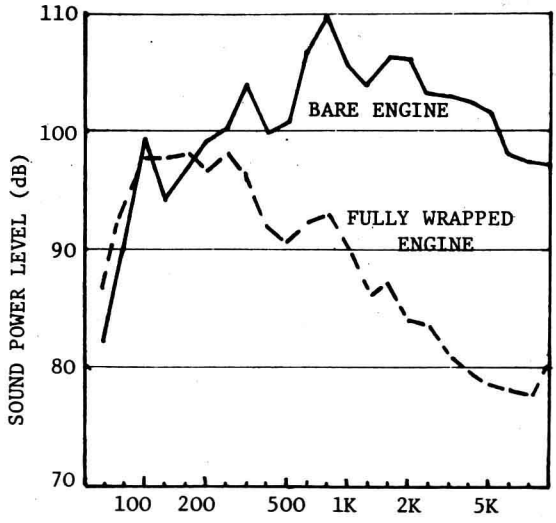

FIG. 2. POWER SPECTRA OF BARE AND WRAPPED ENGINE

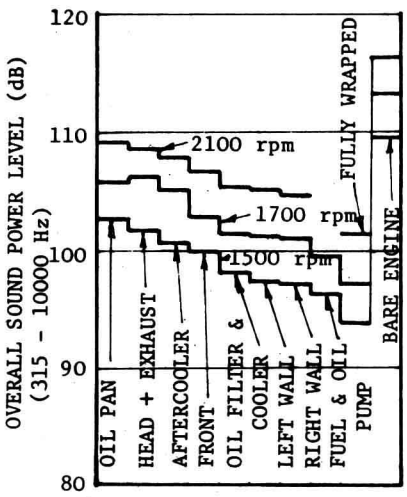

FIG. 3. SOUND POWER RANKING USING SELECTIVE ENCLOSURES

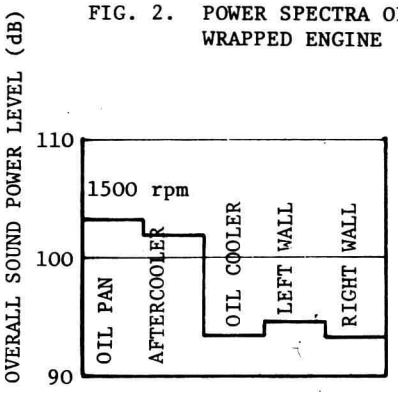

FIG. 4. SOUND POWER RANKING USING SURFACE INTENSITY

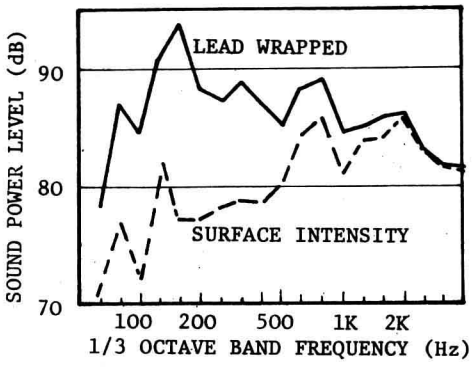

FIG. 5. POWER SPECTRA FOR LEFT BLOCK WALL

The ranking of the various sources in terms of the overall sound power levels for the $^1/_3$ octave bands between 315 Hz and 10000 Hz are shown in Fig. 3. The slight change in the ranking order at the 1700 rpm operating condition may not be significant for this engine although directivity plots, obtained from the 30 microphone readings, also indicated a change in the sound field at this operating condition, whereas at 2100 rpm and 1500 rpm the directivity patterns were essentially the same.

The surface intensity method, described earlier, was then used on five of the eight surfaces analysed with the lead wrapping technique at the 1500 rpm operating condition. The ranking of the various sources shown in Fig. 4, agrees well with the ranking from lead wrapping. However, the overall sound power levels for the oil filter and cooler as well as the left and right block walls are between 4 and 5 dB lower using the surface intensity method than the lead wrapping technique. It is suggested that the lead wrapping results are in error for these lower order sources because only the $^1/_3$ octave levels above 1250 Hz were more than 4 dB above the levels of the fully wrapped engine, whereas the overall power levels were calculated between 315 and 10000 Hz. Furthermore, if the surface intensity power spectrum for the left block wall is compared with the lead wrapping spectrum (Fig. 5) the power levels agree within 1 or 2 dB whenever the power level from the surface exceeds the full wrapped level by about 4 dB.

Since the surface intensity method gives acceleration levels at various points on the surface the mean square velocity of the surface can be calculated. Equation (1) can then be used to obtain the radiation efficiencies for the various surfaces since the power level is known.[4] Figure 6 shows the radiation efficiencies for the four surfaces. Had the radiation efficiency been assumed unity then the power levels would have been over estimated below the 400 Hz $^1/_3$ octave bands for the left and right block walls and below the 500 Hz and 800 Hz $^1/_3$ octave bands for the aftercooler and oil pan respectively.

4. SOURCE RANKING UNDER ACCELERATING CONDITIONS

All the quantitative source ranking methods in terms of sound power require significant averaging times which means that the machine has to operate at steady conditions. If the sound level varies with time, for example during the acceleration phase of an engine, reliable sound power measurements are not possible. However, it is possible to compare the sound pressure levels from various sources by using the selective wrapping technique and measuring the pressure level as a function of time at a number of points in the far

field. By averaging over the number of measurements and over a number of standarised acceleration runs the sources can be ranked at various times throughout the time varying process. This was done while the engine was wrapped in lead and Fig. 7 shows the source ranking at the instant of throttle opening (curve A) and 0.5 seconds thereafter (curve B) as well as at full load 2100 rpm steady operation (curve C). The ranking of full load is similar to the ranking for the power measurement with the exception that the left block wall is indicated as a major source. However, as seen from curves A and B, the ranking during the acceleration process is markedly different from the ranking at full load steady operation. The repeatability of the measurements for successive acceleration runs was generally better than 1 dB so that changes greater than this value would be significant. The reason for selecting a ranking at 0.5 seconds after throttle opening is that for this turbocharge engine with aftercooling the sound level increases most quickly during this time.

The results from this experiment indicate that the source ranking can change significantly with different operating conditions. Consequently, in order to embark on an effective noise control programme on a machine the source ranking procedure should be carried out at an operating condition which is close to that specified by the regulating authorities; for instance if a machine is to meet a noise requirement at ½ or ¾ power then the ranking should be done at these conditions.

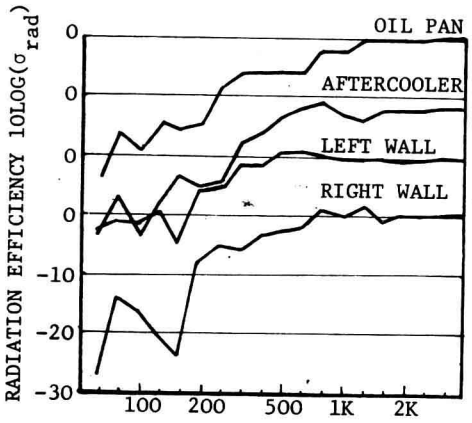

FIG. 6. RADIATION EFFICIENCIES FOR FOUR ENGINE SURFACES

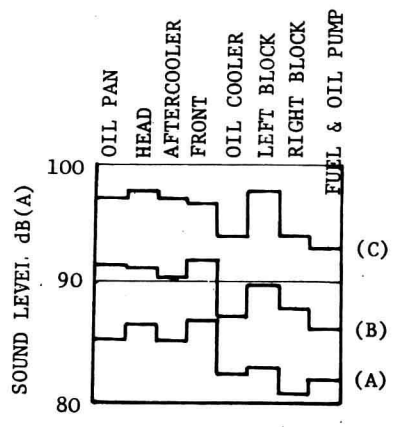

FIG. 7. SOUND PRESSURE RANKING UNDER ACCELERATING AND STEADY CONDITIONS

5. CONCLUSIONS

1. The near field acoustic intensity method is suggested as the fastest and most reliable method available for quantitative source ranking under steady operating conditons. However, the equipment is sophisticated, expensive and requiresexperienced personnel.

2. The near field surface intensity or surface velocity methods are recommended where information about the surface behaviour is required for structural desigr.

3. The selective wrapping technique, although costly and time consuming, can be used with far field sound pressure measurements when the sources are varying with time.

4. For source ranking the operating condition of the machine should be similar to that specified by the noise control programme.

6. REFERENCES

1. Richards E.J., - Private communications.

2. Crocker M.J., "Identification of Noise from Machinery, Review and Novel Methods" Inter-noise 77 p A 201-211.

3. Chan C.M.P. & Anderton D., "Correlation between engine block surface vibration and radiated noise in in-line diesel engines" Noise-Con Eng. 2, 1, 1974 pp 16.

4. McGary M.J., "Noise Source Identification of Diesel Engines Using Surface Intensity Measurements" M.Sc. Thesis Purdue University, Jan. 1980.

5. Chung J.Y., "Cross-Spectral Method of Measuring Acoustic Intensity without Error Caused by Instrumentation Phase Mismatch" J. Acoust. Soc. Am. 64, 6, 1978 pp 1613-1616.

6. Fahy F.J., "Measurement of the Acoustic Intensity using the Cross Spectral Density of Two Microphone Signals" J. Acoust Soc. Am. 62, 4, 1977 pp 1057-1059.

7. Koss L.L. & Alfredson R.J., "Identification of Transient Sounds on a Punch Press" J. Sound Vib. 34, 1, 1974, pp 11-33.

8. Crocker M.J. "Identifying Sources of Noise in Engines and Vehicles" Inter-Noise 79 pp 347-356, Warsaw 1979.

9. Crocker M.J. et al., "Noise Source Identification Under Steady and Accelerating Conditions on a Turbocharged Diesel Engine: SAE paper 800275, Detroit, Feb 25 - 29, 1980.

DESIGN PARAMETERS AND NOISE OF A DIESEL ENGINE

PROFESSOR T. PRIEDE
Institute of Sound and Vibration Research,
The University of Southampton,
Southampton, England.

1. INTRODUCTION

The typical diesel engine noise known as 'diesel knock' is the result of the principle of ignition employed in the diesel combustion process. The spontaneous ignition of the significant volume of fuel pressure rise in the engine cylinder which effectively excites the higher modes of engine structure into transient vibrations which results in the characteristic predominant high frequency impulsive noise. This typical diesel engine noise is most noticeable to the observer at low engine speeds, while at high engine speeds the diesel engine noise is only recognizable by its 'harshness'.

Apart from this typical combustion induced noise, mechanically induced noise generated by the operation of the crank mechanism can also become a controlled factor of diesel engine noise depending on the particular combustion system and mechanical design of the engine employed. The mechanical noise is also impulsive and subjectively it is indistinguisable from the combustion induced noise.

2. GENERAL CONSIDERATIONS OF THE MECHANISM OF GENERATION OF DIESEL ENGINE NOISE

Figure 1 illustrates a typical cross section of a diesel engine and in very simplified form its equivalent vibratory system.

As can be seen, the engine structure consists of two basic structure elements, i.e. internal structure consisting of piston connecting rod and crankshaft and the outer integral basic load-carrying structure consisting of cylinder block crankcase and cylinder head. The internal structure is separated from the outer structure by running clearances.

There are two major sources of noise depending on the specific characteristics of the exciting forces.

1. Unidirectional exciting force (Pg & Pg + Pi) acting axially on the piston resulting from rapid rise in gas pressure and is defined as combustion induced

noise of the engine.

2. Reversible exciting forces (plus or minus F) (forces which change direction) would develop in the crank mechanism and these accelerate internal structure elements across their clearances (piston and bearing slap) causing impacts and resultant vibration and noise. These sources are defined as mechanically induced noise.

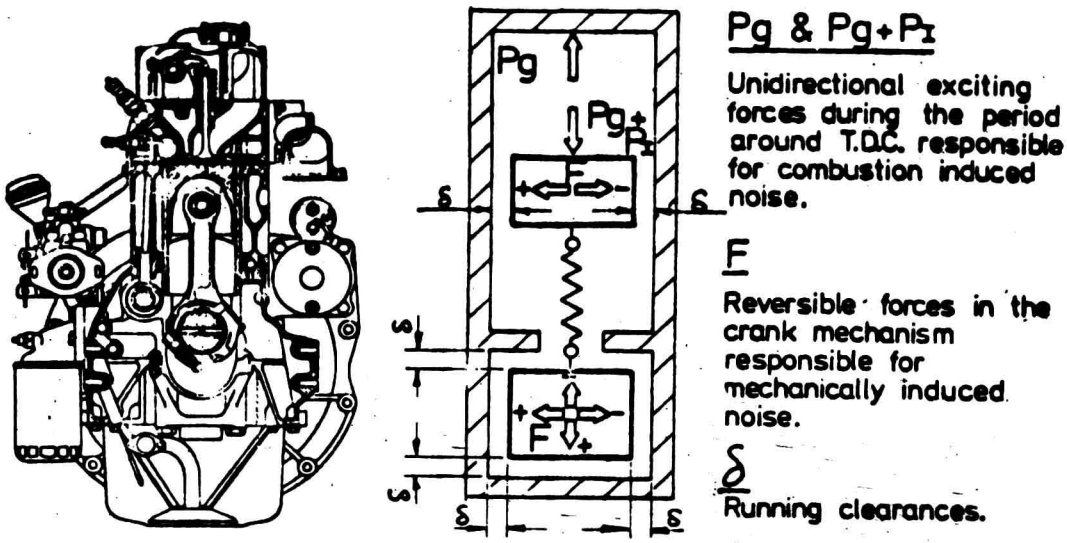

FIGURE 1.

The characteristics of the two categories of exciting forces and the basic mathematical equations are shown in Figure 2a and b.

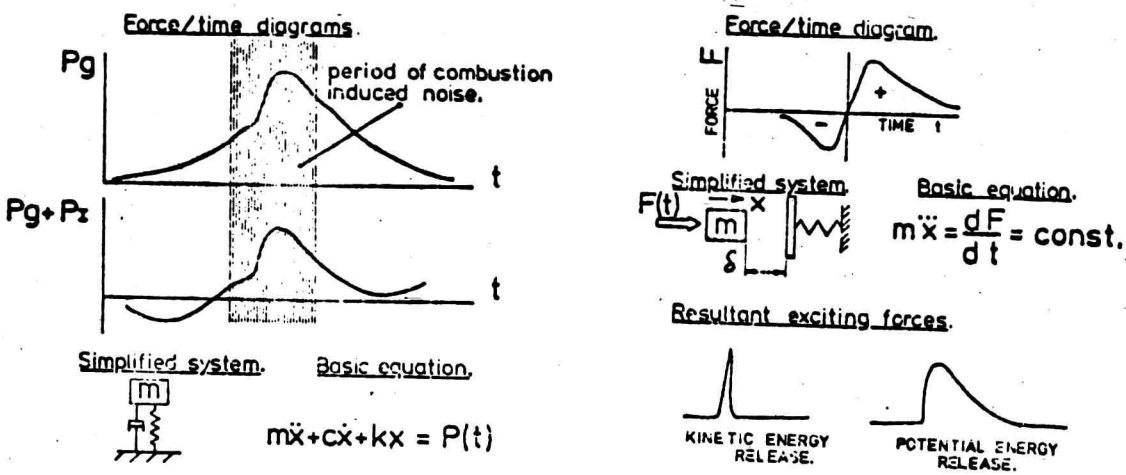

(a) Combustion induced noise (b) Mechanically induced noise

FIGURE 2. CHARACTERISTICS OF EXCITING FORCES IN RECIPROCATING ENGINE

The combustion induced noise is produced by rapid change in the magnitude of the force while mechanically induced noise is produced by the release of kinetic and potential energy in numerous impacts during a single working cycle.

3. RELATION BETWEEN FUNDAMENTAL ENGINE PARAMETERS AND NOISE

Figure 3 summarises the basic relationships between emitted noise and the engine parameters speed, size and load, based on numerous studies of combustion induced noise on a large number of engines.

As can be seen, the choice of the combustion system determines the rate of increase of noise.

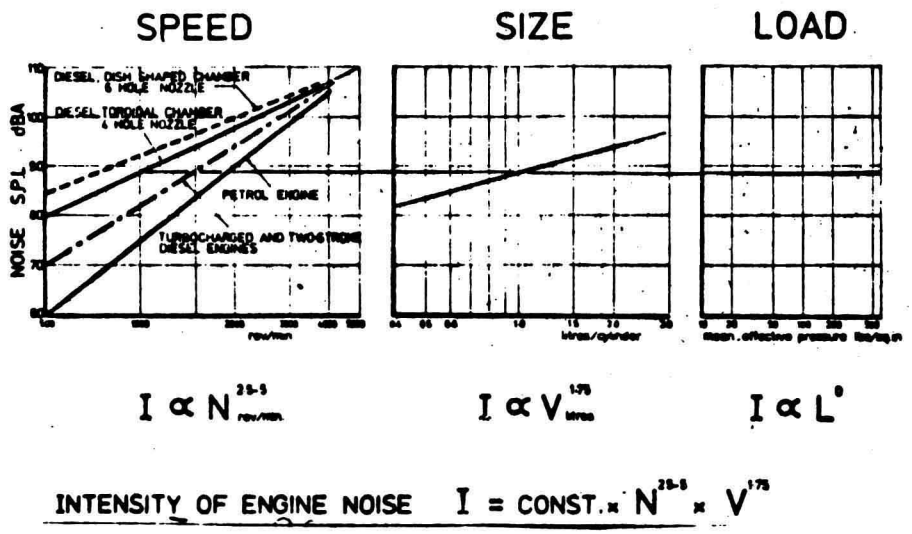

FIGURE 3. RELATION BETWEEN ENGINE NOISE, SPEED, SIZE AND LOAD

For petrol engines it is about 50 dBA per tenfold increase of speed while for a traditional direct injection diesel engine about 25 to 30 dBA per tenfold increase of speed.

As the speed increases, the lines tend to converge clearly indicating that in high speed engines the form of the gas force resulting from combustion is irrelevant.

Measurements again show that the increase of noise with engine size, is relatively less. An increase of size (cylinder capacity) to ten times gives an increase of noise of 17.5 dBA.

Engine load, however, has no effect on noise which is in agreement with the findings that noise is simply due to the initial ignition of the fuel. This occurs at the same intensity whether the engine is running at no load at all or full load.

Based on these considerations and the evidence from experimental data the overall intensity of engine noise can be defined as:

$$I \sim \text{const} \times N^n \times V^{1 \cdot 75}$$

where N = engine speed

n = defines the form of the gas force depending on combustion system used

V = cylinder volume

Further studies revealed that the variations of noise levels for the same cylinder capacity are due to choice of bore to stroke ratio. The shorter stroke engine has a larger bore diameter thus the applied gas force is inevitably considerably greater.

These observations lead to the conclusion that the basic parameters which determine the noise of the engine are speed and cylinder diameter, i.e.

$$I = \text{const} \times N^n \times B^5$$

or

$$I = C_f \, C_s \, (N^n \times B^5)$$

where C_f - defines the level of the gas force

C_s - defines the engine structure characteristics

This simple expression is valuable at the engine design stage for choosing basic parameters for lower noise.

4. ASSESSMENT OF NOISE CHARACTERISTICS OF PRESENT PRODUCTION ENGINES

A considerable amount of research has been directed towards control of the ignition process and quieter combustion systems associated with specific fuel injection systems have been introduced in practice. Some of these are (a) pilot injection system of a traditional DI engine; (b) MAN 'M' systems; (c) Ricardo IDI system with specific fuel injection system; (d) turbocharged DI system and more recently, (e) Perkins 'squash lip' system.

The gains although worthwile, give in practice only 2-4 dBA reductions of engine noise (the lower value usually at rated conditions). Smaller reductions of noise are generally obtained where the smoothness of cylinder pressure

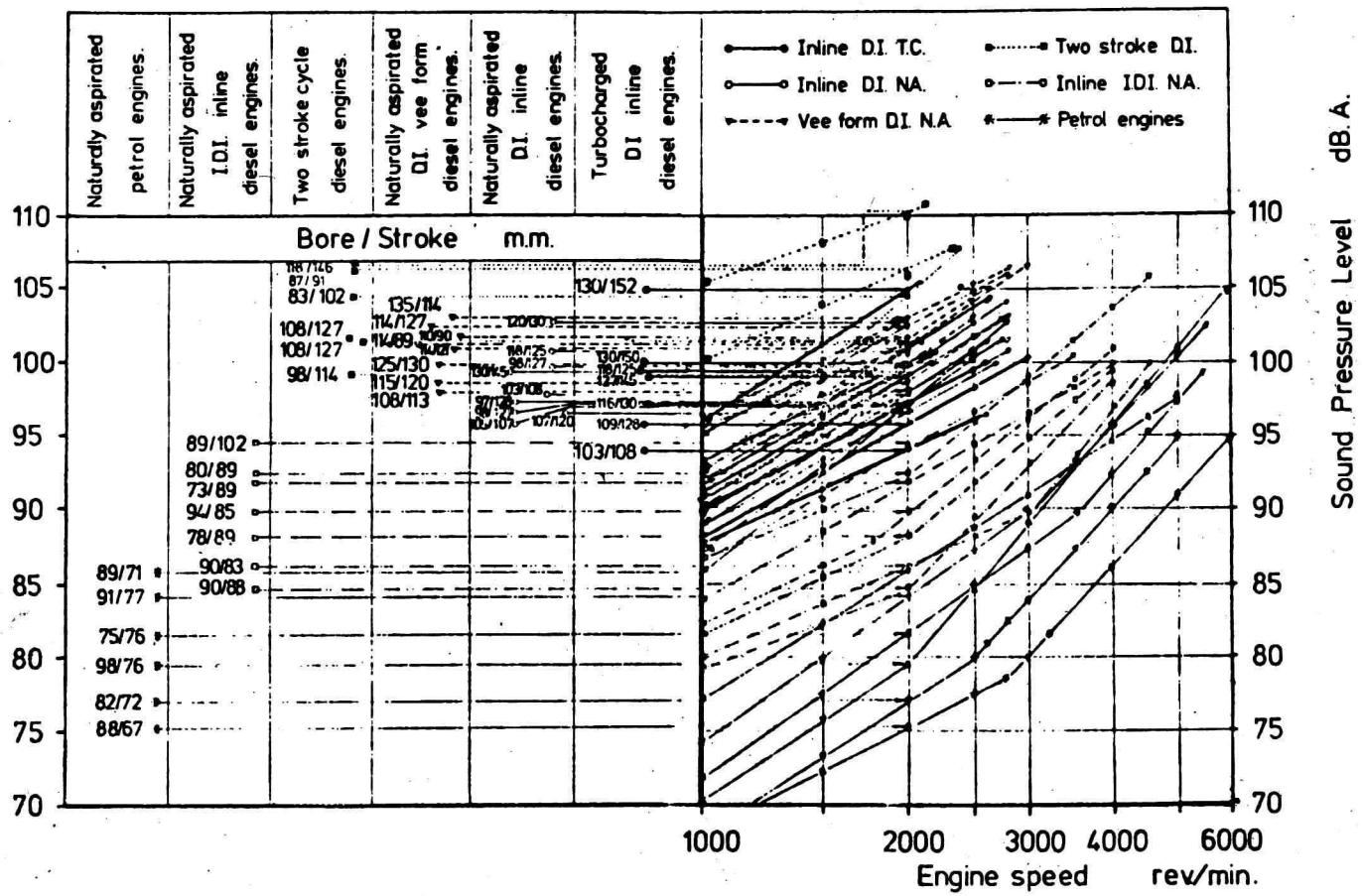

FIGURE 4. RELATIONSHIP BETWEEN ENGINE NOISE AND SPEED AT FULL LOAD

development is obtained at the expense of higher peak cylinder pressure. The smooth combustion in the turbocharged engine is also limited to a relatively small region, namely at high engine speeds and loads. At light load and during acceleration the turbocharged engine behaves, more or less, as a normally aspirated engine.

To establish the relevant differences in noise characteristics of engines of different design and combustion systems a detailed study has been made of the results of all the different engines tested at ISVR laboratories. On each engine gas force diagrams have been taken, and cylinder pressure, noise and vibration analyses have been carried out. The overall noise in dBA at full load conditions of some 50 different engines is summarised in Figure 4. The measured noise is at a distance of 1 metre from the engine complying with the generally accepted practice. The noise of all the engines show straight line relationships with speed, except for small high speed IDI and petrol engines which show two slopes, a low rate of increase in the low speed range and a high rate in the high speed range. If the results are compared on the basis of constant speed the increase of noise with engine size is apparent. At the rated speeds, all engines (except the opposed piston two strokes) reach about the same level of noise within a band of some 10 dBA.

Overall noise levels of the results shown in Figure 4 are plotted against bore diameter at a constant speed of 2000 rev/min which represents a realistic speed for comparison of all engines in this wide range.

It can be seen that the engines fall into specific groups:

(a) All normally aspirated DI engines fit within a 3 dB band of the slope $(\text{bore})^5$. It is clear that there are no differences between overall noise of vee form and in-line engines. Some IDI engines also fall within the same band but these are with abrupt combustion.

(b) The turbocharged engines occupy a band just below.

(c) The remaining IDI engines fall within a band some 8 dBA below the DI engines. These engines generally have smooth combustion.

(d) Two-stroke cycle engines fall within the band some 4 dBA higher than the DI engines.

(e) Opposed piston two-stroke cycle engines fall in a band 12 dB higher.

(f) Petrol engines show considerable scatter but are about 15 dBA below the DI engines.

Many of the differences between these various groups can be explained by the

salient features of cylinder pressure development resulting from combustion. The level of combustion noise devised from ISVR experimental and theoretical predictions is shown in the Figure 5. It will be seen that DI injection four stroke, DI injection two stroke and opposed piston engines noise is primarily combustion controlled.

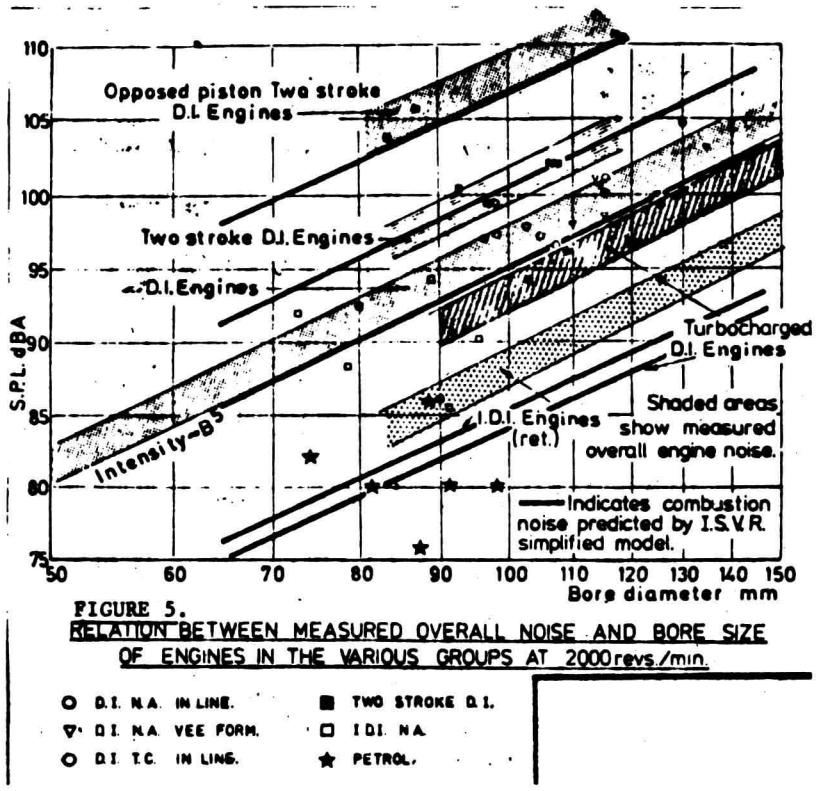

FIGURE 5.
RELATION BETWEEN MEASURED OVERALL NOISE AND BORE SIZE OF ENGINES IN THE VARIOUS GROUPS AT 2000 revs./min.

The turbocharged DI and IDI engines with smooth combustion, however, are controlled by mechanically induced sources of noise.

For example, purely from the combustion point of view the turbocharged diesel engine should be about 10 dBA quieter. It is the high peak gas pressures which are mainly responsible for the high levels of mechanically induced noise.

Typical cylinder pressure diagrams of various combustion systems are shown in Figure 6. It shows that in turbocharged engines the smoothness of cylinder pressure development is achieved at the expense of very high peak pressure which increases the mechanically induced noise.

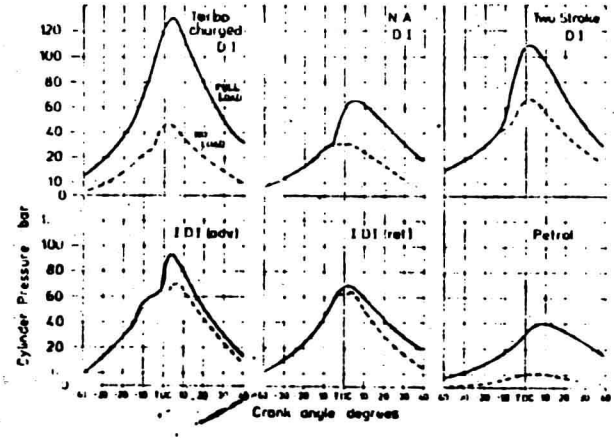

FIGURE 6. Typical Cylinder Pressure Diagram of Various Combustion Systems

In the Figure 6 the noise of all engines despite the different origins of noise (i.e. combustion or mechanically induced) is proportional to $(Bore)^5$. It has been confirmed now that overall noise of engines where combustion induced noise is low, i.e. turbocharged and IDI engines, the predominant mechanically induced noise also increases with $(Bore)^5$ thus confirming the experimental results obtained.

Figure 7 shows that overall noise of most of the engines at present in production lies in the band between 100 to 105 dBA.. Also it will be seen that to a first approximation the noise of all engines, regardless of size, is independent of horse power.

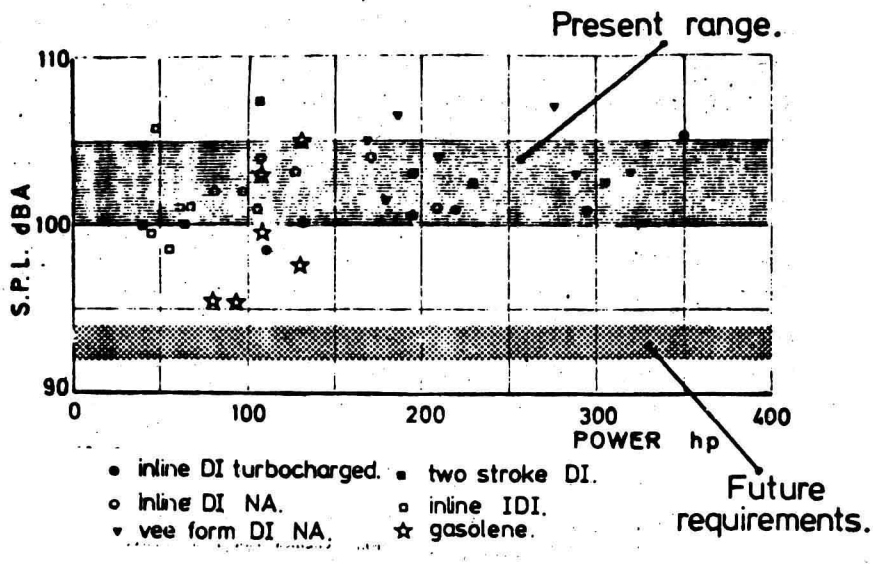

FIGURE 7. RELATION BETWEEN NOISE AND POWER.

This also applies to other machinery as shown in Figure 8.

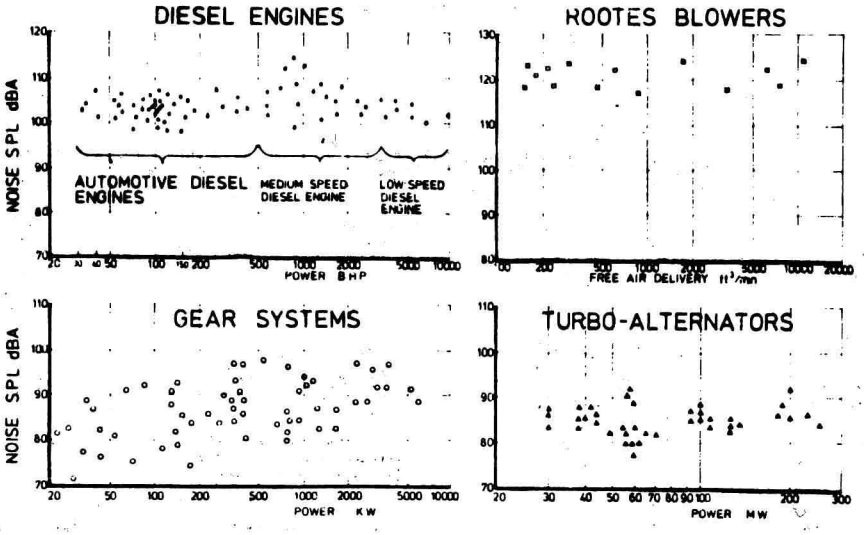

FIGURE 8. RELATION BETWEEN NOISE AND POWER

5. CONTROL OF NOISE

As already discussed there is considerable latitude to select engine design parameters for low noise performance; that is operating cycle, combustion system, bore size and speed. There are, however, good economic reasons which tend to reduce this latitude in practice and to dictate the type of engine design needed for a specific duty. Thus the choice is limited.

It is clear that from the noise point of view the requirement of the combustion system is a smooth cylinder pressure development which must also be associated with a low peak gas pressure and correct matching of gas and inertia forces. From performance considerations alone, it is essential to establish the optimum peak pressure as a compromise between combustion and mechanical efficiency, as mechanical efficiency tends to decrease with increase of gas pressure.

Significant reductions can be achieved by specific design of the main structure and covers accepting existing combustion systems and component parts. Over a number of years, 10 different experimental low noise engine structures have been built embracing all the engine groups described in this report, namely five IDI engines, two normally aspirated DI engines, one vee-form engine, one opposed piston two stroke engine and two high output turbocharged DI engines.

The different principles of design have been explored, to date as shown in Figure 9.

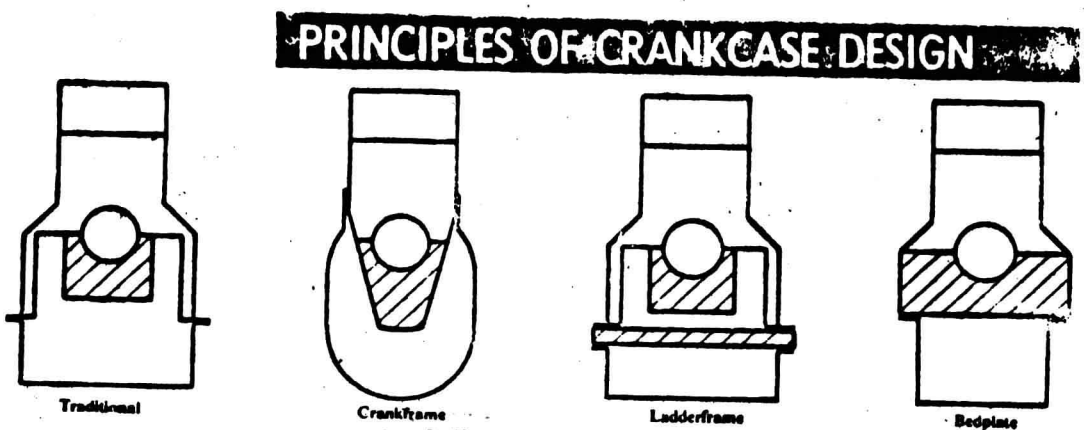

FIGURE 9. PRINCIPLES OF CRANKCASE DESIGN

(a) Skeleton frame both case and fabricated clad with damped materials.

(b) Increased stiffness for the same weight using magnesium alloy.

(c) Reduction of area of cast outer surfaces using crank frame design and replacement with large non-stiff covers.

(d) Increased stiffness using bedplate, ladder frame or split crankcase principles (Figure 8).

(e) Combination of increased damping and stiffness.

(f) Partial enclosure of cast surfaces.

The levels measured from these experimental engines are compared with those obtained from orthodox designs in Figure 10. Reductions range from 7 to 11 dBA.

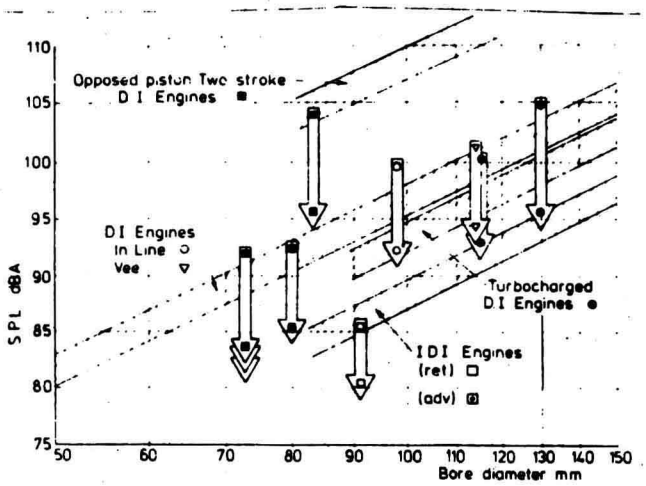

FIGURE 10.

ACOUSTICAL STUDY OF A FORGING DROP HAMMER

N A HALLIWELL and E J RICHARDS

Institute of Sound and Vibration Research
University of Southampton
England

ABSTRACT

The present industrial code of practice in the U.K. recommends a noise exposure limit to workers of 90 dB(A) L_{eq} and drop hammers create noise levels which are typically 110-115 dB(A)L_{eq}. This paper reports an acoustical study of a typical working hammer, and identifies regions for noise control at source. It is shown that acceleration noise from a hammer is not a significant hearing damage risk in L_{eq} terms. Reference is made to initial results from an exact one third scale model under construction at the Institute of Sound and Vibration Research.

1.0 INTRODUCTION

The present industrial code of practice in the U.K. recommends a noise exposure limit to workers of 90 dB(A) L_{eq} normalised to an eight hour working day. Table 1 shows the sound levels recorded from a variety of forging hammers for a final (die to die) blow in a forging sequence. The estimated number of blows required to administer this noise energy dose to a hammer operator is also given.

HAMMER TYPE	L_{eq} (1 sec) dB(A)	Impulse dB(A)	Peak dB(A)	Blows to 90 dB(A)L_{eq} in 8 hours
12 ton Friction Drop	128	134	145	7
10 ton Friction Drop	119	127	139	38
Counter Blow	113	123	136	153
Steam	114	125	136	125

TABLE 1

As is evident from these results the forging industry is one of the leaders in causing industrial deafness and as such the U.K. government makes special provision of deafness allowances for ex-employees.

A drop hammer produces impact noise and fundamental studies of this phenomena[1][2] have shown that it can be divided into two sections acceleration noise and "ringing" noise. The former is caused by the severe acceleration forces which the bodies are subject to during impact and the latter is a result of vibrational energy being transmitted to the structure and re-radiated as noise. For a drop hammer we must include two other types of noise source these being billet expansion and air expulsion noise and note that vibrational energy can escape from the structure into the ground and then be re-radiated as sound. Fig 1 shows a schematic diagram of a drop hammer and Fig 2 shows

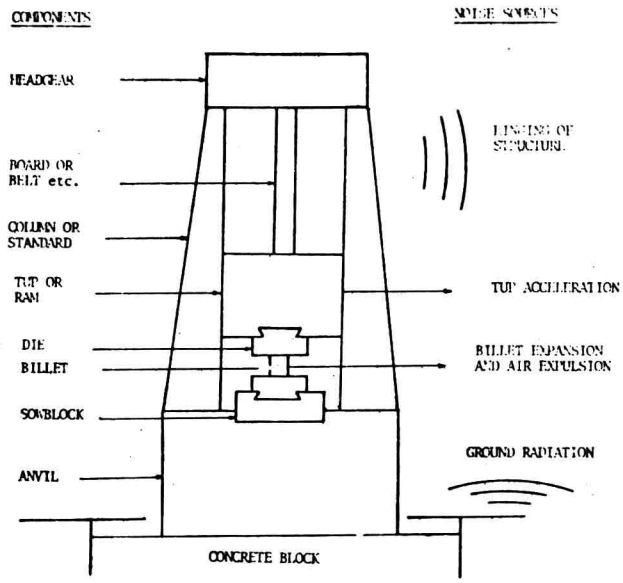

FIGURE 1: SCHEMATIC DIAGRAM OF DROP HAMMER INDICATING SOURCES OF NOISE

a typical sound pressure time history for a single blow. Peak levels reached are usually between 130-150 dB(A) depending upon hammer size and correspond to acceleration, billet expansion and air expulsion noise. The remaining "ringing" noise contains the majority of the sound energy. The percentage of the total kinetic energy developed by the tup which is radiated acoustically is very small indeed typically 10^{-5} to 10^{-6}.

2.0 PEAK NOISE LEVELS

2.1 Tup Acceleration Noise

Acceleration noise arises when a solid body changes its velocity fast enough to compress the air around it. The noise arises as an isolated double pulse radiating only for the period over which acceleration or deceleration occurs. If a body moving with velocity V_o comes to rest instantaneously it can be shown that [1,3] the energy

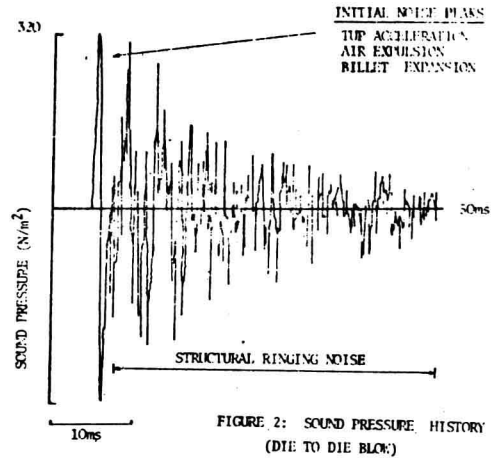

FIGURE 2: SOUND PRESSURE HISTORY (DIE TO DIE BLOW)

(E_{acc}) put into the surrounding air because of compressibility is given by

$$E_{acc} = \rho_o \text{ (vol of body) } V_o^2 /4$$

where ρ_o is the density of air. If the period over which an impacting body changes its velocity is finite (contact time t_o) some of this energy is returned from the surrounding air to the body. The efficiency of this radiation process (μ_{acc}) can be expressed in terms of the ratio of acoustical energy

radiated to the maximum possible if two such bodies impact. The contact time (t_o) can be non-dimensionalised so that $\delta = ct_o/(vol)^{1/3}$ is the ratio of the distance a sound wave can travel in the time of the impact process to a typical body dimension. If the impact time is a larger one which occurs when metal is actually being shaped by the hammer (δ) is larger and the subsequent acceleration noise is smaller. Fig 3 shows the sound energy (μ) normalised to the tup kinetic energy versus δ for forging and die to die blows of a 1 ton friction drop hammer. The universal curve for acceleration noise was produced from

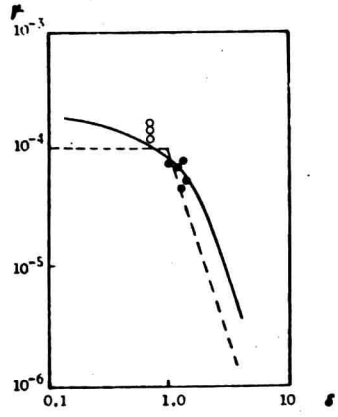

FIGURE 3: NORMALISED SOUND ENERGY μ vs δ FOR FRICTION DROP STAMP

o DIE TO DIE BLOWS
• FORGING BLOWS

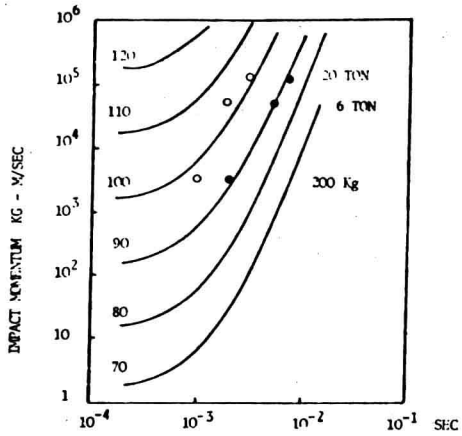

FIGURE 4: MAXIMUM L_{eq} FROM TUP ACCELERATION NOISE

— dB(A)
o DIE TO DIE BLOWS
• FORGING BLOWS

$$\mu = \frac{E_{acc}}{\frac{1}{2}mv_o^2} \quad (1)$$

carefully controlled laboratory experiments . From this curve it is possible to calculate an L_{eq} for a given contact time. This has been done on the basis that the time of raising the hammer is three times that of dropping it and an L_{eq} calculated for an 8 hour period. The results are shown in Fig 4 from which we may conclude that the danger to hearing from acceleration noise is not really significant when risk is assessed on an equal energy basis. Peak sound levels can be shown [3] to increase with tup velocity, volume and contact time. Within the confines of present hammer practice reductions can be obtained by trying to avoid clashing of cold die to die operations for finishing and the use of denser slower speed tups.

2.2 Air Expulsion Noise

Air expulsion noise is created by air being ejected between the dies prior to impact as they close on each other. A large rarefraction pulse is produced as the dies close and suddenly shut off the supply of air. The pressure level produced close to the die centreline is typically 140-150 dB(A). Evensen [4]

has shown that this peak falls away severely with distance from the die edge and we can conclude that it is negligible as a contributor to peak levels in the operator's position where deceleration peaks dominate.

2.3 Billet Expansion Noise

Billet expansion noise occurs due to the sudden deformation and consequent outward radial movement of the billet when the tup impacts[5]. A sharp pressure pulse (typically 100 dB(A)) is produced as the surface of the billet accelerates and this is followed by a smaller longer pulse as the surface decelerates towards the end of the contact time. If hearing damage is assessed on an equal energy basis this noise source is unimportant as the initial pulse only lasts for a few microseconds.

3.0 RINGING NOISE SOURCES

3.1 Ground Radiation

Energy which escapes to the ground will be for the most part dissipated as heat but the ground may indeed re-radiate a portion as sound. This contribution to noise energy is very dependent on the way in which the hammer is mounted and cannot be discussed in great detail. Contributions to the overall level are usually small. In the U.K. spring mounted hammers have been found to be noisier (1-2 dB(A)L_{eq}). Spring mounting reduces energy escape to the ground and this extra energy is more efficiently radiated as sound by the hammer structure.

3.2 Structural Ringing

The structural ringing of the hammer is the most important factor when hearing damage risk is assessed in terms of energy dosage (L_{eq}). In soft hammer blows the majority of the available kinetic energy goes into the shaping of the workpiece whilst for the final coining blows the great majority goes into the structure and the rebound energy of the tup. It is important to be able to trace the escape of this structure-borne sound from the workpiece and to minimise its radiation as air-borne sound.

It has been shown[2] that bodies with preferred flexural modes of vibration will store more vibrational energy under impact excitation and consequently it might be anticipated that the columns of a hammer would be primary radiators. Schroder[6] suggested this but the more recent work of Humbert[7] concluded that the major source of noise was the workpiece area. The latter work surveyed a variety of hammer types but sound measurements were taken on an impulse S.L.M. and can only be interpreted in a qualitative way.

Table 2 shows the A weighted sound energy radiated from a one ton drop hammer based on vibration measurements. For a transient vibration of duration (T) the

sound energy radiated (E_{rad}) by a surface of area (S) can be shown to be [8]

$$E_{rad} = \rho_o c \, S \, \sigma_{rad} \int_o^T \langle v^2 \rangle \, dt$$

where $\langle v^2 \rangle$ is the surface average of the normal surface velocity and σ_{rad} is the radiation efficiency of the surface. The total energy radiated for one blow was some 8 dB less than that measured by microphones but the latter were subject to near and reverberant field errors. It is unlikely that relative magnitudes of sound energy radiated per component and estimated from vibration measurements is in serious error. The results show clearly that ≈ 60% of the total sound energy is radiated from the workpiece area comprising tup, dies, bolster and sowblock.

We can conclude that this is the major source area but even eliminating this at source will only produce ≈3dB reduction overall. The final conclusion must be that significant noise reduction will only result if we treat each component of the hammer individually. We must apply noise control measures throughout.

POSITION	ENERGY RADIATED (Joules)	TOTAL	%
Ram	3.09×10^{-3}	3.09×10^{-3}	12.5
Upper Die Lower Die	1.72×10^{-3} 2.92×10^{-3}	4.69×10^{-3}	19
Bolster Sowblock	1.23×10^{-3} 5.75×10^{-3}	6.98×10^{-3}	28.5
Anvil top Anvil front faces Anvil end faces	1.28×10^{-4} 2.75×10^{-3} 4.35×10^{-4}	3.32×10^{-3}	13.5
Ram guides Frame front faces Frame side faces	6.14×10^{-4} 5.91×10^{-3} 6.17×10^{-4}	7.14×10^{-3}	26

TABLE 2

3.3 Frequency Analysis of Workpiece Area

As the majority of noise is produced in the workpiece area it is of interest to study in more detail the dynamics and vibrational characteristics of the components involved. Figure 5 shows an octave analysis of the A weighted energy from each component for forging blows. As anticipated the tup, frames (columns) and anvil are dominant as radiators of low frequency noise. The majority of energy from the dies, sowblock and bolster, however, appears between 1-2 kHz. Closer inspection of the vibration spectra showed that the tup, bolster and upper die showed a highly damped 1.5 kHz mode. Figure 6(a) shows the integrated (velocity)^2 spectrum for the upper die where

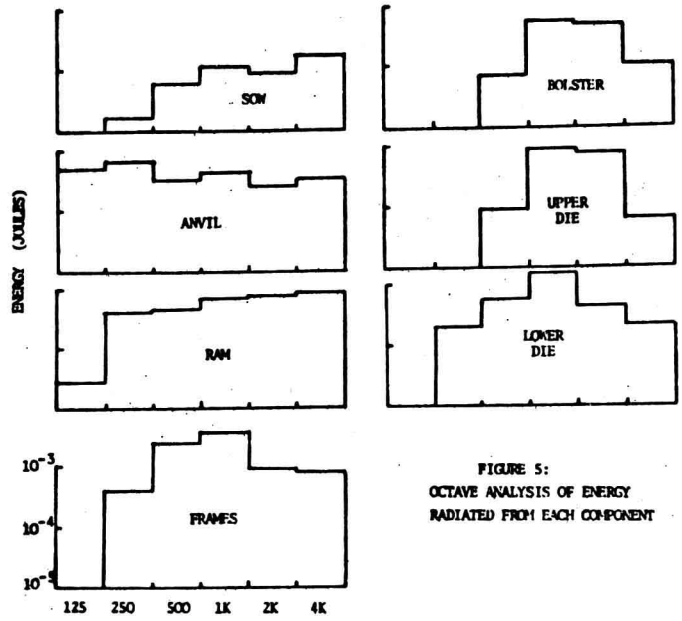

FIGURE 5:
OCTAVE ANALYSIS OF ENERGY
RADIATED FROM EACH COMPONENT

it can be seen that the majority of vibrational energy is indeed in this mode. The lower die and sowblock shared a highly damped but slightly different mode of 1.35 kHz. This is shown in Figure 6(b) for the lower die and compared with a sound pressure spectrum measured simultaneously in the operator's position (Fig 6(c)).

As the natural frequencies of these components might be expected to be much higher than these values the question must be asked are these components behaving as solid bodies oscillating on the springiness of the keying system used. In this way there would be two separate mass-spring systems on either side of the workpiece each with its own frequency response characteristics.

A separate invesitgation was carried out using simultaneously acquired accelerometer signals to examine this phenomena and the results showed that the components do in the main behave as solid bodies in oscillation and Poisson contraction effects appear to be masked by this.

Figure 7 shows the time histories of acceleration levels taken

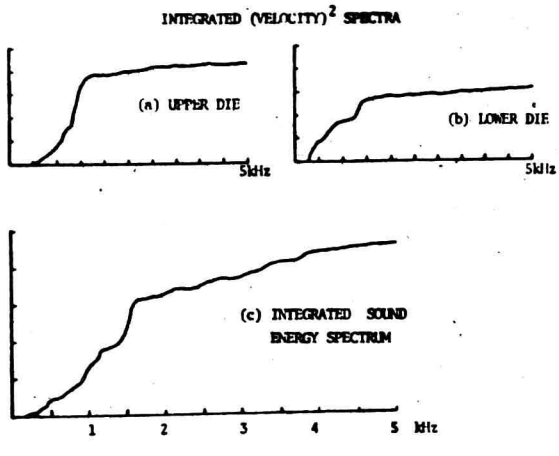

FIGURE 6: INTEGRATED SOUND AND VELOCITY SPECTRA

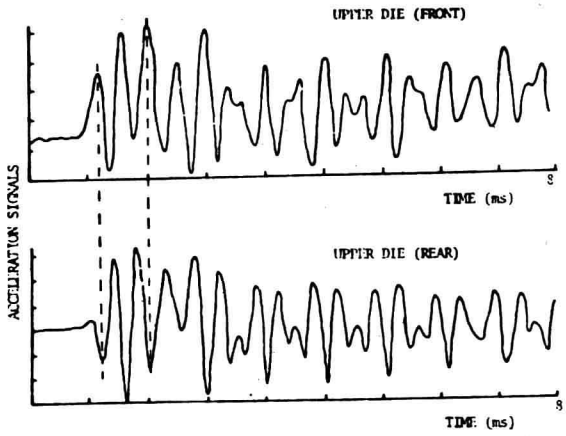

FIGURE 7: UPPER DIE ACCELERATION TIME HISTORIES

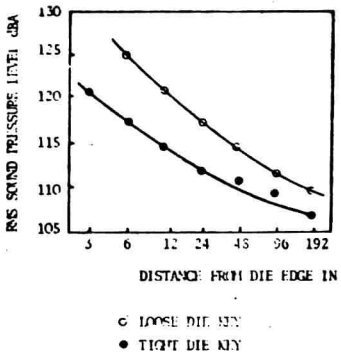

FIGURE 8: EFFECT OF LOOSE DIE KEY ON R.M.S. SOUND LEVEL (AFTER [illegible] (4))

simultaneously on the front and rear of the upper die. They are π out of phase indicating rigid body oscillation. The frequency is ≈ 2 kHz. It can be argued that the state of the keying will have considerable effect on the stiffness of this system. Practical evidence for this idea comes from the fact that forgers assess when a key has loosened by noting the change in noise level produced. Figure 8 shows the change in noise output produced by loose and tight keying.

3.4 Third Scale Model Tests

Tests have shown that the major components of anvil and frames have natural frequencies which agree with the low frequency noise data shown in the octave spectra of Fig 5 for full scale measurements. Model development is at an early stage and components have been tested in free-free conditions. Initial tests do indicate, however, that the major components still carry most energy in their free-free fundamental mode when assembled. Further tests will indicate whether noise control can be anticipated by modal decoupling of components. Figure 9 shows the velocity response of the columns to anvil excitation overlaid on the velocity response of the anvil to load excitation. The anvil couples strongly at 1.7 kHz in its first bending mode.

3.5 Noise Control Measures

Noise reduction at source can be attempted by modal decoupling, re-design of the workpiece area, selective damping increases (particularly columns), re-design of tup and careful use of resilient inserts.

4.0 CONCLUSIONS

Radiated sound energy partition amongst components of a drop hammer is

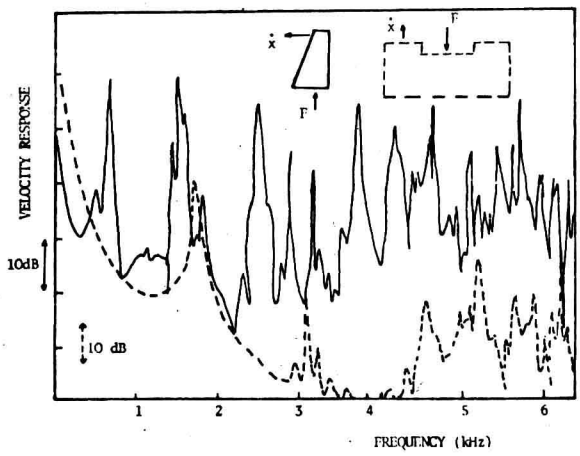

FIGURE 9: MODAL COMPARISON ANVIL/COLUMN FOR LOAD EXCITATION

geometry dependent although in general no one component is a major sound radiator itself. Noise control measures must be applied to every component if significant reduction is to be achieved. The majority of sound arises from the workpiece area which can be considered as a mass-spring system, the stiffness of which is controlled by the type and tightness of the keying system used.

If hearing damage risk is assessed on an equal energy basis tup acceleration noise is not a significant contributor and noise control measures should be applied to the structural ringing. Initial results from third scale model tests are encouraging and relate well to measurements taken full scale.

5.0 REFERENCES

(1) RICHARDS E J et al (1979) On the Prediction of Impact Noise, Part I: Acceleration Noise. J.S.Vib, 62, No.4 pp 547-576.

(2) RICHARDS E J et al (1979) On the Prediction of Impact Noise, Part II: Ringing Noise. J.S.Vib, 65, No.3 pp 419-451.

(3) JUNGER M C (1966) Energy Exchange between incompressible near and acoustic far field for transient sources. JASA, 40, No.5, pp1025-1030.

(4) EVENSEN H et al (1976) Experiments in Forge Hammer Noise Control. International Conference on Forging Noise Control, Oct 26-28, Atlanta, Georgia.

(5) HODGSON D C, BOWCOCK J E (1975) Billet expansion as a mechanism for noise production in impact forming machines. J.S.Vib, 42, No.3, pp 325-335.

(6) SCHRODER P (1974) Dr Ing Dissertation, Technical University of Hannover.

(7) HUMBERT G (1979) Dr Ing Dissertation, Technical University of Hannover.

(8) JEYAPALAN R K, DOAK P E (1980) Sound Energy Calculation of Transient Sound Sources by the Radiation Efficiency Method. J.S.Vib (to be published).

VIBRATION ASPECTS OF PRESS STRUCTURES

L.L. KOSS and J.A. MOFFATT
Department of Mechanical Engineering
Monash University,
Clayton, Victoria, Australia, 3168

INTRODUCTION

Thousands of C frame mechanical punch presses are in use in manufacturing industry in Australia today. Common to most of these machines is the high level of noise generated by them during blanking operations which have high rates of loading and/or unloading. Methods of controlling at the source the noise from such operations consist of shaping the force time history e.g. applying shear to the punch, shock absorption, and structural modification of the press frame. Experimental work on shaping the force time history to reduce the noise [1], [2] has yielded reductions in noise levels up to 10 dB(A) for specific operations. Shock absorption through the use of hydraulic shock absorbers has given reductions up to 6 dB(A) [3] and the use of urethane rubber material placed between the punch plate and bed has given reductions of the order of 2 dB(A) [4]. Almost no work has been reported on structural modification of these presses to reduce their noise output.

A major drawback in developing damping strategies to reduce vibrations and radiated sound is the difficulty in obtaining the transient structural response of the machine as excited by the blanking operation. It is easier to obtain dynamic response data by vibration testing, which can be used for the same purpose as the transient response data. Although some information exists on a computer simulation of the modal response of a simple press frame [5], and on a comparison between frequency response functions obtained experimentally during a blanking operation and shaker testing [6] they are of little help in developing methods of noise control. The research reported here has as its main aim to obtain structural response information based upon vibration excitation of presses so that damping techniques can be further improved and structural modification methods can be developed. Mode shape data from vibration testing and experimental details will be presented herein for a 170 kN punch press. The first low frequency mode shape which shows significant sound radiation will be dealt with in detail.

Experimental Method

The press was excited by a sinusoidal force from an electrodynamic shaker

(Philips, PR9270) having a rated output of 12.5N. A piezo-electric accelerometer (Bruel and Kjaer, 4335) connected to an integrator (Bruel and Kjaer, 1606) and audio-frequency spectrometer (Bruel and Kjaer, 2112) were used to measure the velocity of the press at a number of locations. The phase angle measured with between the velocity signal and a force signal from a transducer (Kistler, 901) in series with the shaker was used to determine relative directions of motion. From the amplitude and phase angle information the motion of the press was obtained. Measurement of accelerations were made at 150 mm spacings on the body of the machine.

MECHANICAL PRESS

John Heine 202A/170 kN Press.

A John Heine 202A/170 kN punch press, resiliently mounted on rubber pads, see Fig. 1, was excited by a vibration shaker to determine its mode shapes. The bed of the press was adjusted to be horizontal and a mass of 10 kg was suspended from the rim of the flywheel to take up slack in the clutch mechanism.

The shaker was first placed on the bed, and the flywheel was turned by hand until the slide moved the pushrod of the shaker to its central position against the bias of its suspension springs. Swept sinewave signals from 20 Hz to 2 kHz were applied to the shaker and the surface velocity of the press was measured at a number of locations. A typical velocity response curve for the crown is shown in Fig. 2, the sweep rate being 3 minutes/decade. The cluster of peaks in the range 300 to 400 Hz corresponded to an increase in emission of sound from the press as the frequency was swept from below 300 Hz.

Although this shaker location would have been preferred, because the force was applied at the same location as the force during normal press operations, it was rejected for further testing because there was insufficient height for a force-transducer to be installed in series with the shaker. Furthermore, the shaker body covered the central part of the bedplate thereby hampering measurements of surface velocity and sound intensity. These disadvantages were overcome by relocating the shaker on a concrete block on the floor near the left front hand side of the press with the pushrod of the shaker acting under the left hand front side of the bed as shown in Fig. 1. With the shaker in this position, similar frequency response plots for the press were obtained as for the shaker held in the jaws of the press. This is shown in Fig. 3 where the velocity response of the crown is given for the shaker at the left front hand of the bed.

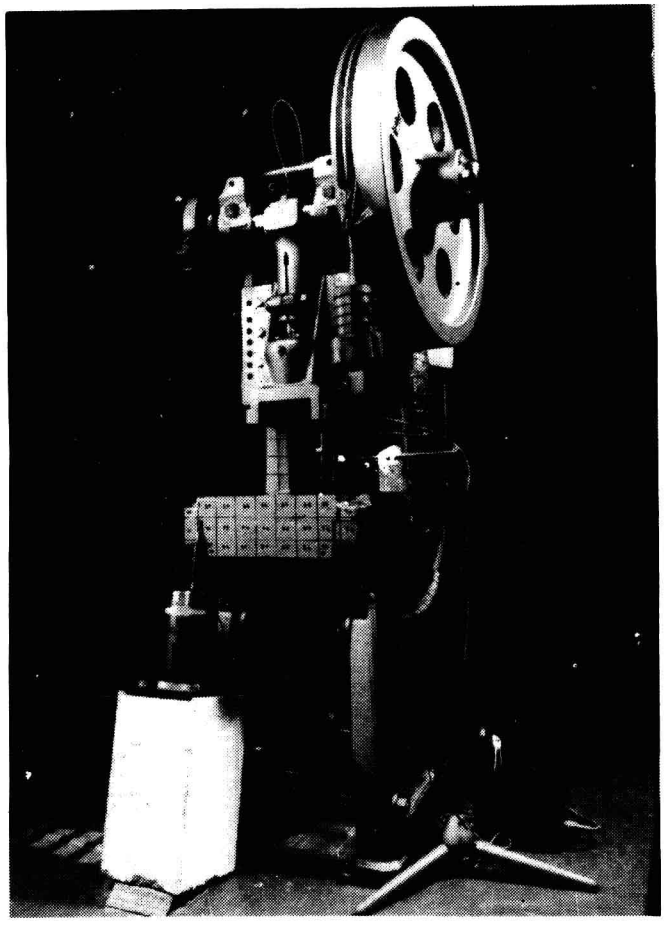

Fig. 1 Photograph of press with vibration shaker at left front position.

RESULTS AND DISCUSSION

A series of resonances exist in the 300 Hz to 400 Hz frequency band as shown in Fig. 2 and Fig. 3. The resonance at 334 Hz is associated with the largest amount of sound radiation in the band as measured by a sound level meter. This frequency was thus first chosen for excitation of the press. To verify that modal overlapping from other modes in this band was not important at 334 Hz, vector diagrams of the displacement at this frequency were constructed for several points on the machine, e.g. Fig. 4 gives the vector diagram for the crown. Information from the vector diagrams shows that the motion at 334 Hz has a very small contribution from the other modes in the 300 Hz to 400 Hz band. The bandwidth determined from the 3 dB down points was about 8 Hz or $\xi = 0.05$, where ξ is the fraction of critical damping of the 334 Hz mode.

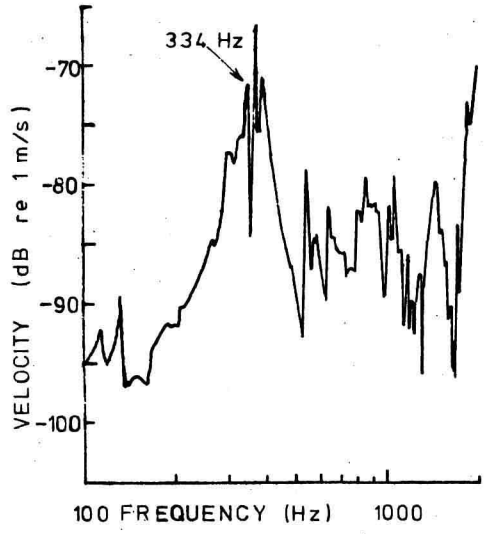

Fig. 2 Frequency response of crown (vertically), shaker between bed and slide.

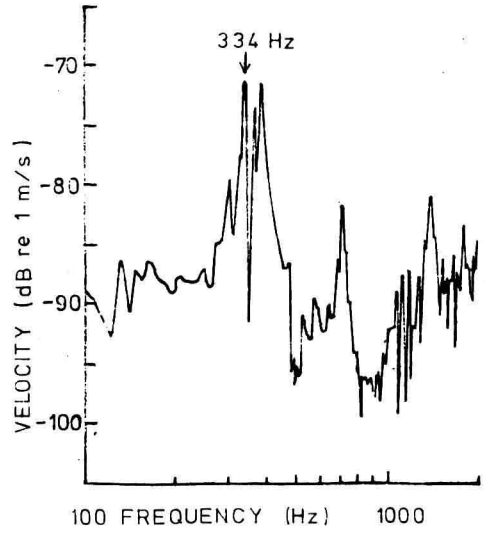

Fig. 3 Frequency response of crown (vertically), shaker at left front position.

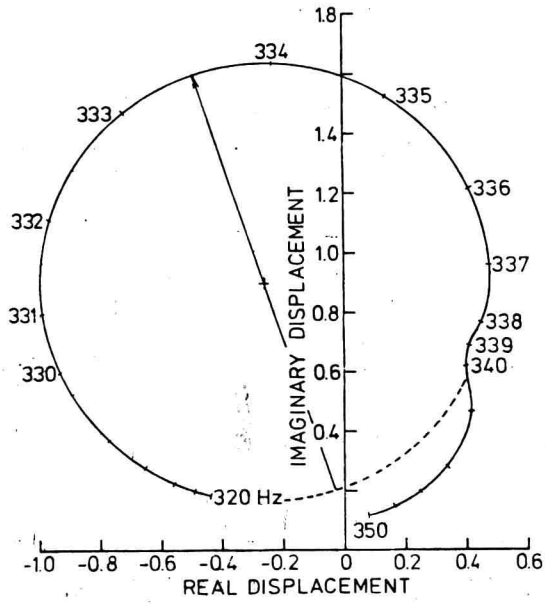

Fig. 4 Vector diagram, complex displacement of crown (vertically) as a function of frequency.

A representation of the mode shape at 334 Hz is given in Fig. 5 where the motion of the slide and flywheel have been left out for the sake of clarity. Displacements are exaggerated in comparison to the size of the press, although to scale. Viewed from the front, the left side of the press has a motion similar to that of a free-free beam, whereas the right side has a similar motion but with an extra node where the frame contacts the pedestal. The side elevations indicate the frame closes in on itself, where the point of minimum closing motion lies at the rear right hand side of the bed when the press is viewed from the front. At this frequency, the bed plate moves as a solid body attached to the press frame. Maximum movements were measured on the pedestal/support structure of the press as can be seen from the front elevation. The motion of the flywheel at this frequency is shown by the broken lines in Fig. 6. The plus and minus signs indicate phase change across the dotted node line. Very small amplitudes of motion occur on the flywheel in comparison to that of the frame and pedestal.

CONCLUSIONS

The mode analyzed herein is a major structural mode of the press, one of a group which exists in the 300 Hz to 400 Hz frequency range. Spatially, the motion shape is similar to that of a free-free beam. Maximum motions exist at the left front hand end of the bed and on the left pedestal, when the press is

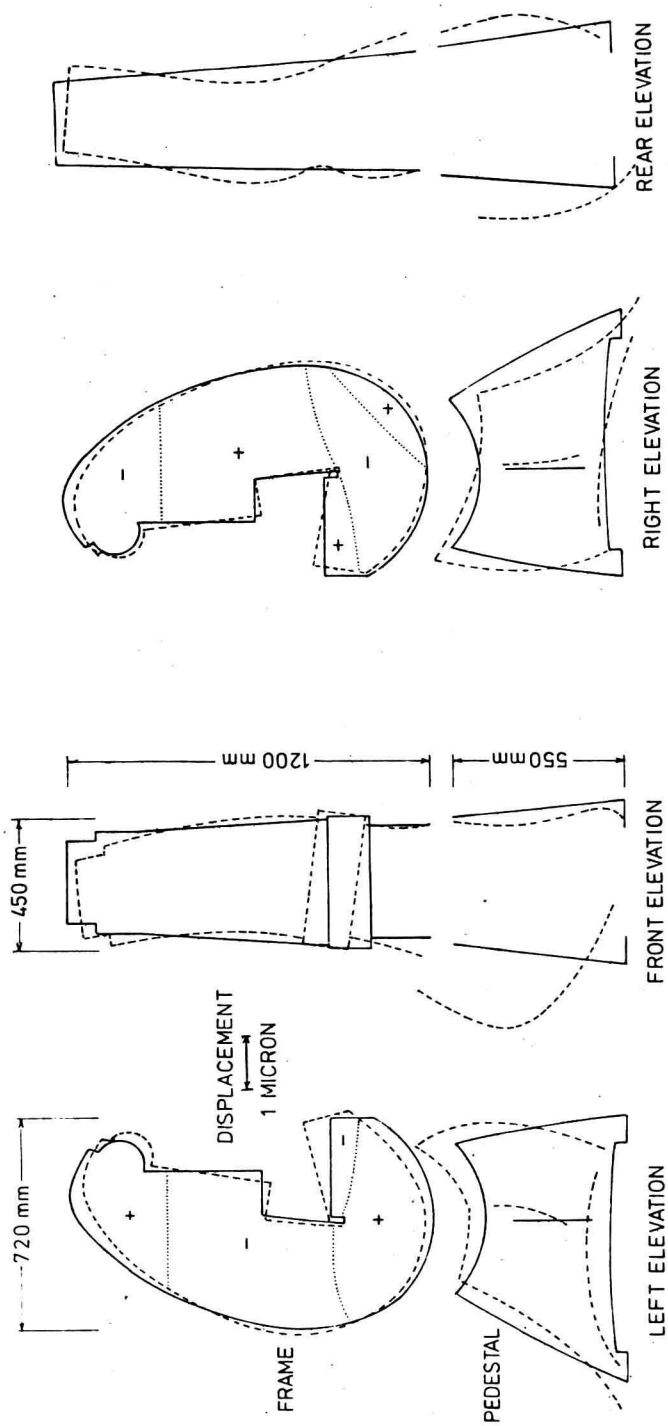

Fig. 5 Mode shape of press at 334 Hz. Solid line - rest position of press, broken line - maximum of motion, dotted line - nodal line. The plus and minus signs indicate relative phase.

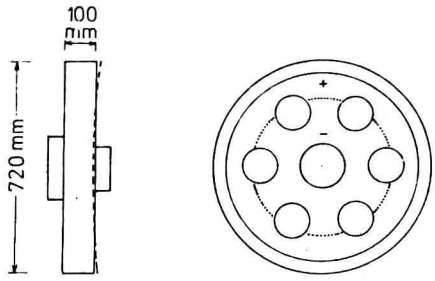

FLYWHEEL

Fig. 6 Vibration of flywheel at 334 Hz.

viewed from the front. As it would be very difficult to dampen the frame due to its large mass and stiffness, a suggested method of reducing the vibration would be to construct the pedestal as a dynamic absorber.

ACKNOWLEDGMENTS

We wish to thank the Repco Corporation, Harold Armstrong Memorial Fund, Australian Research Grants Council, and the Monash University Grant's Committee for supporting this project, and John Heine and Sons for the loan of the press.

REFERENCES

1. Burrows J.M., The Influence of Tooling Parameters on Punch Press Noises. Southampton University, MSc thesis (1979).
2. Evensen H.A., A Fundamental Relationship Between Force Wave Form and the Sound Radiated from a Power Press During Blanking and Piercing. JSV, 68(3), 1980.
3. Bramberger C., Noise Reduction at Punch Presses by Means of Shock Absorber, Noise-Con 79, Machinery Noise Control, 1979, pp.111-117.
4. Koss L.L., Damping of Punch Press Vibrations, Noise Control Engineering, 13(1), 1979, pp.5-12.
5. Brickle B., Punch Press Frame Vibrations and Noise Generation, Akustisk Laboratorium Report No. STF 44 A76053, The University of Trondheim, Norway, May 1976, 40 pages.
6. Koss L.L., Vibrational Analysis of a Punch Press, Noise, Shock and Vibration Conference, 1974. Monash University, Clayton, Victoria, Australia, pp.373-380.

NOISE SOURCE IDENTIFICATION USING THE ENVELOPES OF BAND-PASSED SOUND

K. KIDO, Y. TABEI and T. ITO

Research Center for Applied Information Sciences
Tohoku University
Sendai 980, JAPAN

ABSTRACT

This paper describes a method of noise source identification using the envelopes of band-passed sound picked up at the noise source and the observing point. The coherence function between the source signal and the sound signal at the observing point indicates the contribution factor of the noise source as a function of frequency. But the coherence function decreases in its magnitude when there is some breeze in the transmission path. And the coherence function cannot usually be used as the indication of the contribution factor unless the distance between the source and the observing point is close. The deterioration of the coherence function due to the turbulence in air can be neglected if the period of the sound is much longer than the fluctuation of transmission time. And this paper proposes the use of the envelopes of the band-passed sound instead of the wave form. The method proposed in this paper is suitable for noise source identification when there are various kinds of noise sources which change their characteristics with time.

1. INTRODUCTION

The coherence function is known to be useful for the estimation of the contribution factor of noise source which is important for the noise control. But the fluctuation of the transmission time due to the turbulence in air decreases the coherence function. And the coherence function becomes ineffective when the distance between the noise source and the observing point exceeds several meters in the open air.

Most of environmental noises have their special features in the envelopes when the frequency band is limited through a band pass filter. And the coherence function between the envelopes of the band passed noise picked up at the noise source and at the observing point is a useful measure for the estimation of the contribution of the noise source to the observed noise. The envelope of the band-passed noise shows usually moderate change and the coherence function between the envelopes is hardly affected by the turbulence of air.

2. EFFECT OF THE FLUCTUATION IN TRANSMISSION TIME

When the observing point is not close to the sound source, the coherence function* between the signal $x(t)$ at the sound source and the signal $y(t)$ at the observing point is decreased in the magnitude by the delay in $y(t)$ due to the transmission and by the fluctuation in the transmission time due to the turbulence in air. The delay in the signal $y(t)$ at the observing point introduces the uncorrelated signal in the time window and decreases the coherence function in magnitude. Fig. 1 shows the effect of the time delay in $y(t)$ on the coherence function γ^2, where the duration of the time window (Hanning window) is 43 ms. and the delay in $y(t)$ is 0, 6.7 and 13.5 ms. for each case as indicated in the figure. These results were obtained in an anechoic chamber using a loudspeaker driven by white noise

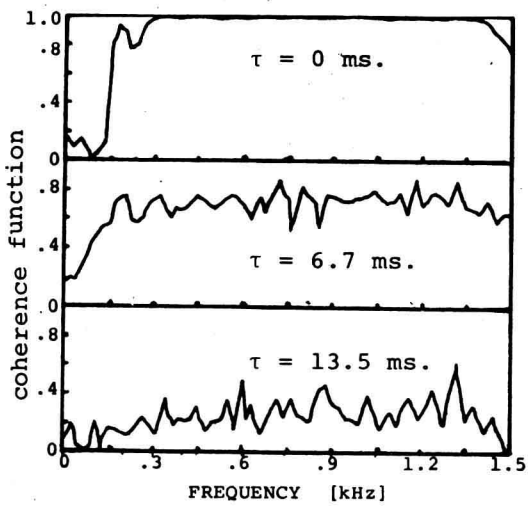

Fig. 1
The coherence function between the source signal $x(t)$ and the response $y(t)$ measured in an anechic chamber. Hanning windows of 43 ms. duration with no shift are used for computation.

---

* The coherence function γ^2 is defined as the followings:

$$\gamma^2 = \frac{Wxy^2}{Wxx\ Wyy}$$

where Wxy : the cross power spectrum of $x(t)$ and $y(t)$
Wxx : the auto power spectrum of $x(t)$
Wyy : the auto power spectrum of $y(t)$
and is the ratio of the frequency component of power spectrum coused by $x(t)$ to the total power of $y(t)$ when $y(t)$ is composed of $x(t)$ and other signals and noise.

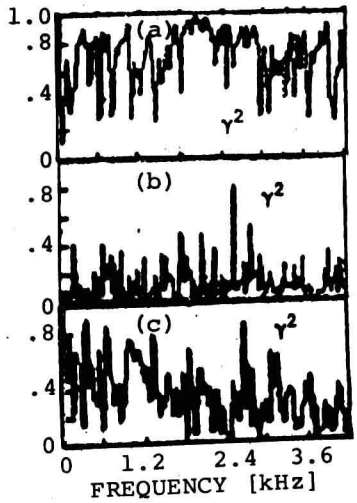

Fig. 2
The coherence functions measured with the noise of electric powered hand drill.
The distance between the sound source and the microphone are 0.35, 15.5 and 15.5 m. for (a), (b) and (c) respectively. The delay due to transmission time is compensated in (c).

as the sound source and there is no fluctuation in the transmission time. And the effect of the delay can be easily compensated giving adequate delay to the signal $x(t)$ at the sound source.

The fluctuation in the transmission time decreases the coherence function in the magnitude as the fluctuation changes the frequency spectrum of $y(t)$.

Figure 2 shows the examples of the experimental results, where the sound source is an electric powered hand drill and the distances between the sound source and the observing points are 0.35, 15.5 and 15.5 meters for (a), (b) and (c) respectively. The magnitude of the coherence function in(a)is less than 1 in all the frequencies, because the signal radiated from the hand drill is not white noise, and the magnitude of the coherence function in (b) is much decreased by the delay due to transmission time and also by the fluctuation in transmission time due to the turbulence in air. Compensating the delay, the coherence function increases in the magnitude as shown in (c) which shows the reduction in the magnitude of the coherence function due to the fluctuation in the transmission time. The weather was almost windless when the experiment was carried out. It seems to be rare according to our experience that the turbulence in air is so little that the coherence function is not decreased.

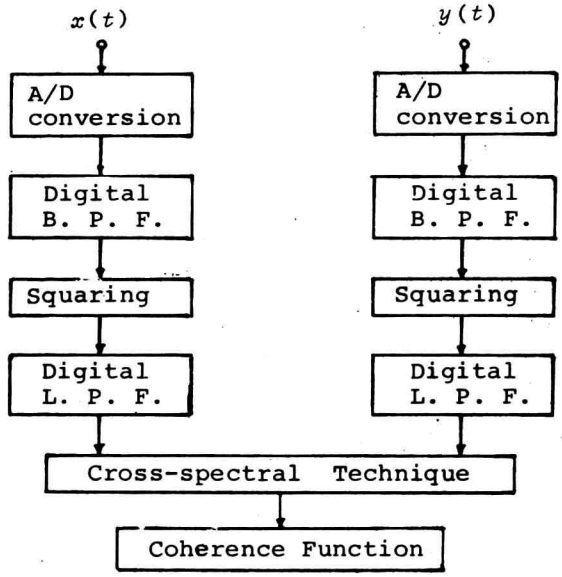

Fig. 3 Block diagram of the all-digital processing to obtain the coherence function between the envelopes of $x(t)$ and $y(t)$.

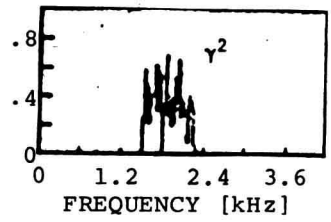

Fig. 4
The coherence function between the band-passed signals.

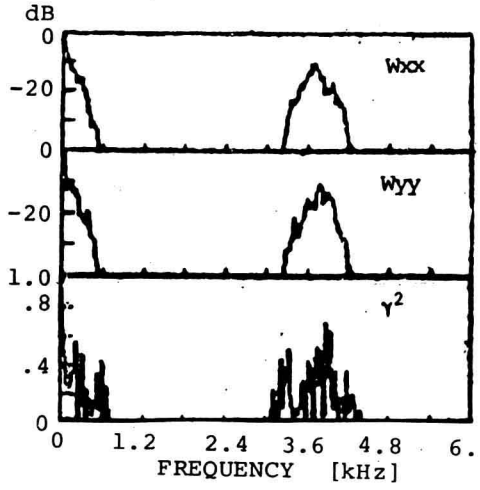

Fig. 5
The power spectra and the coherence function of the squared band-passed signals.

3. USE OF THE ENVELOPES OF BAND LIMITED SIGNAL

We propose, here, the use of the envelopes of band limited signal which is hardly affected by the fluctuation in the transmission time. Fig.3 shows the block diagram of the processing in the first experiment, where the digital processing only is adopted. The signals $x(t)$ and $y(t)$ are sampled at the rate of 12kHz and A/D converted. And the sequences are band limited to the frequencies between 1500Hz and 2250Hz passing through the digital band pass filters. Fig.4 shows the coherence function of the band limited signals which is the same as the part of the corresponding frequency of Fig.2 (c) in principle. And the band limited signals are squared. Fig.5 shows the power spectra (Wxx and Wyy) and the coherence function γ^2 of the squared signals which are composed of the low frequency components and the double frequency components. The spectra of the band limited signals are the same as the low frequency components shown in the top and the middle of Fig.5. And the envelope of the band limited signal is obtained discarding high frequency component by the low pass filtering. The examples of the wave forms of the squared band limited signal and the low passed signal (envelope) are shown in Fig.6.

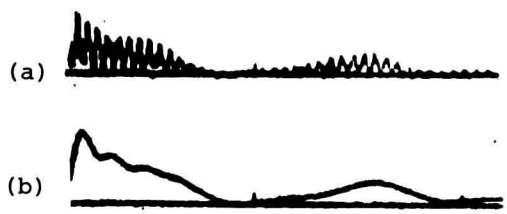

Fig. 6
(a) Example of the wave form of the squared band-passed signal.
(b) Envelope of wave form (a) obtained passing through low pass filter.

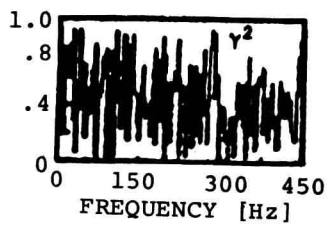

Fig. 7
Coherence function between band-passed $x(t)$ and $y(t)$.

Then, the sampling rate is reduced to 1200Hz and the coherence function between the envelopes is computed. Fig.7 shows the coherence function between the envelopes of the band limited signals which is bigger than the coherence functions shown in

Fig.4 and 5 in the magnitude.

This result will show the effectiveness of the use of the envelopes of the band limited signals. But the method described in the preceedings uses digital processing only, and we have to proceed to simper and more practical method.

4. USE OF ANALOGUE TECHNIQUE IN THE EXTRACTION OF ENVELOPES OF BAND-LIMITED SIGNAL.

Analogue technique is utilized in the extraction of the envelopes of band limited signal. Fig.8 shows the block diagram of the processing utilizing analogue technique before the computation of coherence function. That is, the band pass filter, rectifier and smoother are analogue. The number of computation and the number of data are largely reduced compared with the all digital method shown in Fig.3. After the A/D conversion, the DC components are removed, which show sometimes big value in the cross spectra and deteriorate the accuracy in the computation.

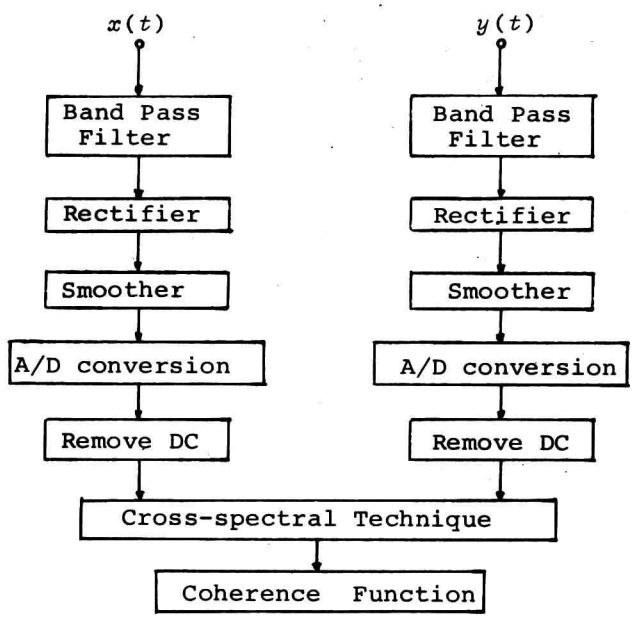

Fig. 8 Block diagram of the processing utilizing analogue technique before the computation of coherence function.

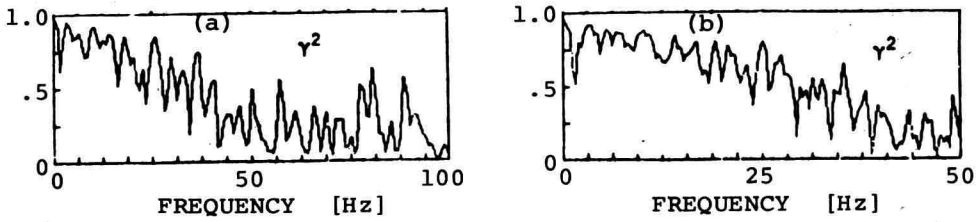

Fig. 9 Coherence function between the envelopes of waves.
(a) : time constant of smoother is 10 ms.
(b) : time constant of smoother is 56 ms.

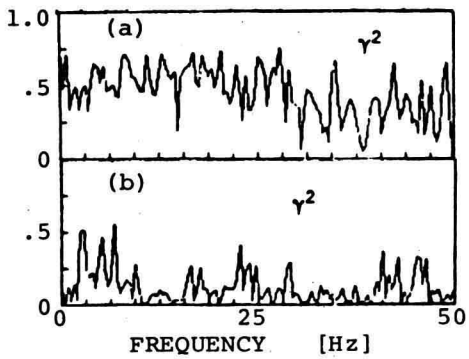

Fig. 10
Coherence functions between the mixed noise and each of noise sources.
(a) : between mixed noise and noise of hand drill.
(b) : between mixed noise and exaust noise.

The time constant of the smoother was investigated using coherence function. Fig.9 shows the coherence functions obtained using two kinds of time constant. The time constant for (a) is 10ms. and that for (b) is 56ms. From such results, it is anticipated that the low frequency components in the envelopes will be useful for the noise source identification.

An experiment was carried out using two noise sources, one is an electric powered hand drill and the other is exhaust noise of an automobil engine. The time constant of the smoother is 56ms. Fig.10 shows the obtained coherence functions between the mixed noise and the noise of the electric powered hand drill and the exhaust noise. In principle, the sum of the coherence functions should be 1.0 unless there are any other noise. The sum is about 0.8 to 0.9 in this example. The result may indicate that the contribution factor of the noise source can be estimated using the coherence function of the envelopes of the band limited signals. Of cource, the estimation includes considerable error, but the error is much less than the error in the estimation using the coherence function between the wave forms when the observing point is not close to the source in the open air.

5. CONCLUSION

A method of noise source identification using the coherence function of the envelopes of band-passed sound picked up at the observing point and the point of noise source has been described. This method cannot give as accurate result as the conventional cross-spectral technique in a still environment as in an anechoic chamber. But, in the actual case of noise control, there is no natural transmission path having no turbulence in the air, and the fluctuations in the transmission time is inevitable. And, in those the actual cases, the method using the envelopes of the band-passed sound is much superior than the conventional cross spectral technique.

We are now developing an extended method using multichannel band pass filter banks. The results will be reported in the near future.

The authors would like to thank Dr. Yoichi Takebeyashi for his valuable discussion and assistance.

NOISE AND SURFACE VELOCITY STUDIES ON A 600 kN PUNCH PRESS

E.C. SEMPLE
University of Adelaide,
Adelaide, South Australia.

R.E.I. HALL
University of Adelaide,
Adelaide, South Australia.

INTRODUCTION

The noise generated by punch presses has been the subject of a number of investigations.[1,2,3,4,5,6] Much of this work has involved making measurements of sound levels at a point in front of the machine corresponding approximately to the positions of the operator. Variations in peak sound power level, or occasionally L_{eq}, have been recorded for different operating conditions, the parameters altered including tool size, tool contact velocity, tool shear, feedstock material and feedstock thickness: in virtually all these investigations a simple punching or blanking operation was involved. Measurements have also been made to study the effectiveness of partial enclosures,[3] and to examine methods by which air noise from ejectors[6] etc. can be reduced.

Such measurements give the integrated noise from the machine but little has been published to provide details concerning which parts of the machine radiate the most noise, and in particular the order of their significance. Large sheet metal components on presses - the flywheel cover is commonly in this category - have been identified as important sources of noise. Herbert,[4] in examining a 1000 kN press, concluded that the sideframe, baseplate and top brace were likely to be the dominant contributors to the noise emitted by the machine. Using multiple coherence methods, Koss[5] examined the noise emitted by a 30 kN press and related this to accelerometer outputs at three points on the structure and one on the support plate for the machine. Those on the structure were adjacent to the crankshaft at the top of the machine, on the ram near the punch, and on base plate: each was mounted at the front of the press in a central position. These points were chosen because a preliminary examination had shown high excitation in these regions and the aim of the experiment was to relate the spectral content of the measured noise to the spectrum of the surface acceleration at points likely to be major sources of this noise.

What has not been available is an extensive study of a press which provides a

detailed picture of the power available in the normal surface motion. Modified by an appropriate radiation efficiency, it is this power which would be translated into radiated acoustic power. This paper reports a study of surface intensity performed on a 600 kN punch press. Extensive measurements of the surface velocity were made - approximately 80 positions on the machine being considered. The aim of the experiment was

a. to obtain at these positions the mean intensity of the surface vibration from the integrated square of the normal surface velocity averaged over the cycle time of the press;
b. to present this data as an intensity map of the machine;
c. to attempt to relate results to the physical characteristics of the machine;
d. to examine broadly how the power spectral density of these intensities varies from one part of the machine to another;

and

e. to relate all this to the measured emitted noise.

METHOD OF MEASURING SURFACE VELOCITIES AND CALCULATING SURFACE INTENSITIES

The punch press used in the investigation is illustrated in Figs. 1(a) and 1(b). It is a second-hand Heine 206A Series 3 600 kN machine specially obtained for punch-press noise investigation. Its exact age is unknown, but it was extensively refurbished about 18 months before purchase and, on an admittedly subjective assessment, can be described as being in good condition: wear on the slides and bearings is minimal though wear in the clutch mechanism is evident from some variability in its noise output between one stroke and another.

As will be seen from the pictures it is a C-frame press. The structure is made from cast iron and the side frames together with the inter-connecting structure are typically about 30 mm thick. Metal thicknesses in the vicinity of the throat, ram and baseplate are about 150 mm. The flywheel is engaged with a dog-clutch and, as is common, this operation is a conspicuous source of noise distinct from that generated by the action of the tool. A typical noise profile for the tool is shown in Fig. 2, the first major peak being caused by the dog-clutch, the second by the tool. The speed of the press is 100 strokes per minute; the stroke length is 90 mm.

For tests the machine was fitted with an industrial tool which produces the pattern of performations shown in Fig. 3 using 36 6.35 mm diameter punches. No shear was applied to the tool. 1 mm thick mild steel strip was used as a feedstock and was put into the machine manually before each test stroke.

Tool clearance is about 10% and the press loading is approximately 300 kN. To obtain the surface intensity at each point sampled on the machine (see Fig. 6 for distribution) a comprehensive measurement of surface velocity was necessary. Velocity measurements were made using a B & K Type 4330 accelermeter in conjunction with a B & K Type 2202 sound level meter operated with an integrator in velocity measuring mode. With this instrument the simplest measurement to make is that of peak velocity using the 'peak hold' facility. But for the present investigation this was considered inadequate, and the velocity/time profile was also recorded for further processing using a TEAC PC-10 tape recorder. The velocity was recorded both directly and also through an A-weighted filter - these A-weighted records being the ones used to produce the data in this paper.

The mean A-weighted acoustic power radiated by a surface on the machine due to a transient event may be defined as

$$L_w\,(A) = 10 \log_{10} \left[\frac{\rho_o\, c\, S\, \sigma}{10^{-12}\, T} \int_{t_1}^{t_2} \langle v \rangle_A^2 \, dt \right] \quad dB \qquad (1)$$

re 10^{-12} watts

where $\rho_o\, c$ = the characteristic impedance of air

S = the area of the surface

σ = the radiation efficiency of the surface

$\langle v \rangle_A$ = the mean A-weighted normal velocity of the surface

T = the stroke period of the press

t_1 and t_2 = time within the stroke period $t \rightarrow t + T$ covering the transient event of interest

If $t_1 = t$ and $t_2 = t + T$, the noise associated with the entire press cycle will be included; however, if t_1 and t_2 cover specific shorter intervals, the radiated power associated with the clutch or the tool impact may be calculated separately. For the purposes of this paper, surface intensity at a point will be defined as

$$I = 10 \log_{10} \left[\frac{\rho_o\, c}{10^{-12}\, T} \int_{t_1}^{t_2} v_A^2 \, dt \right] \quad dB \qquad (2)$$

where v_A = the A-weighted surface velocity at that point. The interval $t_1 \rightarrow t_2$

will cover either the clutch transient or the tool transient.

DATA PROCESSING METHOD

To calculate I at each point, the recorded A-weighted velocity was digitised and processed on a PDP 11/34 computer.

Obtaining a digitised record of one stroke of the press presented some problems since the analog records were unequally spaced on the magnetic tape. To achieve adequate resolution, the analog tape needed to be sampled at 50 μs intervals and only about 20k of core store could be allocated to data storage, consequently the digitised record could be only 1s long. Since the exact position of the recorded transient on the analog tape was not known with great accuracy, it was not possible to start the A/D conversion process at a sufficiently precise time to ensure that the whole of the transient sequence - including both clutch and tool transients - would be contained within the following 1s. To start the A/D conversion process with a trigger from the leading edge of the first transient would eliminate from the digitised record any precursor, or build up in the transient.

This problem was overcome with the arrangement shown in Figure 4. A/D conversion of the record was started manually on a clear piece of tape a few seconds in front of the clutch transient. After 1s the 20k locations in the core store would be full, but A/D conversion continued by overwriting these locations again from the beginning. When the transient was encountered, A/D conversion continued, but the analog signal was used to initiate a delayed trigger from box A. The delay box could retard the leading edge trigger by a variable time interval and this output signal, when it appeared, was used to initiate an interrupt on the computer which halted the A/D conversion process. By setting the delay to (say) 0.7s, the record would run from 0.3s before the clutch transient to 0.7s after this transient - a range that comfortably included the tool transient as well. Software unwrapped the record so that finally the velocity data was stored in a continuous time sequence across the 20k of core store. The system is similar to that employed in digital oscilloscopes to provide "preview" of a transient.

Subsequent processing of each file of velocity data provided plots of $\int v_A^2 \, dt$ plus values for I (equation 2), and L_w (equation 1) with $\sigma = 1$ and S a representative local area. This could be done across the whole record or on the clutch and tool transient separately. Another programme was written to obtain information on the power spectral density of the transient data.

RESULTS

The form of the build-up in integral squared velocity (proportional to integral surface energy) is shown in Fig. 5(a) for a point in the middle of the side-frame. The curve starts with a precursor to the main clutch transient due to the movement of the dog against the flywheel to await the arrival of the dog slot. When the dog engages, the main clutch impact occurs and the structure rings so that an exponential build-up is observed. This is followed by a similar rise due to the tool transient. As is typical for the rest of the machine, the integral squared velocity due to the clutch transient is little different from that due to the tool - a fortuitous situation resulting from the size of the tool chosen for the experiment.

Only in a few special circumstances do the relative amplitudes differ substantially. Measurements on the flywheel (Fig. 5(b)) show that the clutch makes the dominant contribution in this case, while on the ram (Fig. 5(c)) it is the tool impact that is the more important. In each case the adjacence of the impacting source makes the results unsurprising. Other points close to the impact areas also show a weighting in response towards the local source but this is less marked for points on the main structure (see the bedplate in Fig. 5(d)), and the effect diminishes rapidly with distance from the source. In the cases of the flywheel and ram, it appears that their isolation from the remote source is significantly dependent on the fact that they are moving parts - energy transmission through the bearing or slide being poor.

Figures 6(a) to 6(f) give a map of the surface intensities measured; the lower figures correspond to the effect of the tool, the upper figures to that of the clutch. In examining this data the problem is to distil some general observations. High intensities are observed on the flywheel cover and in the vicinity of the tool as expected, but it is apparent that substantial intensities occur also on the foot castings. The general intensity distribution on the main frame of the machine is only 5 to 10 dB less than that observed in these high intensity areas, and truly low intensities are confined to areas on or near the thick cast material at the throat of the press.

The total intensity obtained at any point appears to be dependent on a number of factors, the following being identified as the more important:-

a. Proximity to the impact source is clearly important since machine strain and jerk are at their maximum in these areas. Such positions are characterised by a very rapid rise in the energy curve. This is illustrated in

in Figs. 5(c) and 5(d) where the sharp rise on the ram and bedplate associated with the tool impact may be seen: the more distant impulse due to the clutch produces in each case a sluggish rise.

b. Low material damping causes a substantial build-up in energy due to ringing effects. This is seen most conspicuously on the flywheel cover (Fig. 7(a)) where the ringing from the clutch impact is still significant at the start of the tool impact.

c. With the high internal damping of cast iron, it would be expected that little ringing would be observed on the main frame of the press. While this is often the case, as in Fig. 5(d), the slow exponential rise in the curve associated with ringing is none-the-less more noticable than might be expected in some areas. Figure 6(c) shows the energy buildup at a point on the side frame of the press, and Figs. 6(b) and 6(d) show the same for points on the foot castings. In the latter cases particularly, a remarkably extended buildup may be seen. To some extent this may be attributed to the thin plate-like structures involved - away from stiffeners the foot castings are only about 8 mm thick - but the extended excitation appears also to be due to coupling with the fundamental modes of vibration in the machine which are relatively slow to die away.

In consequence of all this, it is found that there is no simple relationship between peak velocity, as measured with the 'peak hold' facility on the sound level meter, and computed intensity. Figure 8 indicates the wide range of points observed when intensity and peak velocity are plotted against each other. Points on the graph associated with particular areas do, however, tend to be clustered as indicated.

Although quite high intensities have been measured over extensive areas of the machine, it is necessary to examine the variation of power content with frequency to decide on the significance of the results from a noise point of view. Figure 9(a) shows the form of the emitted noise power spectrum up to about 8 kHz, the microphone position being 1 metre from the tool. Figures 9(b) - 9(d) show the form of the velocity power spectrum at a few points on the structure. What is conspicuous from these spectral curves is that the surface intensities on the machine relate mainly to low frequencies which radiate poorly. Figure 9(b) relates to a point on the sideframe and is typical of most points on the main structure: virtually all the power can be seen to be at frequencies below 1 kHz, and in a number of other cases it is well below this. The only records which show any substantial high frequency content are those for the flywheel and the

vicinity of the front of the press. This weighting towards the low frequency end of the spectrum has occurred despite the fact that the velocity signals were fed through an A-weighted filter before recording. The fundamental frequency of the frame can be seen at around 400 Hz in the noise spectrum, and this frequency is conspicuous in the velocity spectrum at all points on the frame: other peaks in this vicinity are associated with frame modes. The broad peak below 2 kHz, and possibly the similar peak above this frequency, appear to be associated with the motion of the front parts of the press near the tool. The flywheel also appears to be a significant contributor above 1 kHz.

A more detailed analysis than this is frustrated at present by the large low frequency content in many of the records. This has led to difficulties in calculating realistic radiation efficiencies, and to inadequacies in the dynamic range of some records.

CONCLUSIONS

The experiments have provided a good insight into the energy flow and surface intensity distribution on the structure of the press during operation. The considerable bias of the velocity power spectrum towards low frequencies despite the use of an A-weighted filter exceeded expectations, and there is need for a somewhat different experimental technique to overcome the difficulties arising from this.

At this stage it it proposed to repeat the measurements using a variable high pass filter to simulate the effect of radiation efficiency. With this it should be practicable to produce surface intensity values relating more directly to radiated noise intensities: the magnitude of the recorded data at high frequencies should also be improved.

ACKNOWLEDGEMENTS

The authors are indebted to Mr. R. Curtin for his assistance in preparing programmes for the digitisation of the experimental data.

This continuing work on punch press is supported by a grant from the South Australian Department of Industrial Affairs and Employment.

REFERENCES

1. STEWART N.D., BAILEY J.R., and DAGGERHART J.A., 'Experimental Investigation of Noise Control for a 60 Ton Power Press' Internal Report: Center

for Acoustical Studies North Carolina State University, Raleigh N.C.

2. KOSS L.L., 'Punch Press Load-Radiation Characteristics' Noise Control Engineering Vol. 8 (1) Jan-Feb 1977.

3. ALLEN C.H. and ISON R.C., 'A Practical Approach to Punch Press Quieting' Vol. 3 (1) July-August 1974.

4. HERBERT A.G., 'Noise and Vibration on a 100 Ton Press' Internal Report: Institute of Sound and Vibration Research Southampton University.

5. KOSS L.L. and ALFREDSON R.J., 'Identification of Transient Sound Sources on a Punch Press', Journal of Sound and Vibration (1974) Vol. 34 (1), p 11 - 33.

6. SAHLIN S and Longhe R., 'Origin of Punch Press and Air Nozzle Noise' Noise Control Engineering Vol. 3 (3) Nov-Dec 1974.

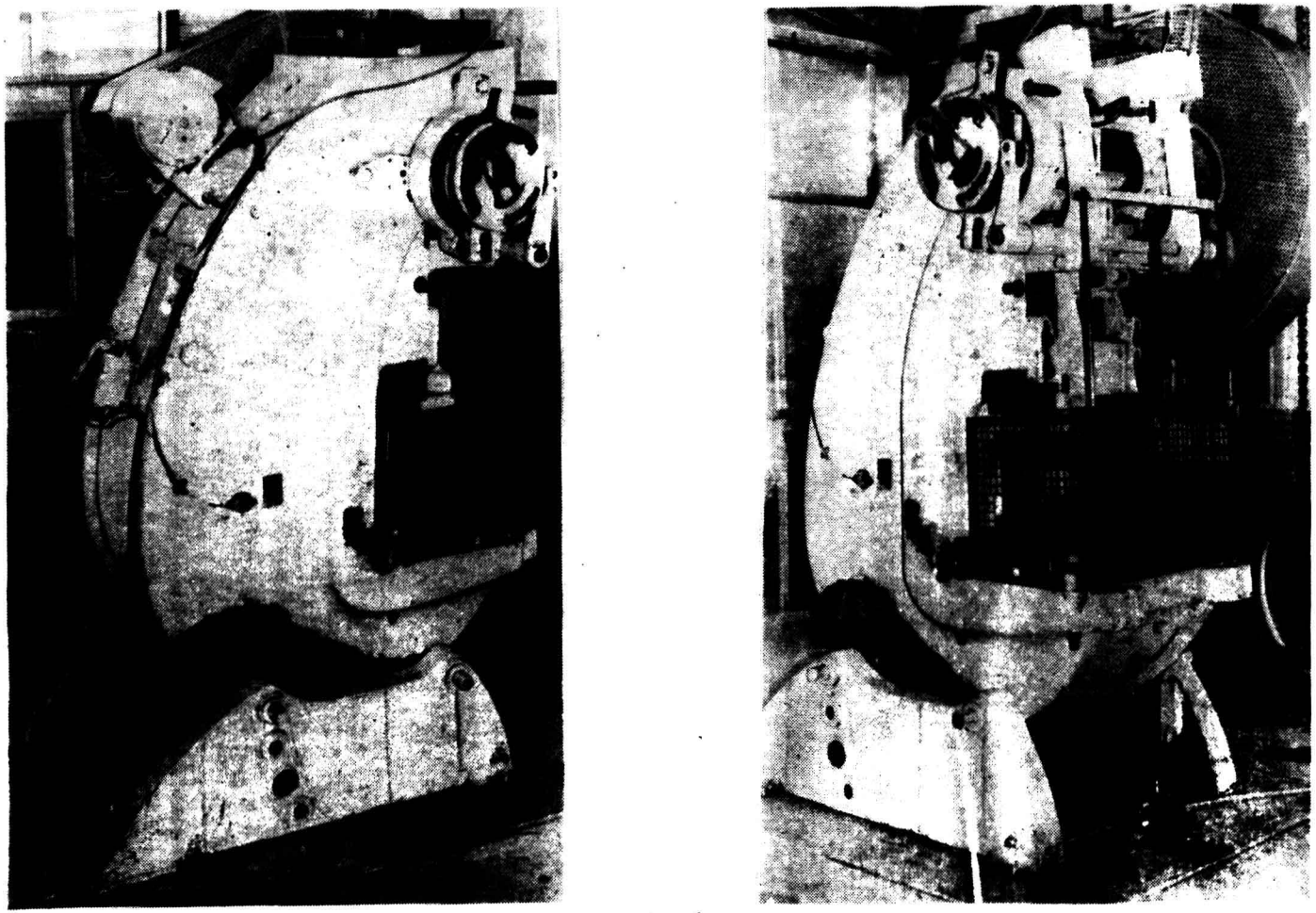

FIG. 1. HEINE 206A SERIES 3 600 kN PRESS USED IN TESTS.

FIG. 2. TYPICAL SOUND PRESSURE VERSUS TIME RECORD FOR PRESS SHOWING TRANSIENT ASSOCIATED WITH THE CLUTCH AND THE TOOL ($L_{eq} \doteqdot 105$ dB AT 1M FROM TOOL).

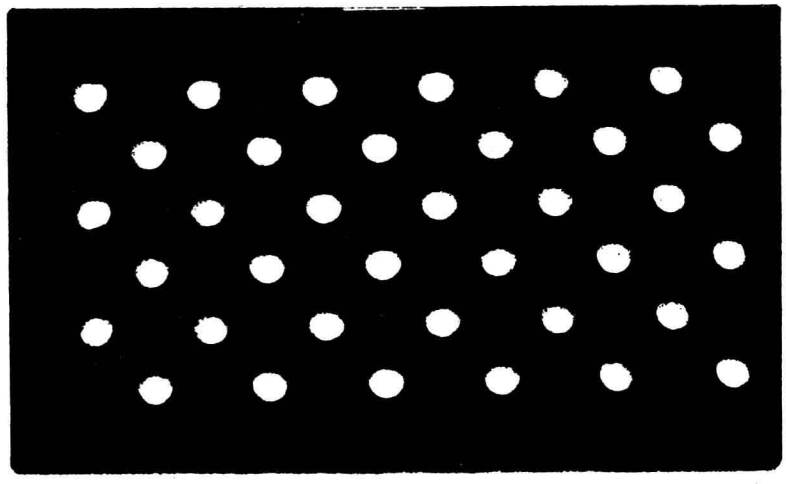

FIG. 3. PERFORATION PATTERN PRODUCED BY TEST TOOL USED IN PRESS FOR THESE TESTS.

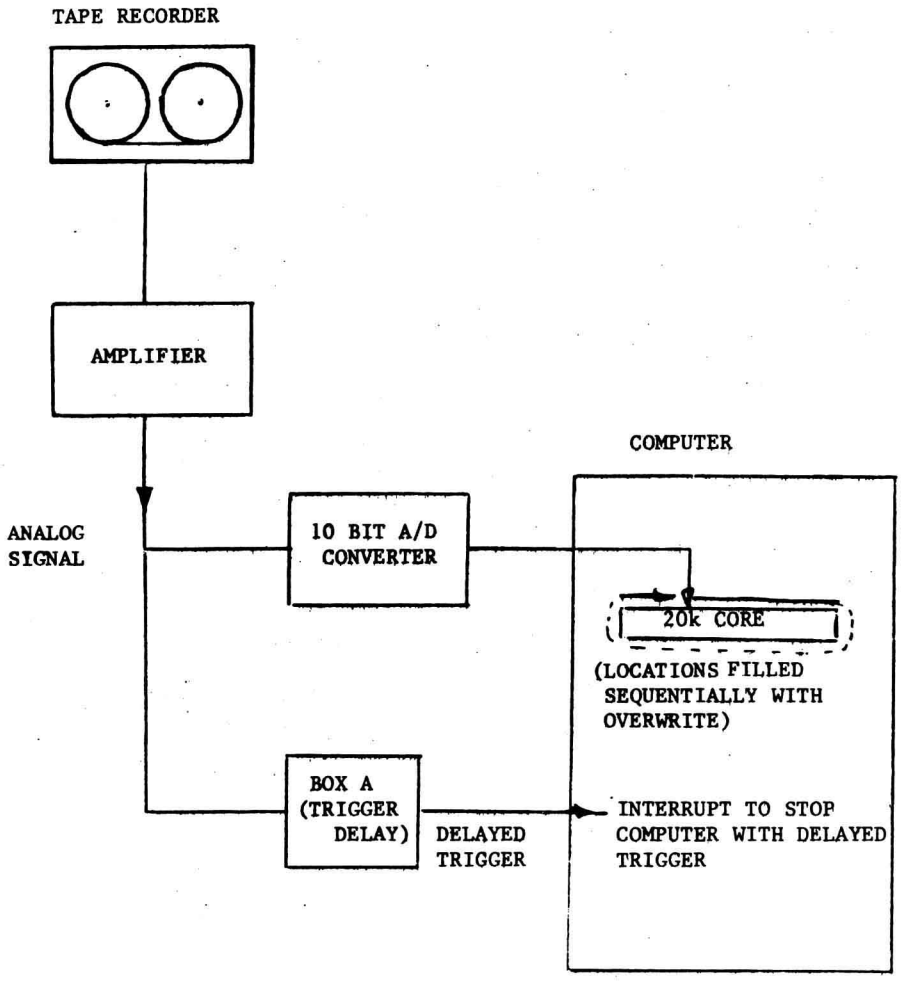

FIG. 4. ARRANGEMENT FOR DIGITISING AND RECORDING TRANSIENT DATA.

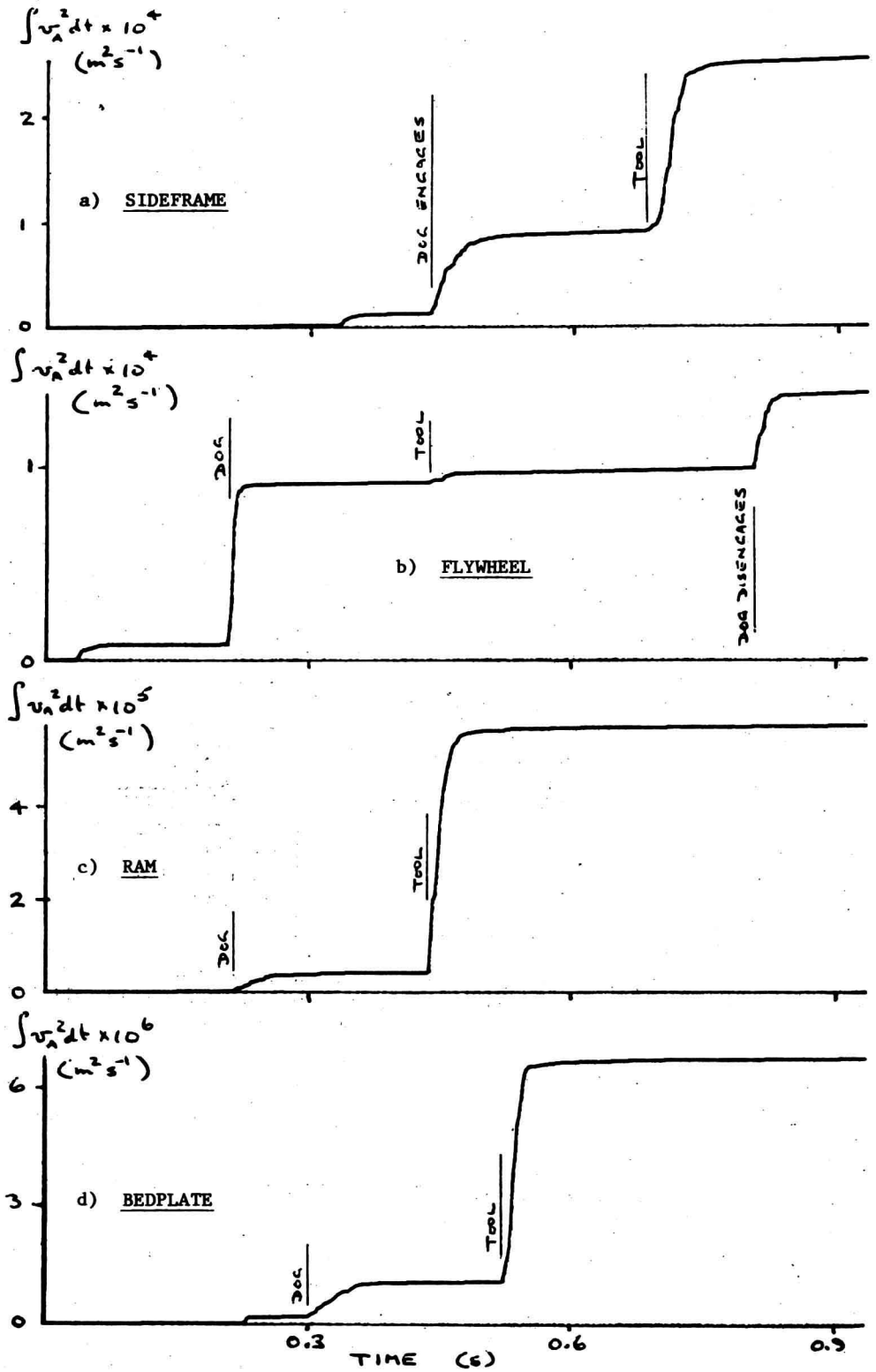

FIG. 5. PLOTS OF INTEGRAL SURFACE VELOCITY SQUARED VERSUS TIME SHOWING THE DIFFERING INFLUENCE OF CLUTCH AND TOOL IMPACTS AT VARIOUS POINTS ON THE PRESS.

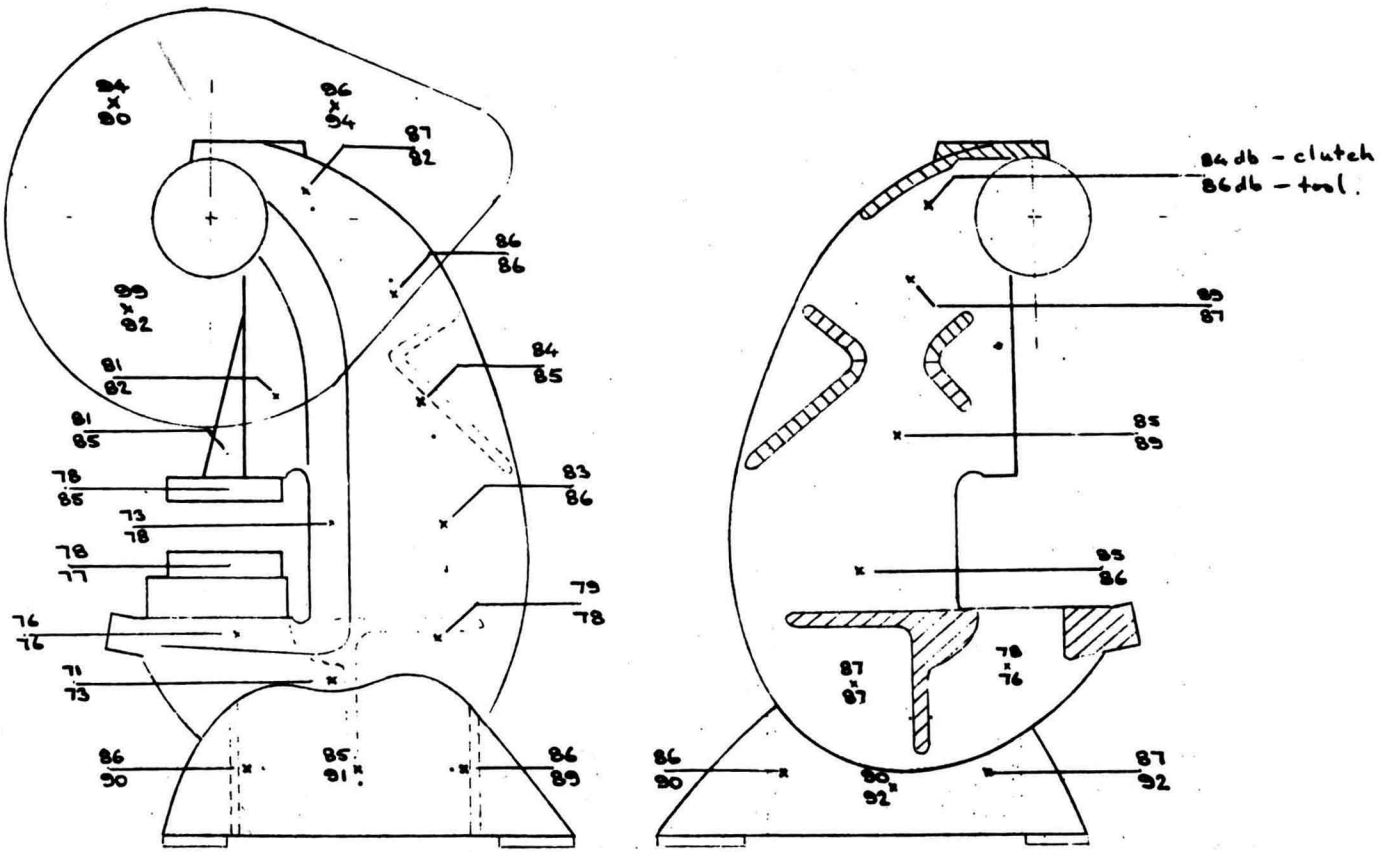

(a) OUTSIDE (b) INSIDE

FIG. 6(A) & 6(b) SURFACE ITENSITIES ON RIGHT SIDE OF PRESS

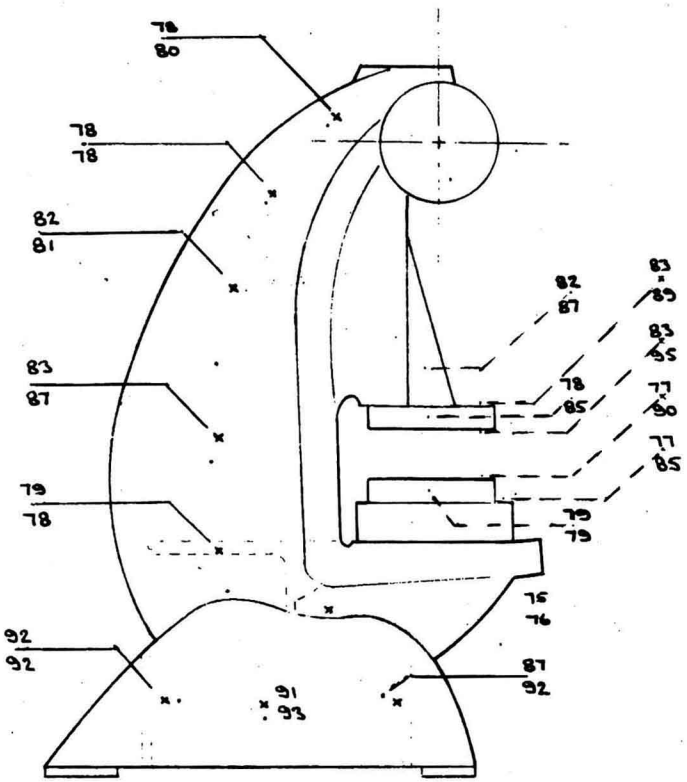

(c) OUTSIDE

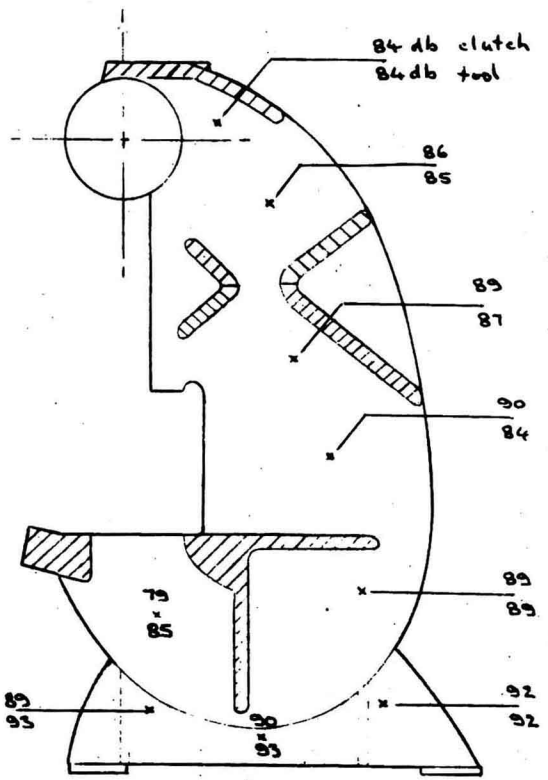

(d) INSIDE

FIG. 6(c) & 6(d) SURFACE INTENSITIES ON LEFT SIDE OF PRESS

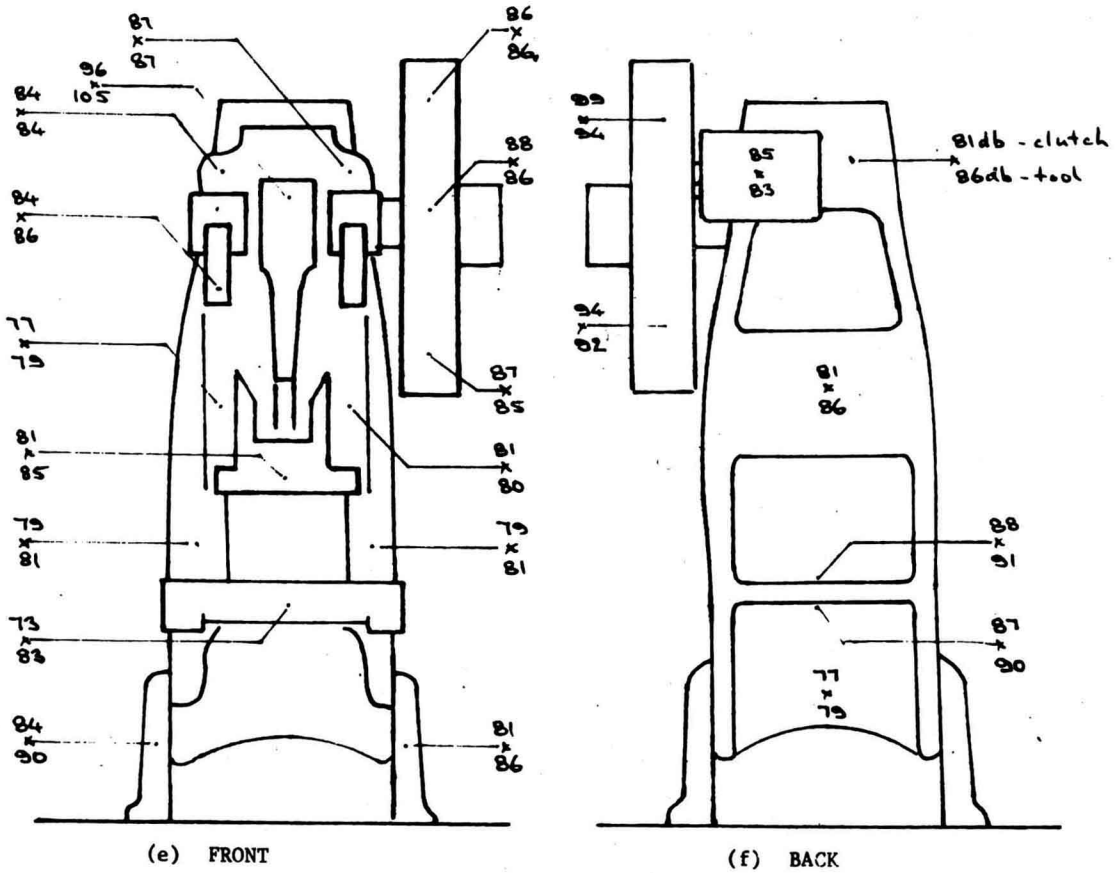

(e) FRONT (f) BACK

FIG.6 (e) & (f) SURFACE INTENSITIES ON BACK & FRONT OF PRESS

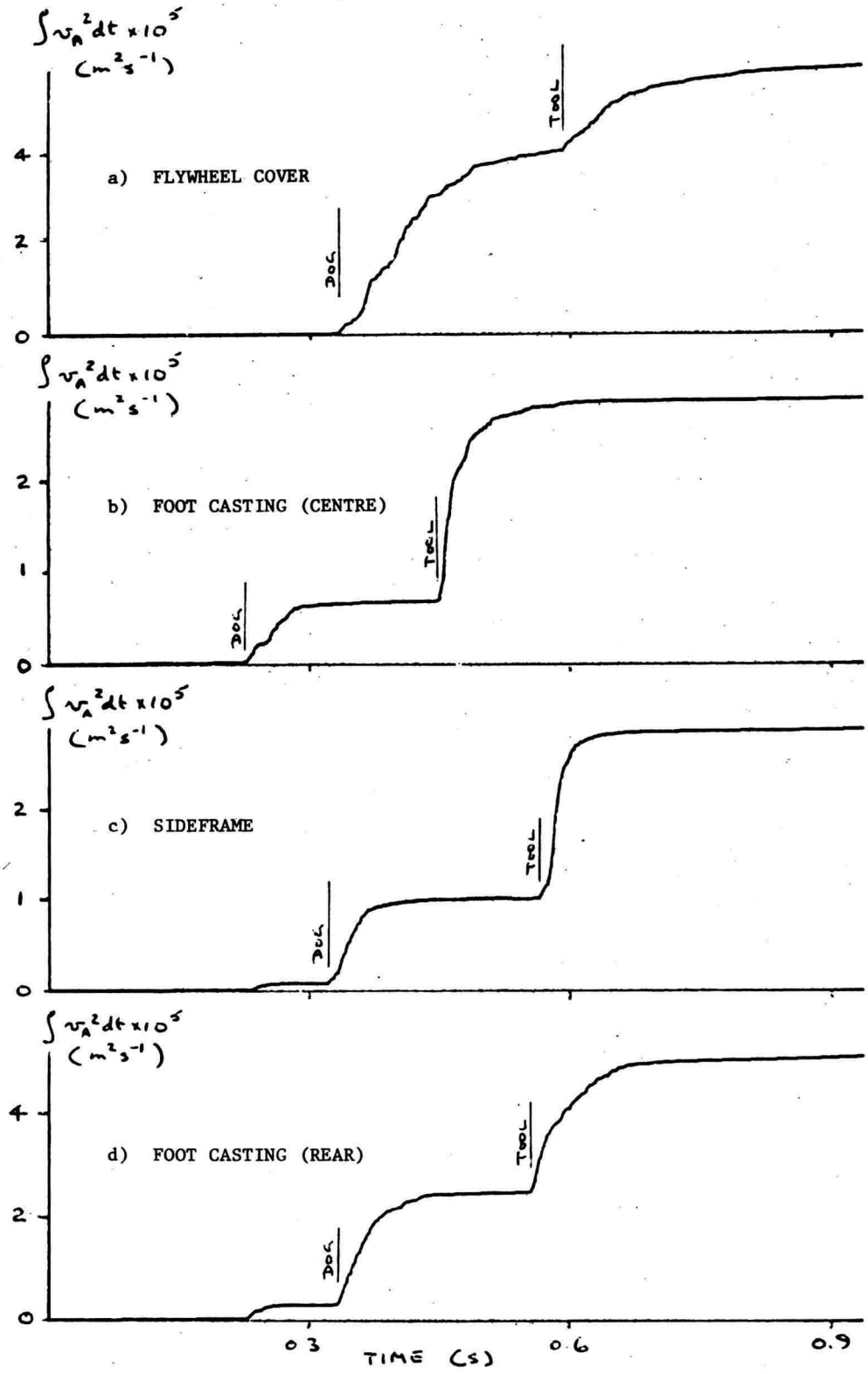

FIG. 7. PLOTS OF INTEGRAL SURFACE VELOCITY SQUARED VERSUS TIME SHOWING RINGING CHARACTERISTICS OF VARIOUS PARTS OF PRESS.

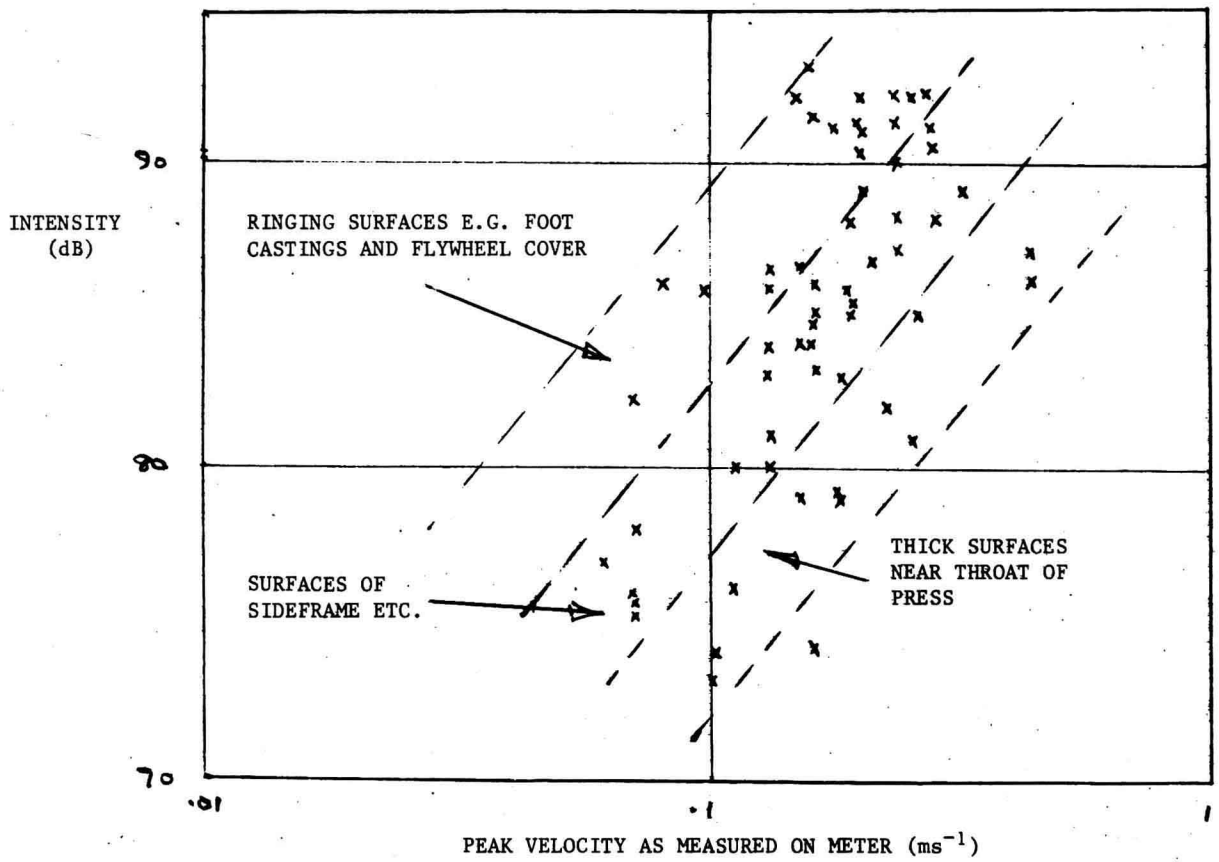

FIG. 8. PLOT OF INTENSITY VERSUS PEAK VELOCITY FOR VARIOUS PARTS OF PRESS SHOWING VARIABILITY OF INTENSITY WITH DAMPING AND MODAL COUPLING.

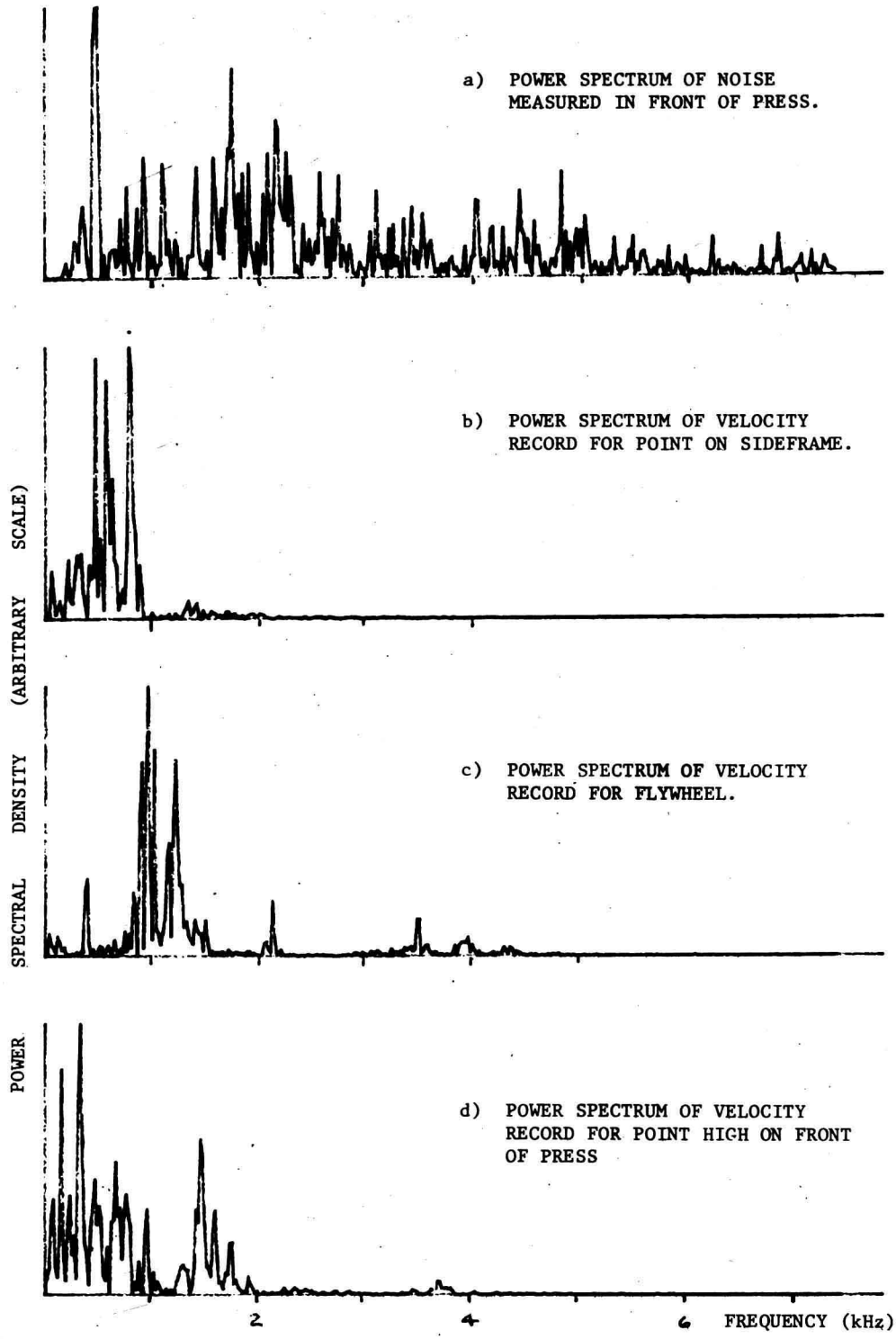

FIG. 9. POWER SPECTRA OF PRESS NOISE AND VELOCITY RECORDS AT VARIOUS POINTS.

THE DYNAMICS OF VEHICLE RESPONSE VIA IMPEDANCE MEASUREMENTS AND FINITE ELEMENT MODELING

D. C. RENNISON

Bolt Beranek and Newman Inc.
P.O. Box 633
Canoga Park, California USA 91305

and

H. BRAUN

Foster Engineering Company
23241 Ventura Boulevard
Woodland Hills, California USA 91364

ABSTRACT

The initial stages of a measurement and modeling program, being conducted with the aim of determining practical modifications to the hull structure of a tracked armored personnel carrier for the purpose of reduction of crew interior noise levels, is presented. A strong directionality in the low frequency invertance functions measured at the idler attachment function is predicted with fair accuracy using a simple finite-element model of the hull structure. The approach promises to allow the conceptual testing and refinement of hull design changes proposed for noise control purposes.

INTRODUCTION

The noise levels inside tracked armored personnel carriers are in the range 115 to 125 dBA, being dependent on vehicle speed and type. Example interior noise spectra are shown in Fig. 1. For the M113 class of vehicles of present concern, these levels result from the impact of the track shoes on drive and suspension elements, in particular and in order of decreasing contributions, the idler mechanism, the drive sprocket and the vehicle roadwheels. The vibrational energy imparted to the hull attachment points feeds into the structure and radiates into the crew compartment. By careful design, the input forces to the attachment points on the hull structure can be reduced (by isolation) by amounts varying between 10 and 15 dB over the critical frequency range 100 to 1000 Hz. However to achieve further noise reductions down to a goal of say 100 dBA, the noise isolation characteristics of the hull structure must be increased. For this, an understanding of the mechanical impedances of the various hull attachment points to the applied forces is of prime importance. This paper reports a measurement and modeling program focused on the idler attachment point of an M113A1 vehicle. Detailed measurements of the idler inertance, defined as the transfer function between acceleration response and force input, both measured at the excitation point (idler), have been made. The influence of small differences in hull

geometry and on excitation direction on these measurements are reviewed by comparison with analytical results produced with a simple finite element model for the hull structure to demonstrate the potential of this modeling technique in investigating the effects of structural design modifications on vehicle vibration response and interior noise levels.

HULL STRUCTURE

Figure 2 presents side and hull section views of the M113A1 hull structure: the side view has been shortened to about two-thirds the actual length. The drive mechanism is located at the left hand forward end of the vehicle and the idler is at the rear end. The hull section view illustrates the essential bilateral symmetry of the hull structure. The aluminum box-shaped hull is composed of thick large plates, the only cross stiffening members being located in the plane of the vehicle floor and at front and rear of the vehicle. Stiff box beams run the length of both sides of the vehicles, and the drive sprocket, roadwheels and idler are attached to these. There are small differences in axial location of the idler spindles on left and right sides of the vehicles due to roadarm suspension requirements. Alignment of the left-side idler pad with the vehicle rear wall and the box beam is shown in Fig. 3. Such small mounting details are important to the local flexibility of the idler attachment points and are reflected in the idler transfer function measurements and calculations as discussed later.

TRANSFER FUNCTION ANALYSIS

Preliminary to developing a model for predicting the vibration response of and noise levels inside the hull structure, detailed noise and vibration measurements were made and some simple power flow analyses performed in an attempt to quantify the contribution of each major structural element to the underway interior noise level. Using measured panel vibration levels and statistical energy methods and assuming the radiation to be controlled by resonant modes of the various structural elements, the floor, roof and rear walls are predicted to contribute approximately equally to the interior noise level, and a fair prediction of the measured noise spectrum can be made, as seen in Fig. 4.

The agreement at lower frequencies (below 250 Hz) is considered fortuitous, since at these frequencies where the structural wavelengths are $\simeq$ equal to vehicle dimensions, a statistical description of the structure is invalid: the power flow from attachment points to hull structure tends to be stiffness-

controlled except at the frequencies of resonant modes of the (complete) hull. This transition from stiffness-controlled to resonance-controlled power flow as frequency increases is indicated in measurements of the idler attachment point inertances. Figure 5 shows a sketch of the experimental configuration and instrumentation used for inertance and transfer function measurements. Inertance is defined as the transfer function between acceleration output and force input viz.

$$H(j\omega) = a(j\omega)/F(j\omega) = (|a|/|F|)e^{j\phi}$$

so that $|H(j\omega)| = |a|/|F|$ is the inertance magnitude and $\phi(j\omega)$ is the inertance phase angle (the phase angle between acceleration and force).

Figures 6 and 7 show representative inertance functions for left- and right-side M113A1 idler spindles for excitation in horizontal and vertical directions respectively. Considering Fig. 6, the inertance magnitude and phase angles for horizontal force input are broadly similar: at low frequency, the inertance magnitude increases sharply with frequency and the phase angles are close to zero, characteristic of a stiffness-controlled system, but as frequency increases above 300 Hz, the phase angle decreases as the power flow becomes resonance controlled. The vertical idler inertances on left and right sides are shown in Fig. 7, where notable deviations from a stiffness-controlled response occurs at low frequencies, shown clearly in the phase data as sharp decreases in phase angle. Strong coupling between a vertical idler force and low frequency vibration modes apparently occurs. At higher frequencies, the phase varies continuously as the power flow is determined by resonant structural modes. Figure 8 shows a comparison of horizontal and vertical inertances on the left idler spindle at low frequencies: vertical idler forces couple effectively to resonant structural modes while a stiffness-controlled response is produced for horizontal idler forces.

FINITE ELEMENT MODEL

A relatively simple finite element representation for the M113A1 hull structures has been developed. Beam and plate elements with six degrees of freedom at 195 connecting nodes were used. Doors and hatches were represented by a set of equivalent point masses distributed along joint boundaries, and the box beam was represented as a series of beam elements. In the model, the

bilateral symmetry of the hull was used to reduce the model matrix size, with centerline boundary conditions being adjusted appropriately to generate symmetric and anti-symmetric modes. Figure 9 shows nodal locations in the structural model. The local stiffness characteristics of the idler spindle were accounted for by means of matrix alterations using the results of a separate static analysis, with the spindle stiffness being represented in the final model by an equivalent beam at the idler position. Figure 10 shows results from the idler static analysis of the flexibilities in the vertical and horizontal directions: it is clear that the horizontal and vertical axes are not the principal axes of the hull and that the inclined rear plate couples in-plane forces to out-of-plane deflections.

The STARDYNE computer library program has been used for dynamic response calculations. Structural loss factors required as input data were determined from octave band 'response-decay' measurements using instrumentation similar to that in Fig. 5. Representative hull mode shapes are shown in Figs. 11 and 12; Fig. 11 corresponds to a low frequency symmetric mode in which roof, sidewalls and floor are all strongly coupled while Fig. 12 shows the shape of the third 'panel' mode of the roof. Approximately 60 vibration modes exist below 250 Hz. Comparison between computed inertance function and the measured results from Fig. 8 are presented in Fig. 13. This initial comparison is considered to be fair in that the general relationship between computed horizontal and vertical inertance function is similar to that shown in the measured data. Differences of about 10 dB exist between computed and measured curves in the range 50 to 120 Hz, corresponding to significant errors in the representation for the vehicle mass or stiffness properties. Further effort is required to improve the model, after which model structure changes such as large variations in local idler attachment flexibility, will be made to reduce the inertance functions in both directions (and the associated interior noise levels) by up to 10 dB and arrive at practical hull modifications without extensive testing.

ACKNOWLEDGEMENTS:

This work was conducted for FMC Corporation, San Jose, California, as part of a continuing program funded by the U.S. Army Human Engineering Laboratories, Maryland. The authors wish to express their appreciation to Mr. Georges Garinther (HEL) and Mr. Steve Hammond (FMC), technical monitors in the program.

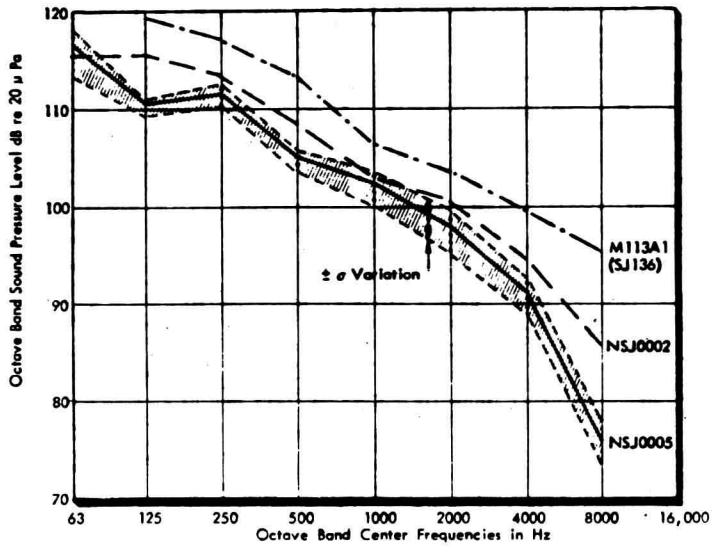

FIGURE 1 . CREW POSITION INTERIOR SOUND LEVEL SPECTRA FOR UNDERWAY AIFV VEHICLES AT 32 KM/H

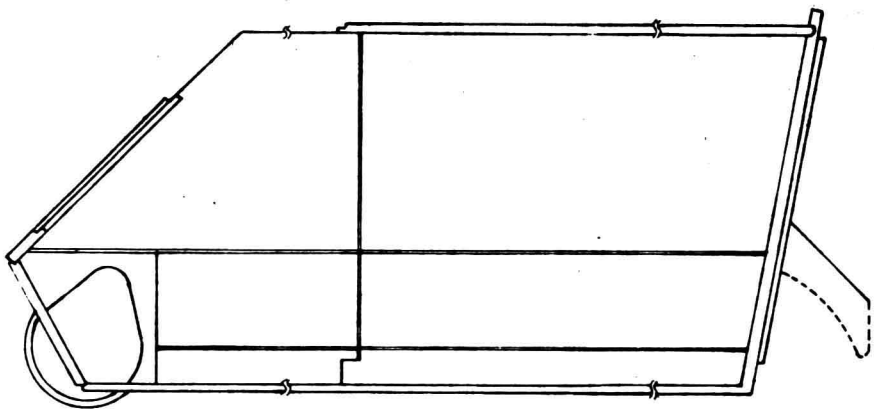

SIDE SECTION VIEW

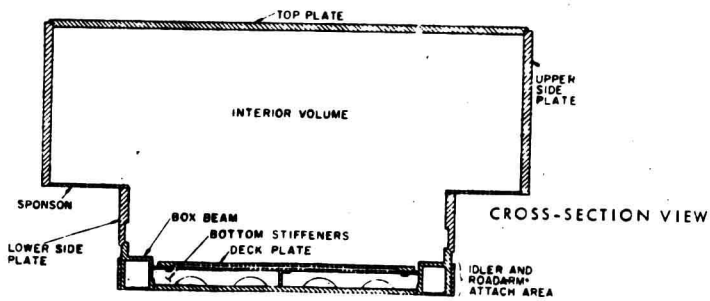

FIGURE 2. SECTION VIEWS OF M113A1 HULL

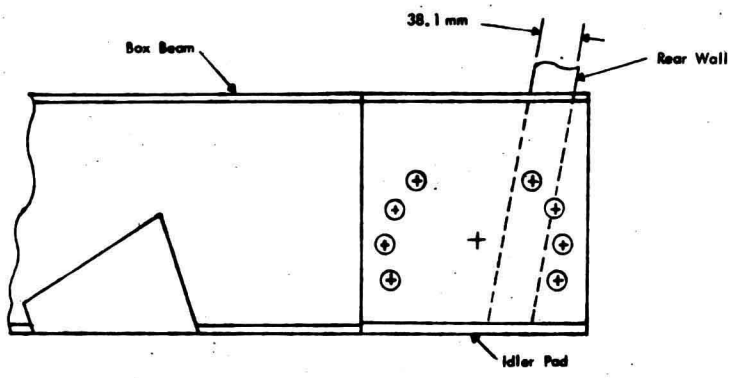

FIGURE 3. SIDE VIEW OF LEFT IDLER PAD

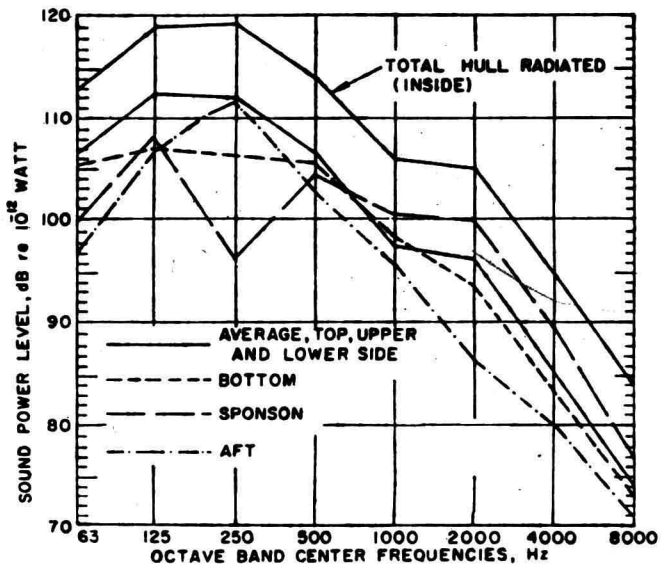

FIGURE 4. CONTRIBUTION OF PANELS TO HULL RADIATED POWER

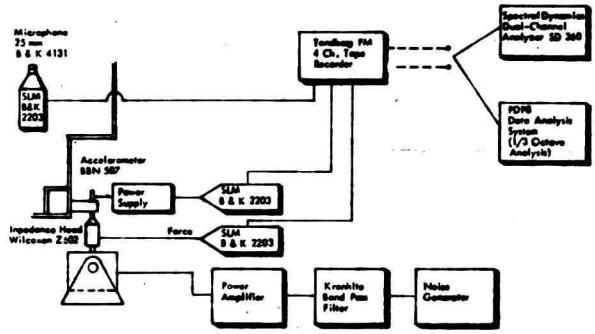

FIGURE 5. INSTRUMENTATION FOR INERTANCE MEASUREMENTS

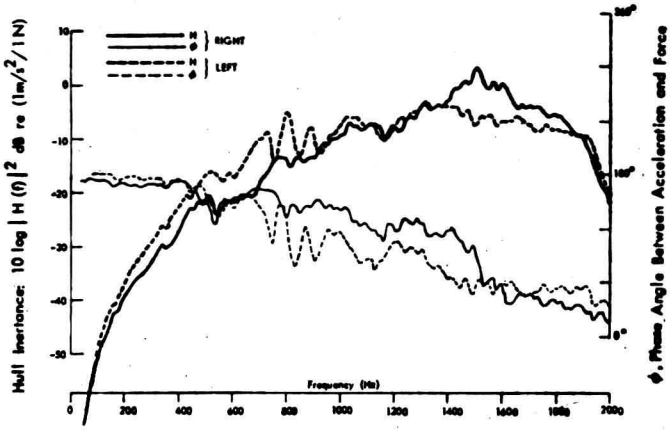

FIGURE 6. COMPARISON OF LEFT- AND RIGHT-SIDE HORIZONTAL INERTANCES ON M113A1 IDLER SPINDLES

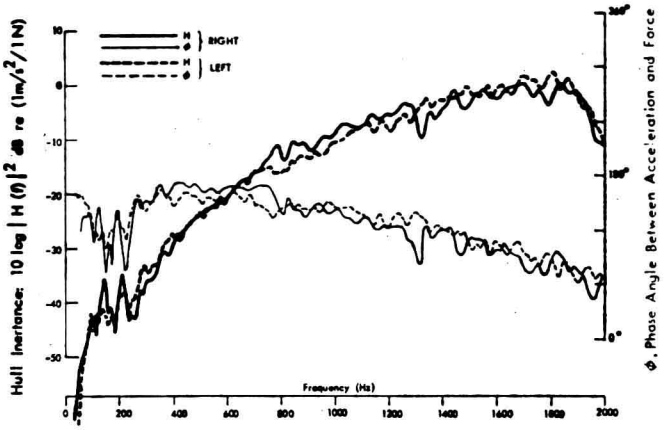

FIGURE 7. COMPARISON OF LEFT- AND RIGHT-SIDE VERTICAL INERTANCES ON M113A1 IDLER SPINDLES

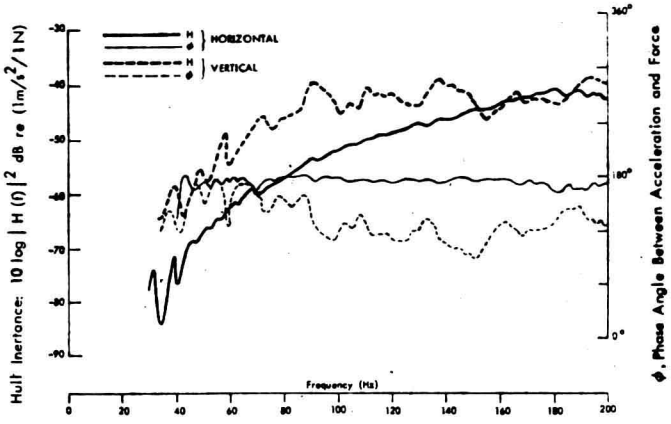

FIGURE 8. COMPARISON OF HORIZONTAL (H) AND VERTICAL (V) LEFT IDLER SPINDLE INERTANCES ON M113A1 VEHICLE

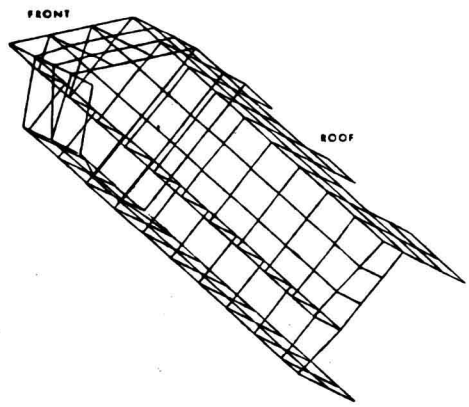

FIGURE 9. NODE LOCATIONS ON MODEL

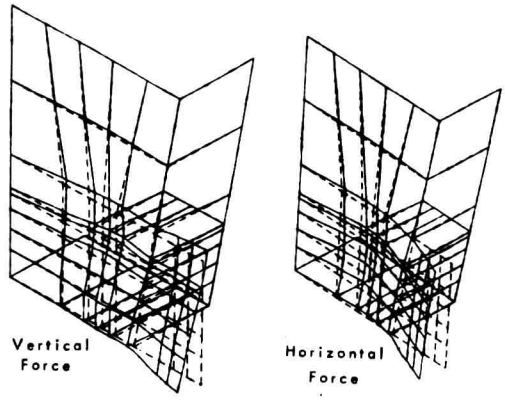

FIGURE 10. IDLER STATIC FLEXIBILITY

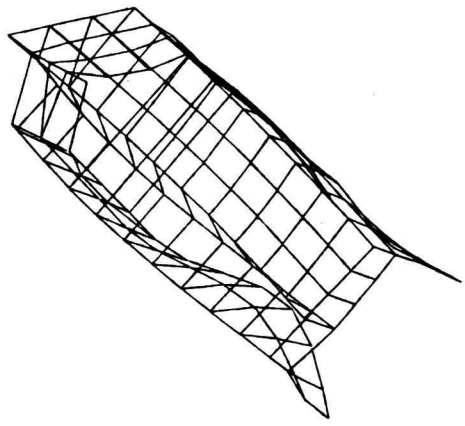

FIGURE 11. SYMMETRIC MODE AT 93Hz

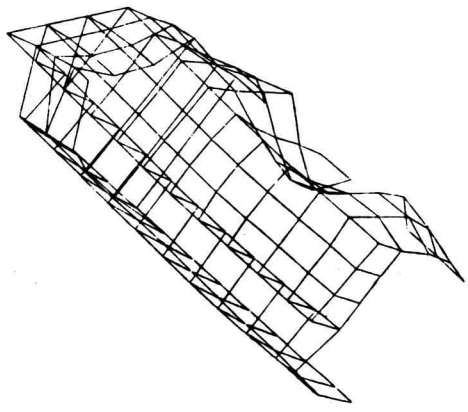

FIGURE 12. ANTI-SYMMETRIC MODE AT 141Hz

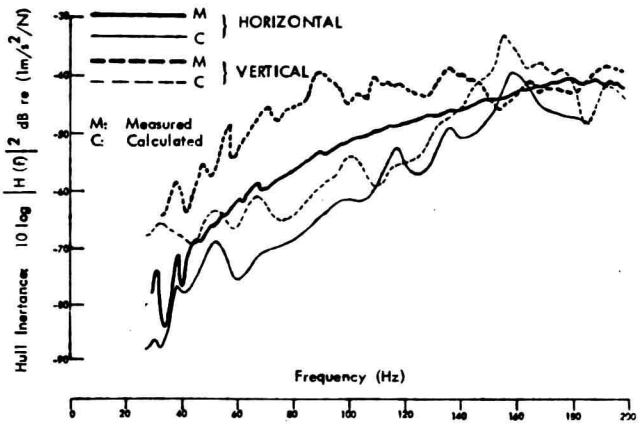

FIGURE 13. COMPARISON OF MEASURED AND CALCULATED OF HORIZONTAL AND VERTICAL LEFT IDLER SPINDLE INERTANCES ON M113A1 VEHICLE

CIRCULAR SAW NOISE GENERATION AND CONTROL

DAVID ALAN BIES
The University of Adelaide,
Adelaide, South Australia.

1. INTRODUCTION

In this paper the complex problem of noise generated by circular saws in operation is considered. While the discussion will be limited to circular saws, many of the points raised could be extended to the consideration of band saws. However, no attempt will be made here to make the extension.

It will be shown that there are three principle sources of noise which are: (1) the unsteady air flow over the teeth which occurs in saws moving at high speed; (2) the resonant and forced vibration of the blade when either the aerodynamically excited blade resonance produces the effect commonly referred to as screaming during idling or the forced vibration at the tooth passing frequency and its harmonics produces the loud noise associated with cutting; (3) work piece radiation. The part being cut may be a significant source of noise and it may possibly couple with the saw blade in resonant response to make the blade a radiator of vibrational energy stored in the work piece.

The work of various investigators as well as work carried out at the University of Adelaide will be reviewed and the various noise source mechanisms, as listed above, will be described in detail as they are presently understood. Various noise control schemes resulting from this understanding will also be mentioned.

Finally a noise suppression guard, invented by the author, will be described which is effective for the control of idling noise. The effect of such control on the overall exposure of a workman will also be considered. A noise suppression guard has been in use in the workshop of the Public Buildings Department of South Australia for more than one year with complete satisfaction. As a result noise suppression guards are now being introduced in the timber mills of the Department of Woods and Forests of South Australia.

2. BLADE VIBRATION NOISE

Blade vibration noise may be important both when the saw is idling and cutting. If it is important when the saw is idling then it will be associated with a very loud tone. Such a saw is said to scream or whistle and whistling noise

may be 10 to 15 dB louder than the broad band aerodynamic noise associated with an idling saw. During cutting whistling is never observed but in this case the blade will be driven at the tooth passing frequency and its harmonics. Furthermore the work piece being cut will be driven at the same frequencies so that both the saw blade and the work piece will radiate sound at these frequencies. If resonances in either the blade or work piece or both happen to coincide with the driving frequencies then the response can be very large and the radiated sound very large.

2.1 Idling Noise

When a saw whistles the blade vibrates in one of its normal modes of vibration which may give rise to an amplitude of displacement of the order of a few tenths of a millimeter near the perimeter.[1-10] The modes of vibration of a saw are described by classical plate theory which teaches that there will always be frequencies of vibration for which a wave travelling around a closed circuit will return upon itself in phase so as to enhance its own motion. Classical theory also teaches that there will always be such closed circuits in any bounded medium capable of transmitting waves. If two resonant waves of the same amplitude are driven at once but in opposite directions around a resonant closed circuit then a standing wave will result. The standing wave will be characterised by nodes which are positions of wave cancellation and antinodes which are positions of wave maximal enhancement. Thus, although our usual experience with resonance is with standing wave systems as in rooms and strings in the case of saws and combustion chambers with cylindrical symmetry travelling wave resonance is possible and observed.

When an object such as a plate is driven at a fixed point waves travelling in all directions will be produced. If the excitation frequency corresponds to one of the resonant frequencies of the object then the waves travelling in opposite directions around the corresponding resonant circuit will be enhanced and a standing wave pattern will be produced. In the case of the circular saw the standing wave pattern will consist of nodal radial and circumferential lines of minimal displacement.[1,5,11,12] The resonance is usually identified by the number of these nodal lines called the mode numbers. An example is shown in Fig. 1.

Modal patterns in circular saw blades are commonly identified by mounting the blade horizontally and sprinkling a bit of fine sand on the blade while at the same time exciting the blade by some means. The sand will collect at the displacement nodes being driven away from the antinodes when the blade is driven

hard enough. We have used time average holography to identify the mode shown in Fig. 1.

When an object is driven in resonant response its motion is controlled by the internal damping of the object. If the internal damping is quite small, as is the case for the ordinary saw blade, then the response can become quite large. Thus an obvious strategy for controlling whistling is to increase the damping of the blade and various schemes for accomplishing this end have been proposed and demonstrated.[6,9,10,13-17] It is also clear that if the damping is small then small forces will be sufficient, if of the right phase and frequency, to strongly drive a saw blade in resonant response.[3,18]

While modal response in the form of standing wave patterns is readily identified in a stationary saw blades identification of modal response in spinning saw blades is by inference.[1,2,3,5,11,12] What is generally observed is a strong resonant frequency with perhaps an accompanying slightly different secondary resonant frequency. When considered as a travelling wave the observed frequencies are readily explained. In this case the apparent frequency of the forward travelling wave is $(f + nR)$, where f is the resonant frequency of the stationary blade in standing wave response, n is the number of full waves around the blade circumference which corresponds to half the number of radial nodes or the number of diametral nodes and R is the rotational frequency of the saw blade. In the case of the backward travelling wave the apparent frequency is $(f - nR)$. Careful investigation of whistling saws rotated at various speeds has confirmed the presence of forward and backward travelling waves. Furthermore, it has been observed that as the speed of rotation is increased the mode which is driven may abruptly change to the next higher order mode, that is n increases in discontinuous steps as the rotational frequency is increased.[2,3] In each case the resonance takes some while to establish itself. Generally the establishment of a loud steady tone takes of the order of ten seconds.

Various experimenters have investigated the phenomenon of tone production and there is agreement that it is the result of blade modal response which is aerodynamically driven. The nature of the driving mechanism may still be the subject of some controversy and the selection of the mode which is driven remains to be explained although an hypothesis has been put forward.[3,13] It had been suggested that the blade tone was due to a coupling between regular von Karman type vortex shedding and a resonance of the blade. When the two frequencies coincided blade resonance would result. However careful

investigation has failed to verify the presence of regular vortex shedding.[3,18] Rather the blade resonance driving mechanism appears to be a galloping oscillation associated with a laminar boundary layer wake shedding. Based on such a model a theory for aerodynamically driven oscillations in a circular saw blade has been formulated. The theory provides stability criteria which seem to agree with experiments. The theory also predicts that the phenomenon will depend strongly upon detail of the tooth design.[8]

According to the galloping oscillation theory a mode will be driven if laterial deflection of the saw teeth results in an increase in the force which initially caused the deflection. The theory is similar to the more familiar theory of flutter phenomenon. The model is like that of the well known galloping bridge driven by a strong wind.

As a matter of interest the manner of noise radiation of a tone by a blade in standing wave resonance has been investigated in our laboratory. Figure 2 shows the areas of positive intensity and Figure 3 gives areas of negative intensity, that is, sound power is returned to the blade at the places indicated. This latter phenomenon appears to be encountered quite often. The nett energy flux, however, is always positive.

2.2. Cutting Noise

The phenomenon of screaming or whistling is never observed during cutting. Thus while cutting noise is generally louder than idling noise, the cutting noise may actually be less than the whistling idling noise.

Spectrum analysis of cutting noise shows that it is characterised by the strong presence of the tooth passing frequency and all of its harmonics.[6,7,10] The noise which is produced is the result of the forced response of the blade and possibly the work piece to the cyclic impact of the teeth on the material being cut. In consequence very little can be accomplished by adding damping as the forced response is not controlled by damping. Thus resonances can be suppressed by this means but the peak stresses are unaffected.[10] Typical spectra without and with damping are illustrated in Fig. 4(a) and Fig. 4(b) respectively.

Of interest is the observation that a well damped blade gives a much cleaner cut. Induced resonant vibration can cause the teeth to vibrate laterally enough to degrade the blade performance. Thus an alternative reason, besides noise for suppressing blade resonances is provided.

2.3 Controls for Blade Noise Radiation

Various schemes have been proposed and demonstrated for the control of screaming. Few investigators, however, have made any claims for the control of cutting noise. Of the various mechanisms proposed for the control of screaming only those which provide significant damping can be expected to have any effect upon cutting noise and then the effect may be quite limited. Of the various other proposed mechanisms which seek to control screaming by altering the modal response of the blade or by altering the aerodynamic driving mechanism so that it becomes ineffective none can be expected to effect cutting noise.[4,8,19,20]

Blade damping mechanisms include laminated blades constructed of sheets fastened together so as to contain a viscoelastic medium between them. Such blades are effective but they are expensive. Alternatively damping may be applied to the sides of the blade in the form of a constrained viscoelastic layer. Commercial materials are available but we have found that simple shim stock and double backed adhesive may be used successfully.[15,17] To be effective the constrained layer should extend to 0.6 of the saw blade radius. Alternatively various damping constructions which are contained in the saw blade collet seem possible.

The use of a damping material on the sides of a saw blade may restrict the depth of cut if the kerf is not greater than the total thickness of the blade and damping materials.[13] Thus an alternative damping mechanism is provided by air pads which ride on a thin layer of air on the top half of the blade.[14] This device works on the principle that motion of the blade normal to its surface will cause the contained thin layer of air to move laterally. This mechanism provides viscous damping which increases as the inverse cube of the separation distance between the rigid pad and the vibrating surface of the saw blade. Such a device is available commercially and has been shown to be quite effective under appropriate circumstances.[14]

Devices which have been proposed for the control of screaming and which are expected to have little or no effect upon cutting may be listed as follows. Expansion slots, both open and plugged, have been shown to be effective by some investigators and shown to make things worse by other investigators.[8.11] When they are effective the reasons why have not yet been convincingly provided so that their use for noise control is problematical. Plugging an expansion slot with a soft metal probably does provide a bit of damping which may be sufficient to control screaming but is probably insufficient to affect cutting noise.

Screaming may be prevented by altering the induced air flow in the region of the teeth. Thus surface roughening applied to the region peripherally just below and including the teeth has been shown effective in preventing screaming.[4] Alternatively closing of the gullet will prevent screaming.[4] In this case the teeth would have to cut alternatively opposite sides of the cut. This fix, however, has the deleterious effect of reducing cutting speed by about ten percent.

Finally some forms of teeth have been shown to be stable while others have been shown to be unstable. Unfortunately, the popular tungsten carbide tip saw tooth is unstable.[18]

3. WORK PIECE RADIATION

During the cutting of any extended body, characterized by many possible modes of vibration in the frequency range of the tooth passing frequency and its harmonics, the modes of the body will be excited and strong sound radiation may follow. The sound radiation from the work piece will be determined by the radiation efficiency of the latter body. Its response will be modal to a point input force at the point of contact with the teeth.

Our experiments have provided some suggestion of a possible coupling between the resonant response of the work piece and the saw blade. Thus, a solid piece of aluminium when cut with the same saw used to cut aluminium extrusion produced markedly less noise then when cutting the extrusion even though the volume of metal cut was significantly greater. The solid piece of aluminium was a very short piece chosen for the test to insure that its lowest order resonant mode was well above the audio frequency range and the range of our A-weighted reading. On this basis one might expect that damping of the work piece might result in reduction of noise radiated by the saw as well. The opposite phenomenon may also be true.[14]

Noise radiation from the work piece may eventually limit possible noise reduction associated with the sawing operation. We have observed that noise along the length of an aluminium extrusion being cut at one end is very nearly of constant level along the entire length. Similarly, it has been shown that the noise level along the length of a piece of timber decreases very slowly as the observation point is moved away from the saw and parallel to the timber.[21] Thus noise control for cutting with saws requires consideration of the noise radiated by the work piece as well.

For certain flat stock the air damping pad described above might be adapted to control noise radiation from this source. Alternatively a tight fitting elastomeric substance placed over the first 10 centimeters or so of an extended extrusion next to the cut has been shown to be effective in reducing radiated noise.[6,7] Foams applied in the area of the cut have also been shown to be effective.[13] However, all of these schemes involve processes which would slow production and add cost thus the problem is at present without an acceptable solution.

4. IDLING NOISE

When a saw is turned on and allowed to run freely, but without cutting, it produces a noise commonly referred to as idling noise. One may immediately ask why is idling noise of any importance. Certainly the best control would be to shut the saw off when not in use. However, observation in the field has shown that even when a saw is in continuous use the actual cutting time may be relatively short. Thus we have determined by actual measurement that cut-off saws in continuous use at one of the timber mills in South Australia are actually cutting only 20% of the time that they are in use. Thus the saw idles while the operator disposes of timber which he has cut and aligns a new piece for cutting. His total noise exposure could be significantly reduced if idling noise could be suppressed or eliminated. Shutting the saw off between cuts would be completely impractical and in the case of very large saws the on-off cycling would place an unacceptable heat load on the motors. Consequently means are required for the control of idling noise.

Screaming has been described and means for its control have been suggested. When screaming is absent a running saw produces a broad band A-weighted sound level at the operators position of around 90 dB(A). Consideration will hence forth be restricted to this broad band aerodynamic noise which for convenience will be termed "idling noise". Experimentation by many researchers has shown that for any blade the idling noise sound pressure level increases rapidly as the saw rotation speed increases.[4,10,11,17-20,22,23] For example, for a doubling of rotational speed increases in noise level ranging from 13.8 to 18.0 dB(A) have been reported. We have observed increases ranging from 13.8 to 16.8 dB(A) with an average from our experiments of about 15 dB(A) for each doubling of rotation speed. Clearly a reduction of rotation speed, or equivalently a reduction in blade diameter, which reduces the tip speed, can be a very effective means for reducing idling noise.

4.1 Model for the Noise Source

Various mechanisms for the generation of idling noise have been suggested but the one which seems best to explain the observations of experiment is based upon an assumed dipole model.[3,18] In this model each tooth is considered to be a little air foil moving through the surrounding air at a speed of the order of the blade tip speed. Each tooth passes successively through the wake of the preceeding tooth and in consequence each tooth experiences a highly turbulent flow. The result is that each tooth experiences a fluctuating lateral force as well as a fluctuating drag. However, it has been shown that the fluctuating drag force is negligible compared to the side to side fluctuating lateral force.[18]

In the model the tooth is assumed to remain stationary in its frame of reference. Thus the fluctuating side forces due to the passage of the turbulent stream over the surface of the tooth do not include motion in the tooth but the equal and opposite force of the tooth on the air stream has the same effect as though the tooth moved. The fluctuating lateral forces tend to push the air stream from side to side just as would an acoustic dipole. The result is dipole radiation with the axis of the dipole normal to the surface of the saw or parallel with the axis of rotation. The consequence of the model is that sound should be loudest along the axis of rotation of the saw and least in the plane of rotation and this expectation has been verified giving further support to the dipole model.[19] As will be shown a dipole model implies that noise generation should increase as some power of the tip speed approaching the sixth power which is in further agreement with observation mentioned earlier.

Based upon the assumption that each tooth of the saw acts like an independent dipole source with axis parallel to the axis of rotation the sound pressure level at any angle ϕ relative to the axis of rotation and distance r (significantly larger than the diameter of the saw) is given as follows.[18,24]

$$\langle p^2 \rangle = N(\dot{L}^2) \sin^2\phi/(16\pi^2 C^2 r^2) \qquad (1)$$

where $\langle p^2 \rangle$ is the mean square sound pressure

N is the number of teeth

$\dot{L}$ is the time rate of change of the lateral fluctuating force

and C is the speed of sound, 341 m/sec.

According to the model it should be possible to calculate the sound pressure anywhere given the quantity $\dot{L}$.

A convenient alternative form of expression for the resulting sound pressure is to describe the total sound power radiated by the N dipoles. Simple integration of the mean square pressure over a spherical surface at distance r from the source provides the following expression for the radiated sound power.

$$W = N(\dot{L}^2)/(6\pi C^3\rho) \tag{2}$$

where W is the radiated sound power
and ρ is the air density.

The fluctuating lateral force on several tooth models has been measured.[18] The experimenters showed that the lateral force L is dependent upon the tooth geometry as well as the proximity of other teeth, that is the gap or gullet width between teeth. Unfortunately they seem to have passed up the opportunity to measure the time rate of change of the fluctuating force ($\dot{L}$) so to proceed we will have to resort to estimation of this quantity.

The results of the study mentioned gives the following expression for the root mean square amplitude of the fluctuating lateral force (L) as

$$L = \alpha(\tfrac{1}{2}\rho S U^2) \tag{3}$$

where α is a function of tooth geometry and is of the order of 0.12
S is the lateral surface area of a tooth
and U is the peripheral speed of the saw or speed of the tooth in a stationary reference frame.

We now make the assumption that the time derivative of L is approximated as follows.[3]

$$\dot{L} = (\tfrac{1}{2}\rho S U^2)(U/h) \tag{4}$$

where h is the blade thickness at the tooth.
The expression for the sound pressure at any point (r,ϕ) becomes

$$\langle p^2\rangle = N\alpha^2\rho^2 S^2 U^6 \sin^2\phi/[64\pi C^2 h^2 r^2] \tag{5}$$

The expression for the sound power becomes

$$W = \alpha^2 N\rho\, S^2 U^6/[24\pi C^3 h^2] \tag{6}$$

Consideration of the above equations for sound pressure and sound power shows that they both exhibit U to the sixth power dependence provided that the quantity

α does not depend upon U and provided that our approximation for $\dot{L}$ does not imply a further dependence upon U not explicitly shown. In fact neither assumption appears to be correct but for the present purpose the assumptions are good enough. As will be shown reasonable estimates can be made with the equations given for sound pressure and sound power.

At this point it may be of interest to consider the proposed model in a bit more detail from a classical point of view. Thus we imagine the teeth of a saw replaced by a corresponding collection of classical dipoles each of two volume sources of strength Q in antiphase separated by a small distance d. The sources on opposite ends of the dipole pulse out of phase at the single frequency ω (radians per second). The axes of all of the N dipoles are parallel to each other and to the axis of rotation of the saw. The acoustic power radiated is

$$W = NQ^2\omega^6\rho d^2/3\pi C^3 \tag{7}$$

where it is assumed that each dipole radiates independently of the rest.

To proceed we let $Q\omega$ equal Sv where v is the assumed normal velocity over a surface S equal to the replaced tooth laterial surface. Furthermore we replace v^2 at a single frequency ω with $v^2(\omega)\Delta\omega$ where $\Delta\omega$ is a narrow frequency band about ω and $v^2(\omega)$ is the spectral density of the assumed normal velocity. The expression for the radiated power becomes

$$W(\omega) = NS^2\rho d^2\omega^4 v^2(\omega)/3\pi C^3 \tag{8}$$

We now assume that $v^2(\omega)$ is proportional to U^2, and $d^2\omega^4$ is proportional to U^4/h^2, then the expression for the acoustic power radiated becomes

$$W(\omega) = \beta N\rho S^2U^6/3\pi C^3h^2 \tag{9}$$

We see by comparison that equation (9) and the previously derived equation (6) are the same provided $\beta = \alpha^2/8$. Either constant may be interpreted as an energy conversion factor, that is, a measure of the conversion of free stream power $S\frac{1}{2}\rho U^3$ to acoustic power. The implied energy conversion is in line with that observed for subsonic jets.[25]

Various investigators have attempted to determine empirical expressions for radiated sound pressure level at some point, generally at one meter and 45° to the axis of saw rotation, this point being roughly described as the operator's position.[4,10,19,23] As a result of this study several prediction schemes are available. Additionally we may use the equation (5) on the assumption that α is approximately 0.12 as mentioned earlier to predict expected sound

pressure level.

In Table 1 the measurements of radiated sound pressure level at the operator's position are summarized for eleven blades chosen at random with widely varying numbers of teeth and tooth design. In the same table results for the estimated sound levels are presented using the procedures given in several references. We also show the results of using equation (5). Consideration of the data in the table shows that reference 10 gives the most consistently correct predictions but it was based upon a fit of the experimental data shown. On this basis the equation derived here is as good as any. What is required of course is a measurement of the time rate of change of the lateral force on a tooth ($\dot{L}$) which would provide the crucial test of the proposed model.

4.2 Control by Modification of the Source

Having established the nature of the source with reasonable assurance a great many means for reduction of the source strength have been proposed and tested. These have all proceeded by cut and try modification of the saw blade, mainly tooth and gullet design with various degrees of success.[4,18,19,22] For example, on the basis of tests on more than one hundred blades one experimenter has proposed that the radiated noise is proportional to a power of the gullet area.[4] On this basis he recommends a blade with closed gullet and has demonstrated a reduction of the order of seven or eight decibels by this means.[4] A saw with a closed gullet would cut on alternate sides with alternate teeth. No trouble with chip removal was encountered but cutting rate was reduced about ten percent with the model tested.

Other authors have made various specific recommendations but none promise more than a few decibels reduction and the effect upon cutting rate has not been reported. In summary the best that such research has been able thus far to provide is the observation that the noise generated is very strongly dependent upon tooth speed. Consequently the smallest diameter saw, turning at the lowest acceptable rotational speed is recommended for minimum noise.

5. NOISE CONTROL GUARD

The observation that the idling noise is dipole in nature has lead to a much different approach to the saw noise control problem at the University of Adelaide. Rather than modify the saw blade we have sought to control the production of noise by an appropriately designed guard. This is possible since a dipole placed between two rigid planes and oriented with its axis normal to the planes will not radiate sound below the cut off frequency determined by the spacing

between the planes.[25] That is, at frequencies for which the free space wavelength is greater than twice the spacing between the rigid planes, the radiation impedance seen by the source will be imaginary. The images of the dipole in the rigid planes tend to unload the source and only a local non propagating disturbance is generated.

Consideration of the effect on the radiation impedance as seen by the saw of two closely spaced rigid planes provided the motive for trying the experiment. The effect on the idling noise was dramatic; it was completely suppressed. Further experimentation, however, showed that as the space between the rigid planes was increased resonances were encountered which greatly increased the noise radiated. This effect is illustrated in Figure 5. Other experimenters have orally reported observation of such guard induced resonances to the author and thus they have purposely avoided such configurations. Where attention has been given to the guard it has taken the form of introduction of acoustic liners to dissipate the noise already generated.[7,14] It should be noted that a dissipative liner makes possible dipole radiation at all frequencies i.e. a soft wall cannot provide sound radiation cut-off.

When a noise suppression guard, based upon the idea of dipole radiation cut-off was constructed and tested, it was determined that when enclosed the rotating saw acts like a strong pump. Furthermore, it was determined that the sealing of small unnecessary leaks reduced the residue noise. Thus with careful attention to detail it is possible to completely suppress idling noise. The sealing of small leaks in a guard, which does not extend excessively past the perimeter of the saw, is necessary to achieve this end. In practice we have found that a guard which extends of the order of three times the spacing between guard plates is sufficient.[17]

The apparent pumping of the rotating saw is at present not fully understood.[26] It does have the added, and unexpected advantage that it greatly simplifies wood dust collection. It also suggests the distinct possibility that the guard is successful for quite another reason than the one given. Thus as mentioned earlier, the source strength is dependent upon the relative speed between the saw teeth and the stationary surrounding air to a power varying between 4.6 and 6. When the saw induces a strong flow within the confines of the closely spaced plates of the guard it obviously does so by decreasing the relative speed of the teeth with respect to the surrounding air. The surrounding air is moving at high speed in the same direction as the saw and thus the dipole source strength can be expected to be greatly decreased. The result, however, is the same;

noise generation is suppressed.

A docking saw, fitted with the guard, is shown in Figure 6. This saw has now been in use for more than a year with complete satisfaction. It should be noted that the noise suppression is in no way dependent upon tooth design. [7,9] The device works to suppress idling noise of any saw.

It is of interest to determine the possible effect in commercial use of the guard. Before modification, the docking saw shown in Fig. 6 idled at 90 dB(A) and cut 50 x 100 mm timber at 96 to 97 dB(A) as measured at the operator's position. After installation of the guard the saw idled at 76 dB(A), which is the noise level of the saw motor. With the aid of damping shims on the blade [17] the saw cuts the same timber at 90 dB(A).

Alternatively, if the use observed in the timber mills of South Australia is typical, so that the saw normally idles about eight percent of the time, then in terms of exposure the treated saw may cut at 97 dB(A) and still meet South Australia's noise dose criteria for 8 hours operation. In the United States which accepts a 5dB(A) increase for each halving of exposure time instead of the 3 dB(A) increase allowed in South Australia the cutting noise level could be raised to 101 dB(A) before a workman's maximum permitted exposure was reached.

6. CONCLUSION

The generation and control of the various sources of noise associated with the use of circular saws has been considered in this paper. It has been shown that although various means involving optimal choice of the tooth design have been proposed for noise control it is not necessary to modify the saw to suppress idling noise. A simple redesign of the guard may be sufficient. Screaming commonly encountered during idling has been shown to be aerodynamically induced but the coupling is quite weak and very little damping will suppress it. Thus, while tooth design modifications are possible to suppress screaming, the phenomenon may be avoided by the application of just a bit of damping. The requirement for adequate damping is readily met and may easily be implimented. Alternatively, the guard described in this paper will probably suppress screaming.

Cutting noise involves forced response of the blade and work piece. These sources may in turn respond resonantly thus damping of the blade is again recommended. Practical means for work piece damping are needed but have not yet been invented thus cutting noise remains as a troublesome phenomenon to receive

further attention. The suppression of idling noise, however, has been shown to ease the problem of cutting noise control.

REFERENCES

1. C.D. Mote, Jnr., and R. Szymani, "Circular Saw Vibration Research" Shock and Vibration Digest, 10 (6), June 1978 pp 15-30.

2. C.D. Mote, Jnr., and M.C. Leu, "Whistling Instability in Idling Circular Saws", ASME publication 79-WA/DSC-18, December 2-7, 1979.

3. C.D. Mote, Jnr., and H.S. Cho, "Aerodynamically Induced Whistling in Circular Saws" (May 1978 submitted to Journal of the Acoustical Society of America).

4. Wyle Laboratories - Research Staff Mechanical Memorandum TM 78-1, Aerodynamically Quiet Circular Saw Blades. A Design and Application Manual, prepared for Woodworking Machinery Manufacturers of America, August, 1978.

5. D.S. Dugdale, "Discrete Frequency Noise from Free Running Circular Saws", Journal of Sound and Vibration 10 (2), 1969, pp 296-304.

6. J.G. Bollinger and M.F. deVries, "Origin and Control of Noise in Aluminum Extrusion Cut-off Saws", University of Wesconsin Publication, 1978.

7. J.G. Bollinger, M.F. DeVries and Kian T. Yap, "Control of Noise in Sawing of Aluminum Extrusions", Second Year Progress Report Number 1, 1979, Mechanical Engineering Department, University of Wisconsin - Madison.

8. F.B. Malcolm, "Expansion Slots, Symmetrically Placed, Solve Problem of "Screaming" Saws", World Wood March 1972 pp 10-11.

9. Anon., "Control of Noise in Sawing of Aluminium Extrusions", Precision Metal June 1979 pp 52-54.

10. M. Zockel and S.G. Page, "Noise Reduction on Circular Saw Blades", Engineers Australia, Proceedings of Conference of Machinery, Vibration and Noise, 1978, Adelaide, 29-30 May pp 37-42.

11. G. Pahlitsah and B. Rowinski, "Vibration Behaviour of Circular Saw Blades, Part IV, The Causes of Screaming in Circular Saw Blades, and its Prevention",

Translated from: Holz alsoRoh - und Werkstoff 25 (10), 1967, pp 393-397, Commonwealth of Australia CSIRO Translation No. 9211 (d).

12. C.D. Mote and R. Szymani,"A Review report on Principal Developments in Thin Circular Saw Vibration and Control Research Part 1: Vibration of Circular Saws", Holz also Roh - und Werkstoff 35 (1977) pp 189-196.

13. John H. Burnham, "Control of Aluminum Extrusion Sawing Noise", paper presented at the Aluminum Association Workshop, Chicago, Illinois, June 9-10, 1976.

14. C.H. Allen, "Vibration Damper for Circular Saws", The Journal of the Acoustical Society of America, 60, Supplement Number 1, Fall 1976, p S51, Abstract W7.

15. F. Kirschner, "New Materials for Vibration Damping Control", Proceedings Inter-Noise 75, Sendai August 27-29, 1975 pp 499-505.

16. Anon., "Woodtape Company Introduces Quiet Circular Saw Blade", Noise Control Engineering, November-December 1975 pp 138-139.

17. M. Zockel, D.A. Bies and S.G. Page, "Solutions for Noise Reduction on Circular Saws" Chapter 14, Proceedings Noise-Con 79, Purdue University, Lest Lafayett, Indiana pp 373-383.

18. Hyung S. Cho, "Aerodynamically Induced Vibration and Noise in Circular Saws", Doctor of Philosophy Thesis, Department of Mechanical Engineering, College of Engineering, University of California Berkeley, August 1977.

19. John S. Stewart, "An Investigation of the Aerodynamic Noise Generation Mechanisms of Circular Saw Blades", Noise Control Engineering 11 (1), July-August 1978, pp 5-11.

20. John S. Stewart, "Noise Generation Mechanisms for Machines Employing Circular Saw Blades", Proceedings of Noise-Con 79 Machinery Noise Control, 30 April-2 May 1979, pp 53-61.

21. P.D. Wheeler and W.I. Acton, "Wood-Radiated Noise from Woodworking Machines", paper presented at the 9th International Conference on Acoustics, Madrid, Spain, 1977.

22. H.S. Cho and C.D. Mote, Jnr., "On the Aerodynamic Noise Source in Circular Saws", Journal of the Acoustical Society of America, 65 (3), 1979, pp 662-671.

23. K.D. Korkan, S.L. Petrie and T.S. Rice, "Experimental Investigation of Aerodynamic Noise from a Circular Saw Blade", Proceedings of the Technical Program, Noisexpo National Noise and Vibration Control Conference, Chicago, Illinois, March 14-17, 1977, pp 190-195.

24. A.S. Hersch and W.C. Meecham, "Sound Directivity Pattern Radiated from Small Airfoils", Journal of the Acoustical Society of America 53 (2), 1973 pp 602-606.

25. L.L. Beranek, Editor, "Noise and Vibration Control", Chapter 16, McGraw-Hill Book Company, New York, 1971.

26. J.A.T. Stafford, T.B. Ferguson, E.S. Hirst and R.W. Asquith, "An Expirmental Investigation Observing Some Unsteady Flows Induced by a Rotating Disc", Proceedings of the 5th Conference on Fluid Machinery 2, 1975, Budapest, pp 1071-1079.

TABLE 1 COMPARISON OF RESULTS OF SEVERAL NOISE PREDICTION SCHEMES

Blade Number Table 1 References 17	Experimentally Determined Sound Pressure Level in dB(A) (operator's position)	Predictions and Errors of Given References Sound Pressure Levels in dB(A) at operator's							
		references 17		references 4		references 19		equation (5)	
1	85.5	83.3	-2.2	82.5	-3	84	-1.5	88	2.5
2	83.0	84.6	1.6	80.5	-2.5	84	1.0	85.5	2.5
3	88.0	90.0	2.0	81.5	-6.5	79	-9.0	93.0	-5.0
5	88.0	84.5	-3.5	86.5	-1.5	90.5	2.5	92.0	4.0
6	76.0	75.9	-0.1	75.5	-0.5	64	-12	72.0	-4.0
7	88.0	87.4	-0.6	84.5	-3.5	86	- 2	92.0	4.0
8	86.5	84.0	-2.5	82.5	-4.0	84	-2.5	89.0	2.5
9	86.5	83.6	-2.9	80.0	-6.5	82.5	-4	84.5	-2.0
10	93.0	90.0	-3.0	88.0	-5.0	92	-1.0	96.0	-0.5
11	86.5	82.6	-3.9	85.5	-1.0	85	-1.5	86.0	-0.5
12	77.5	77.9	0.4	77.5	0.0	62	-15.5	76.5	-1.0
error range		+ 2 to - 3.9		0.0 to - 6.5		2.5 to -15.5		2.5 to - 5	

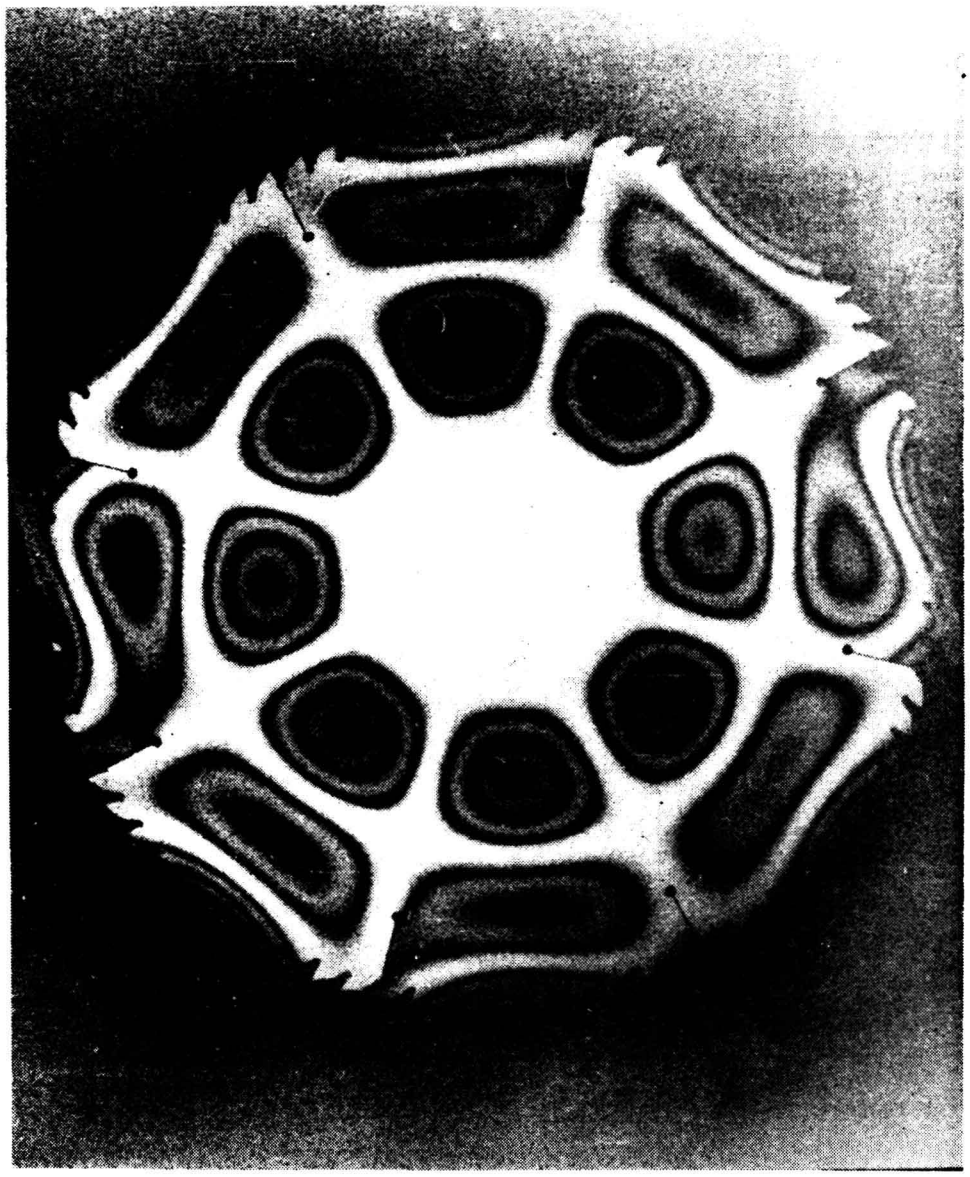

FIG. 1. HOLOGRAM OF VIBRATING SAW BLADE

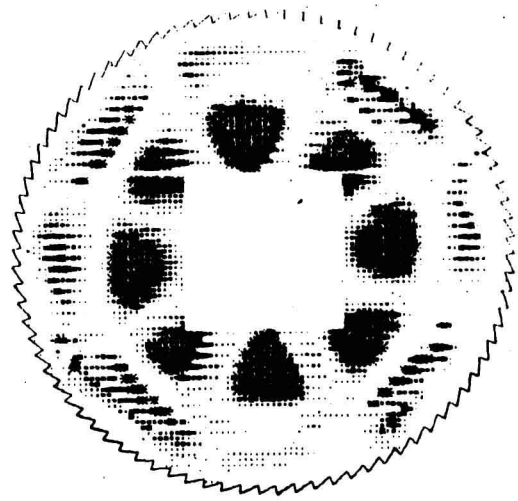

FREQUENCY OF VIBRATION = 2305HZ
MEAN SAW RADIUS = 220.3MM.
SAW THICKNESS = 3.2MM.

FIG. 2. POSITIVE INTENSITY. MEASURED RESISTIVE SURFACE INTENSITY DISTRIBUTION FOR SOUND RADIATION FROM A CIRCULAR SAW BLADE CENTRE CLAMPED TO A RADIUS OF 68.3MM.

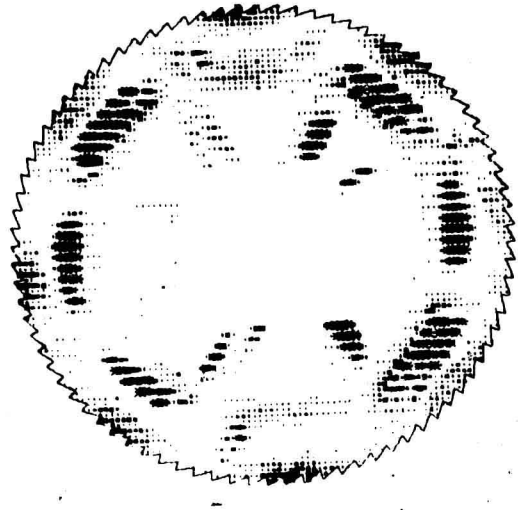

FREQUENCY OF VIBRATION = 2305HZ
MEAN SAW RADIUS = 220.3MM.
SAW THICKNESS = 3.2MM.

FIG. 3. NEGATIVE INTENSITY. MEASURED RESISTIVE SURFACE INTENSITY DISTRIBUTION FOR SOUND RADIATION FROM A CIRCULAR SAW BLADE CENTRE CLAMPED TO A RADIUS OF 68.3MM.

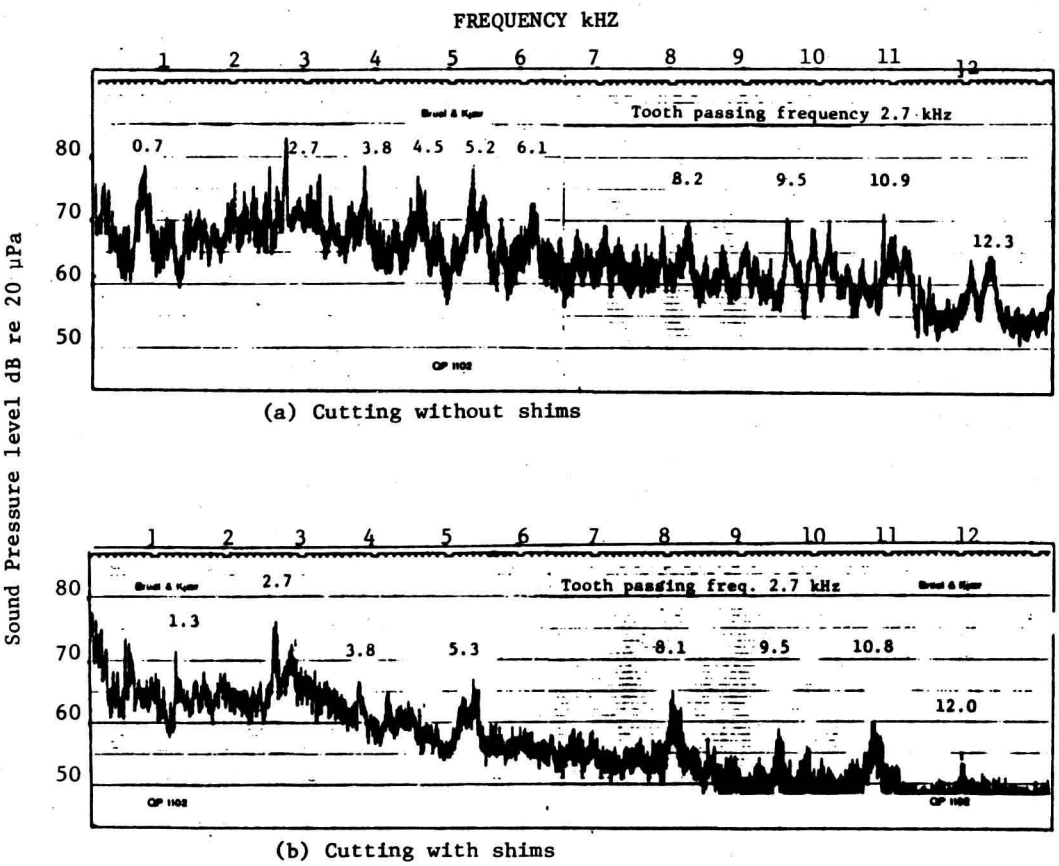

FIG. 4. CUTTING NOISE SPECTRA

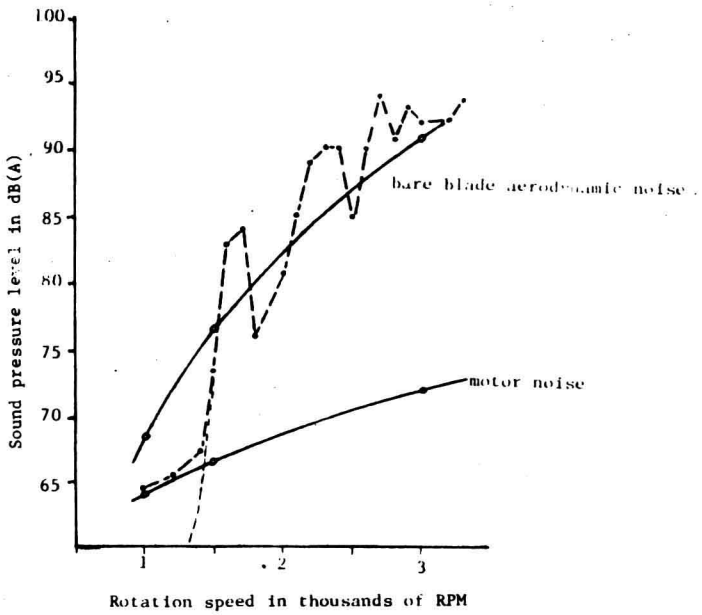

FIG. 5. IDLING NOISE OF A DAMPED BLADE ROTATING BETWEEN PARALLEL SQUARE BOARDS. (TUNGSTEN CARBIDE 300 MM DIAMETER BLADE, BOARDS 60 MM APART AND 570 MM SQUARE)

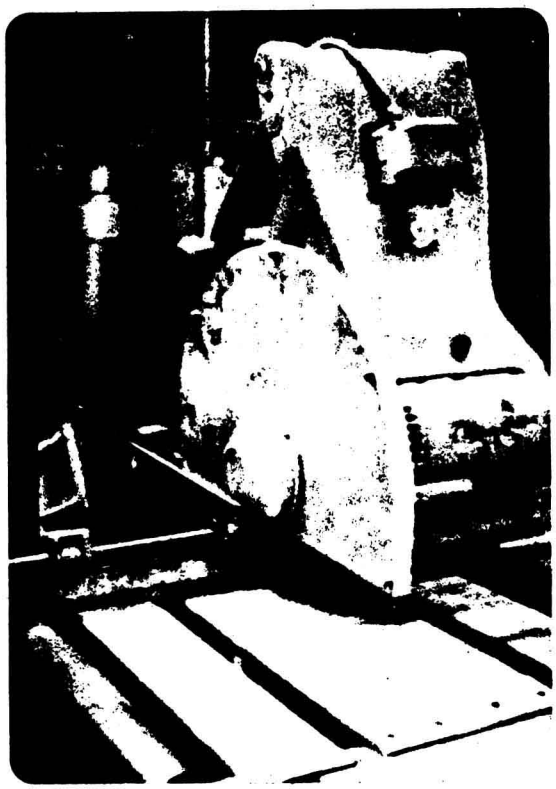

FIG. 6. DOCKING SAW WITH NOISE SUPPRESSION GUARD.

PREDICTION OF NOISE RADIATION FROM PIPES WITH DISTURBED INTERNAL TURBULENT FLOW

M.K. Bull
University of Adelaide,
Adelaide, South Australia.

M.P. Norton,
CSIRO Division of Mechanical Engineering,
Highett, Victoria.

1. INTRODUCTION

Severe disturbance of a turbulent pipe flow, such as that due to a valve, mitred bend, tee-junction, or orifice plate, gives rise to flow separation from the pipe walls and increased turbulence levels in the vicinity of the disturbance. This results in the generation of an intense internal acoustic field consisting of propagating plane waves and higher order modes. At a distance of about ten pipe diameters from the disturbance normal turbulent pipe flow is re-established, but it has this acoustic field superimposed on it. The acoustic waves will propagate throughout the piping system and can be a major source of external acoustic radiation. In particular, coincidence of higher order acoustic modes with flexural waves in the pipe walls leads to very efficient excitation of pipe wall vibration and sound radiation into the external fluid. In the case of severe flow disturbances such waves will be the dominant source of external radiation at frequencies at which they can propagate, and it is this phenomenon to which attention will be directed here.

2. COINCIDENCE

Both the acoustic waves (apart from plane waves) which can propagate in the fluid inside an infinitely long pipe and the flexural waves which can propagate in the pipe wall are dispersive - their axial phase velocities vary with frequency. The (p,q) -th acoustic mode is characterised by p nodal diametral planes and q nodal cylindrical surfaces concentric with the pipe axis. For such waves in the presence of an idealised uniform flow with velocity U and corresponding Mach number M = U/c parallel to the pipe axis at all points over the cross-section, the relation between (radian) frequency ω as seen by a stationary observer and the axial component k_x of the wavenumber vector can be expressed as

$$\bar{\nu} = (\omega a/c)/M_L = [\sqrt{(\kappa_{pq} a)^2 + K_x^2} \pm MK_x]/M_L \quad , \qquad (1)$$

where a is the pipe radius, c is the speed of sound in the

internal fluid, $K_x = k_x a$, M_L is defined below, and κ_{pq} is the wavenumber component in the plane of the cross-section as determined by the boundary condition at the pipe wall (see Morse and Ingard [1], Chapter 9). κ_{pq} represents the lowest (resultant) wavenumber at which the (pq) -th mode can propagate; it determines the cut-off frequency of the (pq) -th mode when there is no flow. The term MK_x in the equation represents the Doppler shift of frequency, and the + and - signs correspond to upstream and downstream wave propagation (relative to the fluid) respectively. The n-th flexural mode in the pipe wall is characterised by an integral number n of (trace) wavelengths around the circumference of the pipe. The relation between ω and k_x for such waves, as given by Heckl's [2] approximation, is

$$(\omega a/c_L)^2 = (\omega/\omega_r)^2 = \bar{\nu}^2 = \bar{\beta}^2 \, (n^2 + K_x^2)^2 + K_x^4/(n^2 + K_x^2)^2, \qquad (2)$$

where $c_L = \sqrt{E/\rho_s}$, $\bar{\beta} = h/a\sqrt{12(1 - \mu^2)}$, h is the thickness of the pipe wall, E, μ, and ρ_s are respectively Young's modulus, Poisson's ratio, and density of the pipe wall material, $\bar{\nu} = \omega/\omega_r$, $\omega_r = c_L/a$ is the "ring" frequency of the pipe, and M_L (as used above) $= c_L/c$.

Coincidence of structural and acoustic modes may take the form of wavelength matching only ("wavenumber coincidence") or both wavelength and frequency matching ("complete coincidence"). We therefore define wavenumber coincidence as the condition in which the circumferential distance along the pipe surface between diametral nodes of the (p,q)th acoustic mode is equal to half the wave-length of the n-th structural mode in the same direction (n = p), and in which also the structural and acoustic wavenumbers k_x in the axial direction are equal. Complete coincidence is defined as wavenumber coincidence with, in addition, matching of frequencies of the structural and acoustic waves.

Complete coincidence is represented by the intersection of the acoustic and structural curves on plots of axial wavenumber against frequency, with n = p, such as Figure 1. There are two complete-coincidence frequencies for a given flow Mach number; they become identical when M = 0. Because the frequency of a given acoustic mode varies very slowly from the cut-off frequency with increasing axial wavenumber while that of the structural modes varies rapidly with axial wavenumber, complete coincidence occurs at frequencies which are very close to the cut-off frequency of the acoustic mode. It will also be observed that the effect of flow is to reduce the acoustic cut-off frequency (by a factor of $\sqrt{1 - M^2}$ on the no-flow value, Mason [3]).

In practical piping systems we are concerned with finite lengths of pipe, for example the lengths between flanges. In such cases a section of pipe will have

a set of characteristic resonance frequencies corresponding to particular allowed values of k_x. For example, if as an approximation (which will improve with increasing frequency) we assume that a finite section of pipe of length ℓ has simply-supported ends, then the values of K_x are restricted to

$$K_x = K_m = m\pi/\Lambda \quad , \quad (m = 1,2,3,.....) \quad , \tag{3}$$

where $\Lambda = \ell/a$, and equation (2) gives for the resonance frequencies

$$\bar{\nu}_{mn}^{\,2} = \beta^2 \, (n^2 + K_m)^2 + K_m^4/(n^2 + K_m^2)^2. \tag{4}$$

In piping systems there is also the possibility that, by reflection, standing acoustic waves will be set up, and that these waves also will be restricted to a set of discrete frequencies. However in the present work we consider only finite sections of pipe excited by travelling acoustic waves. In this case, because of the restriction of K_x for the structural modes to the discrete values K_m, complete coincidence will not, in general, occur at a structural resonance frequency; it will occur only in the particular case of a length-to-radius ratio Λ of the pipe section given by

$$\Lambda = m\pi/K_{cc} \quad , \tag{5}$$

where K_{cc} is the value of K_x corresponding to complete coincidence. If Λ has a value other than one of the discrete values represented by equation (3), only wavenumber coincidence at a resonance frequency is possible.

3. PREDICTION OF ACOUSTIC RADIATION

It can be shown (Bull and Rennison, [4]) that the power spectral density of the velocity response of the wall of a finite length of pipe, averaged over the area S of the vibrating surface, $[\![\phi_{\dot{\zeta}}(\omega)]\!]$, to a random pressure field whose power spectral density is ϕ_p, is given by

$$[\![\phi_{\dot{\zeta}}(\omega)]\!] = \frac{\omega^2 \phi_p(\omega)\, S^2}{2} \sum_{\alpha} \frac{j_{\alpha\alpha}^2(\omega)}{|Z_\alpha(\omega)|^2} \quad , \tag{6}$$

where $Z_\alpha(\omega)$ is the complex obstructance of the α-th resonant mode of the pipe ($\alpha \equiv (m, n)$),

$$|Z_\alpha(\omega)|^2 = \omega_\alpha^4 (\rho_s Sh/4)^2 \, [(1 - \omega^2/\omega_\alpha^2) + (\omega/\omega_\alpha Q_\alpha)^2] \tag{7}$$

$j_{\alpha\alpha}^2(\omega)$ is the joint acceptance of the pressure field and the pipe wall, ω_α is the resonance frequency of the α-th pipe mode and Q_α its damping quality factor. The relation between the spectral density of the pipe wall velocity and that of the radiated acoustic power ϕ_Π is

$$\phi_\Pi(\omega) = \sigma \rho_e c_e S \, [\![\phi_{\dot{\zeta}}(\omega)]\!] \quad , \tag{8}$$

where ρ_e and c_e are respectively the density of and speed of sound in the external fluid and σ is the radiation ratio for all contributing pipe modes at frequency ω. Combining equations (6) and (8) we obtain

$$\frac{\phi_\Pi}{\rho_e c_e c S a} = \frac{\rho_{fs}^2 M^3}{6\beta^2} \cdot \Phi_p \cdot \sum_\alpha \frac{\sigma_\alpha \cdot j_{\alpha\alpha}^2(\omega) \cdot A_\alpha(\omega)}{(\omega_\alpha a/c)^2}, \tag{9}$$

where $\Phi_p = 4\phi_p/\rho_f^2 U^3 a$, ρ_f is the internal fluid density, $\rho_{fs} = \rho_f/\rho_s$, $\beta = h/2\sqrt{3}a$, σ_α is the radiation ratio for the α-th pipe mode, and

$$A_\alpha(\omega) = (\omega/\omega_\alpha)^2 \left[(1 - \omega^2/\omega^2{}_\alpha)^2 + (\omega/\omega_\alpha\, Q_\alpha)^2\right]^{-1}. \tag{10}$$

For the higher order acoustic modes the joint acceptance can be expressed as the product of axial and circumferential components:

$$j_{\alpha\alpha}^2 = j_{mm}^2 \cdot j_{nn}^2, \tag{11}$$

where $j_{nn}^2 = 1/4$ for $n = p$, but is otherwise zero, and

$$j_{mm}^2 = \frac{2(1-\cos\Lambda K_m \cos\Lambda K_x)}{\Lambda^2 K_m^2 (1-K_x^2/K_m^2)^2} \tag{12}$$

j_{mm}^2 (see figure 2) has its maximum value, 1/4, at wavenumber coincidence ($K_x/K_m = 1$); $j_{\alpha\alpha}^2$ then has its maximum value of $(1/4)^2$. The formal expression for the acoustic power radiation in a frequency band ω_1 to ω_2, $\Pi_{\Delta\omega}$, due to higher order modes can now be obtained from equation (9). If the assumption is made that $\sigma_\alpha = 1$ for the structural modes involved, then we have

$$\frac{\Pi_{\Delta\bar{\nu}}}{\rho_e c_e c^2 S} = \frac{\rho_{fs}^2 M^3}{6\beta^2 M_L} \sum_\alpha \sum_{(p,q)} \frac{1}{\bar{\nu}_\alpha^2} \int_{\bar{\nu}_1}^{\bar{\nu}_2} (\Delta\Phi_p)_{pq} \cdot j_{\alpha\alpha}^2(\bar{\nu}) \cdot A_\alpha(\bar{\nu}) \cdot d\bar{\nu}, \tag{13}$$

where $(\Delta\Phi_p)_{pq}$ is the contribution of the (p,q)-th acoustic mode to the total power spectral density of the internal wall pressure field, and the summation is in principle over all combinations of acoustic modes and structural modes for which wavenumber (or complete) coincidence is possible at frequencies within the band. However significant structural response will occur only if the structural resonance frequency (which in principal could even be outside the band under consideration) is not too far removed from the acoustic excitation frequency corresponding to the same axial wavenumber. This implies that significant structural response and radiation due to wavenumber (but not complete) coincidence will only occur when both the acoustic frequency giving rise to the wavenumber coincidence and the structural resonance frequency are close to the complete-coincidence frequency. The summation will therefore in effect be confined to acoustic

modes giving complete coincidence at frequencies within the band, and to one or two resonant structural modes with frequencies close to (or at) the complete-coincidence frequencies. Furthermore, since the complete-coincidence frequency is in general not very far removed from the cut-off frequency of the acoustic mode, the summation will in general be confined to acoustic modes with cut-off frequencies in the band in question.

However, even with the restrictions just noted, equation (13) indicates that the acoustic power radiation due to a given higher order mode will still depend critically on whether complete or only wavenumber coincidence occurs. Suppose that complete coincidence of the (pq)th acoustic mode and a p-th order structural wave in the pipe wall occurs at a non-dimensional frequency of $\bar{\nu}_{cc,pq}$ and a non-dimensional axial wavenumber of $K_{xcc,pq}$. If the length-to-radius ratio of a pipe section is such that $(\Lambda K_{xcc}/\pi)$ is an exact integer m then complete coincidence of the (m,p)-th structural mode and the (pq)-th acoustic mode will occur. In this case the functions $A_\alpha(\bar{\nu})$ and $j^2_{\alpha\alpha}(\bar{\nu})$ will both have their maximum values at $\bar{\nu} = \bar{\nu}_{cc,pq}$. The main lobe of the curve of $j^2_{\alpha\alpha}$ versus K_x/K_m (figure 2) is confined to acoustic wavenumbers in the range $K_x = (1\pm 2/m)\, K_m$, which corresponds to a narrow frequency bandwidth $\Delta\nu \simeq (c_g/c_L).(4\pi/\Lambda)$, where $c_g(<c)$ is the group velocity of the acoustic mode at the acoustic frequency corresponding to $K_x = K_m$. Despite this, the damping of metal pipes will generally be sufficiently low (high Q) to ensure that the effective bandwidth of the function $A_\alpha(\bar{\nu})$, namely $\Delta\bar{\nu} \simeq \bar{\nu}_\alpha/Q_\alpha$ where $\bar{\nu}_\alpha$ is the resonance frequency of the pipe mode, is much less than that of $j^2_{\alpha\alpha}$. Hence in this case $j^2_{\alpha\alpha}$ will depart little from its maximum value of $(1/4)^2$ over the bandwidth of $A_\alpha(\bar{\nu})$ and from equation (13) the contribution of the complete coincidence to the radiation becomes

$$\frac{\Pi}{\rho_e c_e c^2 S} \simeq \frac{\rho_{fs}^2 M^3}{96\beta^2 M} \cdot (\Delta\Phi_p)_{pq} \cdot \frac{Q_{pq}}{\bar{\nu}_{cc,pq}} \qquad (14)$$

If Λ is such that $(\Lambda K_{xcc}/\pi)$ is not an exact integer the peaks of $A_\alpha(\bar{\nu})$ and $j^2_{\alpha\alpha}(\bar{\nu})$ will occur at different frequencies $\bar{\nu}_\alpha$ and $\bar{\nu}_{c\alpha pq}$ respectively (see Figure 3). These may be separated sufficiently for $A_\alpha(\bar{\nu})$ to be independent of modal damping Q_α and to be a slowly-varying function of $\bar{\nu}$ over the bandwidth of the joint acceptance curve. In this case $A_\alpha(\bar{\nu})$ can be approximated by its mid band value $A_\alpha(\bar{\nu}_{c\alpha pq})$ and the contribution to the acoustic power radiation becomes

$$\frac{\Pi}{\rho_e c_e c^2 S} \simeq \frac{\pi\rho_{fs}^2 M^3 M_g}{24\beta^2 M_L^2 \Lambda} \cdot \frac{A_\alpha(\bar{\nu}_{c\alpha pq})}{\bar{\nu}_\alpha^2}, \qquad (15)$$

where $M_g = c_g/c$, evaluated at $\bar{\nu}_{\alpha pq}$. Experiments performed so far [5] indicate that the power radiated corresponds to a summation of terms such as that given by equation (15), rather than the potentially higher value represented by equation (14). A comparison of experimental data and estimates based on equations (13) and (15) is shown in Figure 4. It therefore appears that equation (15) can be used as the basis for prediction of the external radiation.

Experiment also indicates that $\Delta\Phi_p$ varies as $M^2/(\omega a/U)^2$ and that ϕ_p varies as $\bar{\nu}^{-1}$. The power radiation in one-third-octave bands is then independent of $\bar{\nu}$ and, for steel pipes, given roughly by the empirical relation

$$\frac{\Pi_{1/3}}{\rho_e c_e^3 S} \simeq 7 \times 10^{-5} \cdot \frac{\rho_{fs}^2 M^7}{\beta^2 \Lambda} \qquad (16)$$

An example of experimental data and comparison with the spectral density of the power corresponding to equation (16) is shown in Figure 5.

ACKNOWLEDGEMENT

This work is part of research programme supported by the Australian Research Grants Committee.

References

[1] P.M. MORSE and K.U. INGARD 1968 Theoretical acoustics. McGraw-Hill, New York.

[2] M. HECKL. 1962. Vibration of point-driven cylindrical shells. J. Acoust. Soc. Am. 34, 1553-1557.

[3] V. MASON 1969. Some experiments on the propagation of sound along a cylindrical duct containing flowing air. J. Sound Vib. 10, 208-226.

[4] M.K. BULL and D.C. RENNISON. 1974. Acoustic radiation from pipes with internal turbulent gas flows. Proceedings of Noise Shock and Vibration Conference, Monash University, pp. 393-405.

[5] M.P. NORTON. The effects of internal flow disturbances on the vibrational response of and the acoustic radiation from pipes. Ph.D. Thesis.

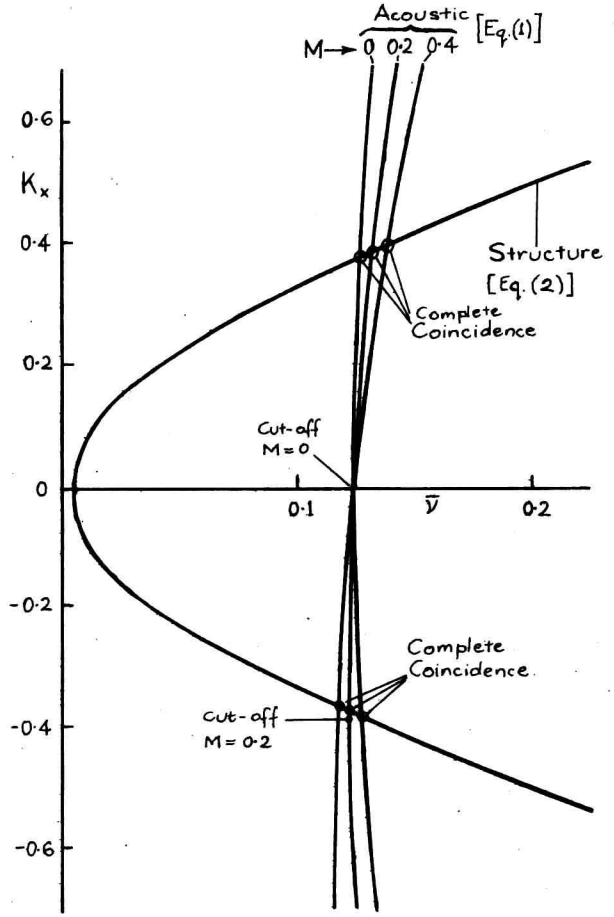

KK7

Figure 1. Complete coincidence of first order structural modes with the (1,0) acoustic mode at various flow Mach numbers.

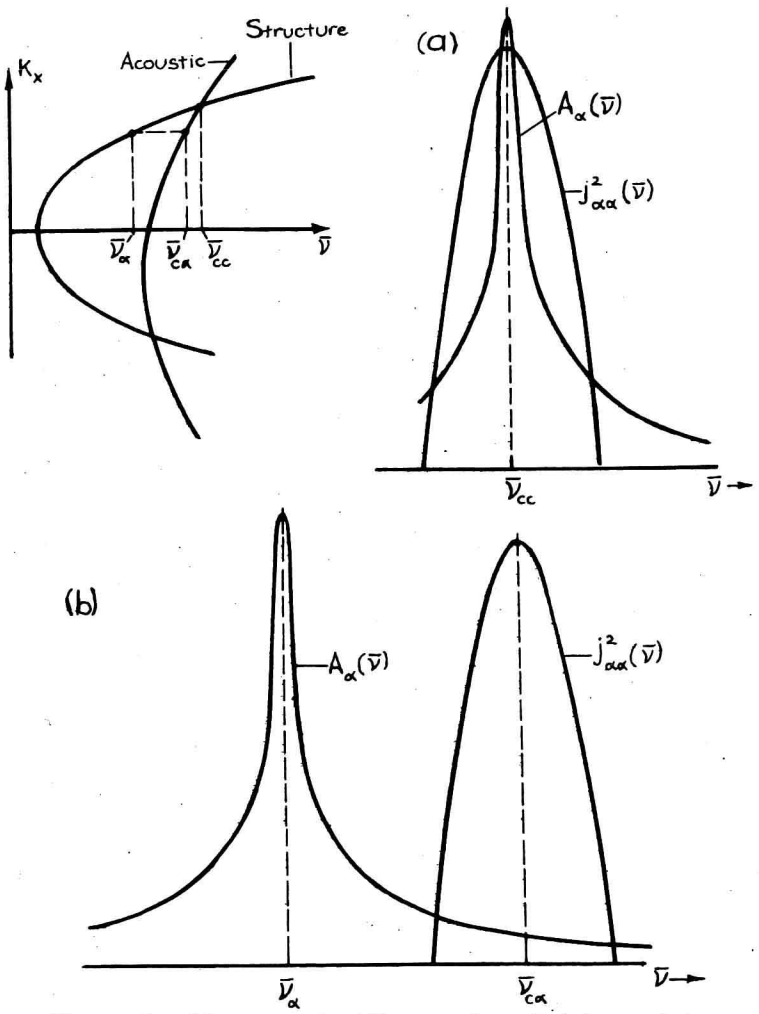

Figure 3. Diagrammatic illustration of (a) complete coincidence and (b) wavenumber coincidence.

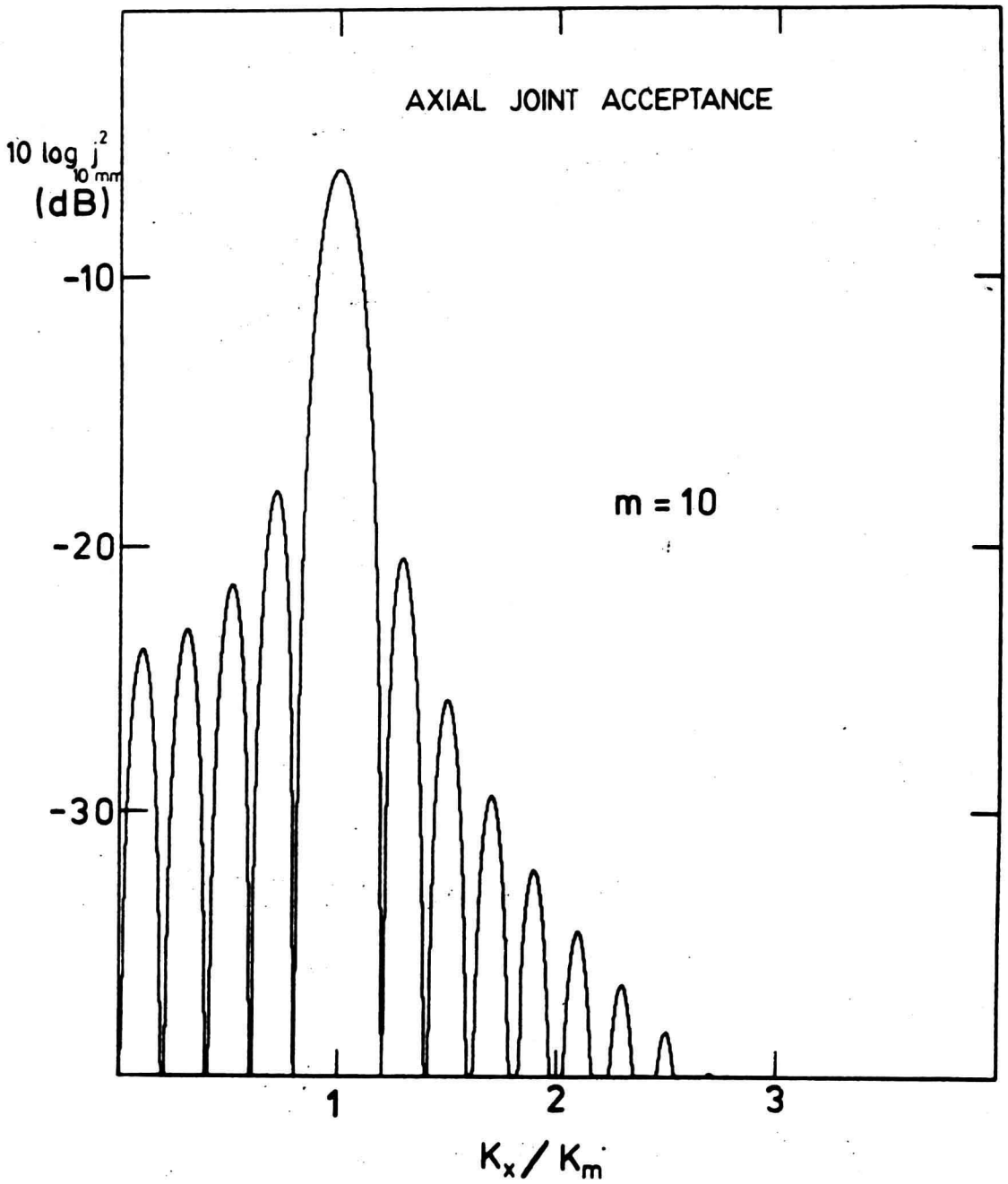

Figure 2. Example of the joint acceptance function j^2_{mm} for m = 10.

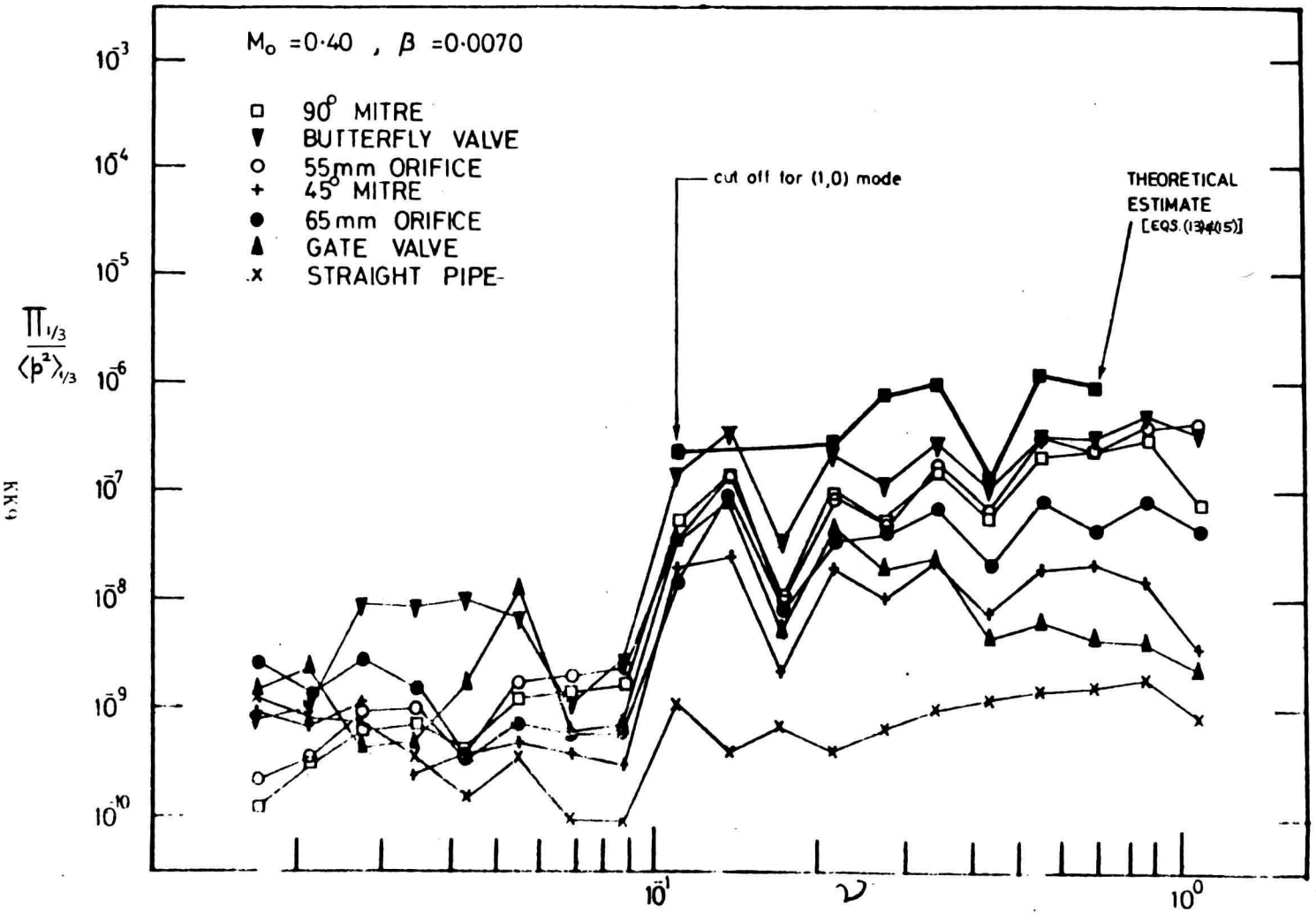

Figure 4. Ratio of acoustic power radiation in a one-third octave band to the mean square wall pressure fluctuation in the same band: comparison of theoretical estimate with measured values.

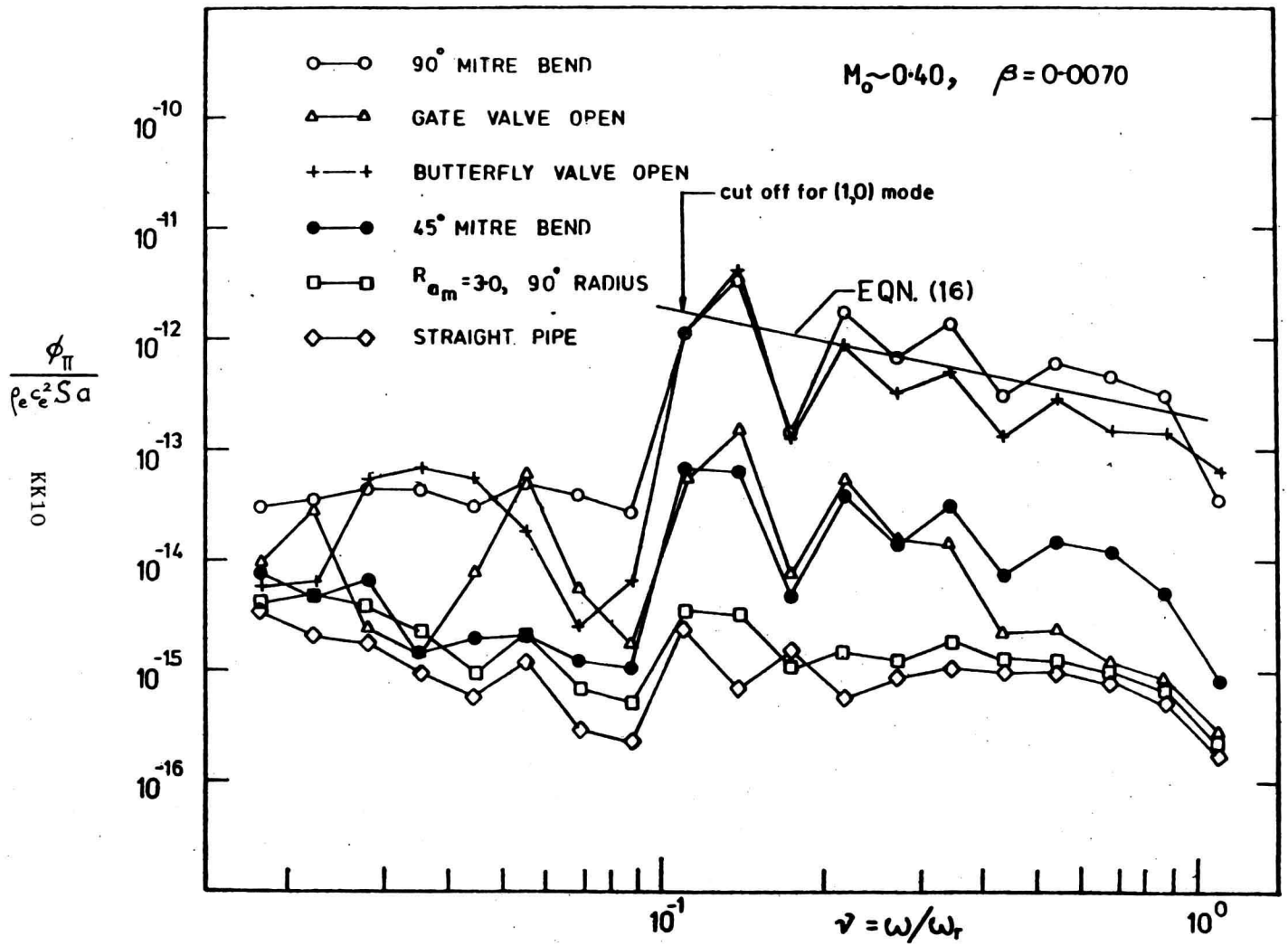

Figure 5. Spectral density of acoustic power radiation: comparison of empircal estimate with experiment.

BACK PRESSURE CONSIDERATIONS IN THE DESIGN OF DUCT SILENCERS AND CLASSIFICATION OF PERFORMANCE

G.N. MURPHY
Department of Mechanical and Production Engineering,
Royal Melbourne Institute of Technology,
Melbourne, Victoria.

1. INTRODUCTION

The purpose of a duct is to transport its contents as economically as possible and hence any device which causes resistance to the flow represents a continual power loss. In most instances such a loss is a small percentage of the total power involved, but savings that may be achieved without additional outlay are attractive however small they may be.

In the case of internal combustion engines, the power required to move the gases through inlet and outlet ducts may seem insignificant, but the effects on the power production may be quite dramatic due to the restricted "breathing". The Motor Industry Research Association (UK) conducted a series of tests (reference 1) which indicated power reductions up to 14% associated with silencer back pressure. Such reductions lead to larger engine requirements and the implications where maximum power/weight ratios are important are obvious. This aspect can cause a tendency to ignore noise reduction obligations.

The silencing and back pressure effects for selected components and combinations have been evaluated here, both theoretically and experimentally. In general the silencing characteristics may exhibit huge variation with frequency, particularly when reactive components are used. This raises difficulties in expression of the silencing/back pressure relationship as a single number classification. This feature warrants special consideration.

The problem has analagous aspects to the single number classification of sound barrier performance devised by the American Society of Testing and Materials described in the Society's "Tentative Classification for Determination of Sound Transmission Class" ASTM Designation E413-70T. There are severe limitations to the use of such a classification where the resultant performance is the interaction between a noise spectrum and an attenuation spectrum. However the concept now appears to have wide acceptance. The brochures of the suppliers of acoustic materials provide ample evidence of this.

2. COMMENTS ON SOME COMMONLY USED DUCT COMPONENTS

In general all duct components have both noise attenuation and flow restricting characteristics. Evaluation of these is possible in most cases by either analytical means, reference to fairly comprehensive handbooks on either subject, or by experiment. There is however an enormous variety of components and combinations and, on the acoustic side, components may interact with each other to produce complicated results. It is therefore advisable to look at both the acoustic and flow restricting characteristics in a qualitative manner. This is done in Table 1.

TABLE 1 SILENCING AND BACK PRESSURE EFFECTS OF DUCT COMPONENTS

Component	Silencing Effect	Back Pressure Effect
Sudden Expansion	Moderate value, independent of frequency	Severe
Sudden Contraction	As for sudden expansion	Moderate
Expansion Chamber	Although a combination of the previous two the combination gives silencing of moderate value which is periodic with frequency	Severe
Diffuser	Small value at low frequency. Value reduces as frequency increases	Low
Bell mouthed entry to contraction	Moderate value at low frequency. Value reduces as frequency increases	Low
Surface roughness	Small value. Appears independent of frequency	Moderate
Sound absorption material	Good for high frequencies. Moderate to small for low frequencies	Severe to low depending on placement
Bends	Small. Can have splitters arranged to provide by-pass paths giving reactive cancellation of selected frequencies.	Moderate. Effect can be reduced by use of aerodynamically shaped splitters.
Side Branch entries or perforations	Large silencing effects are possible. Resonating cavities can be tuned to suit noise spectrum to be treated.	Moderate
End Branches in expansion chambers	As for side branches	Low

Consideration of Table 1 shows immediately that the sudden expansion type of component is one of the most undesirable. A casual observer will have noticed that the motor cycle manufacturers are well aware of this aspect. The relative virtues of the other types of component are not so obvious and it is desirable to attempt some quantitative classification.

3. PROPOSED METHOD OF CLASSIFICATION

The back pressure characteristics can be considered proportional to the square of the velocity for low Mach numbers (less than 0.2). In this paper the term "back pressure" (BP) will mean the pressure loss referred to the fluid velocity in some basic portion of the duct. It will be what the fluids reference books commonly refer to as the total head loss, but expressed in pressure units. The low Mach number requirement is reasonably valid for industrial duct work.

$$\text{Thus } BP = K \frac{\rho V^2}{2} \qquad - - - (1)$$

where ρ is the fluid density

V is the fluid velocity referred to a basic cross section

K is a dimensionless factor depending only on duct component configuration

The back pressure is therefore readily expressed by a single factor.

One method of deriving the "average" silencing effect when the attenuation is frequency dependent is to determine the overall attenuation of a flat spectrum noise. This can be derived by evaluating the average transmission coefficient and converting it to a transmission loss (dB). The "average" derived in this manner will be an unreasonably low figure for a silencer which exhibits some very low or zero transmission loss values at certain frequencies. This would give a false impression of the value for a component which, when combined with other such components tuned to different frequencies, may produce a much higher "average". A supplementary method of arriving at an "average" attenuation is proposed as an average dB transmission loss based on a linear frequency scale.

For a silencer with a flat transmission loss spectrum, both figures are identical. For a silencer with a tuneable spectrum, the average dB loss is larger and it is more appropriate where the noise spectrum to be treated suggests a tuned silencer.

The frequency range specified for both methods of averaging is 20 Hz to 2,500 Hz. Where a component such as a simple flat-ended expansion chamber or side-branch resonator exhibits a periodically repeating characteristic, the averages are more simply taken for one half cycle.

The performance of a silencer component, or a combination of silencer components, can therefore be related effectively to its back pressure effects by two figures, one termed the "Average Transmission Loss (dB)/Back Pressure Constant (K)" and one termed "Average dB Transmission Loss/Back Pressure Constant (K)". The following examples illustrate this method.

Classification of a Sudden Expansion

$$\text{Transmission Loss TL (dB)} = 10 \log \frac{(S1 + S2)^2}{4\ S1\ S2} \qquad \text{- - - (2)}$$

(Reference 2)

where S1 and S2 are the two duct areas. Using an area ratio 1:10 gives a TL of 4.8 dB and is independent of frequency. The back pressure (BP) is expressed by equation (1) and for this component

$$K = \left(1 - \frac{S1}{S2}\right)^2 \qquad \text{- - - (3)}$$

(Reference 3)

The area ratio 1:10 gives K = 0.81

The classification of this component in accordance with paragraph 3 would therefore be 4.8 ÷ 0.81 = 5.9. With no frequency dependence, the "Average Transmission Loss", and "Average dB Transmission Loss" would be identical and thus the full classification would be 5.9, 5.9.

Classification of a Simple Expansion Chamber

$$\text{Transmission Coefficient } \tau = \frac{4}{4\ \cos^2\left[\frac{2\pi f l}{c}\right] + \left[\frac{S2}{S1} + \frac{S1}{S2}\right]^2 \sin^2\left[\frac{2\pi f l}{c}\right]}$$

where f is the frequency, Hz

c is the speed of sound

l is the length of the expansion chamber

For an area ratio 1:10, this gives the transmission loss characteristic shown in Figure 1. The "Average Transmission Loss (dB)" is 6.9 dB. The "Average dB Transmission loss" is 9.7 dB.

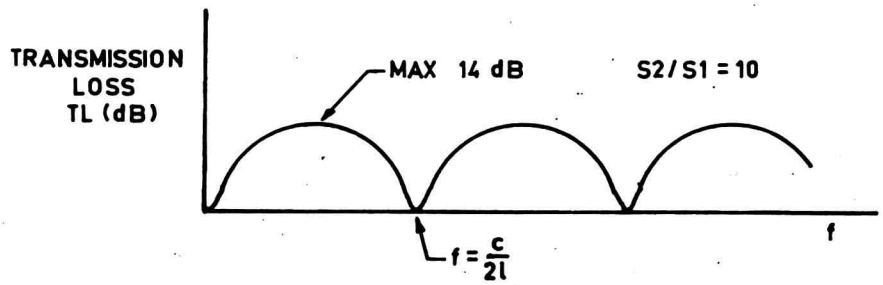

FIG.1. SILENCING CHARACTERISTIC OF SIMPLE EXPANSION CHAMBER

The pressure drop is the sum of that for expansion and that for a contraction. From reference 3, this is evaluated as K = 1.17. The classification for this silencer would therefore be 5.9, 8.3.

Some Experimental Results

Figure 2 shows some results where both transmission loss and K factors were measured experimentally.

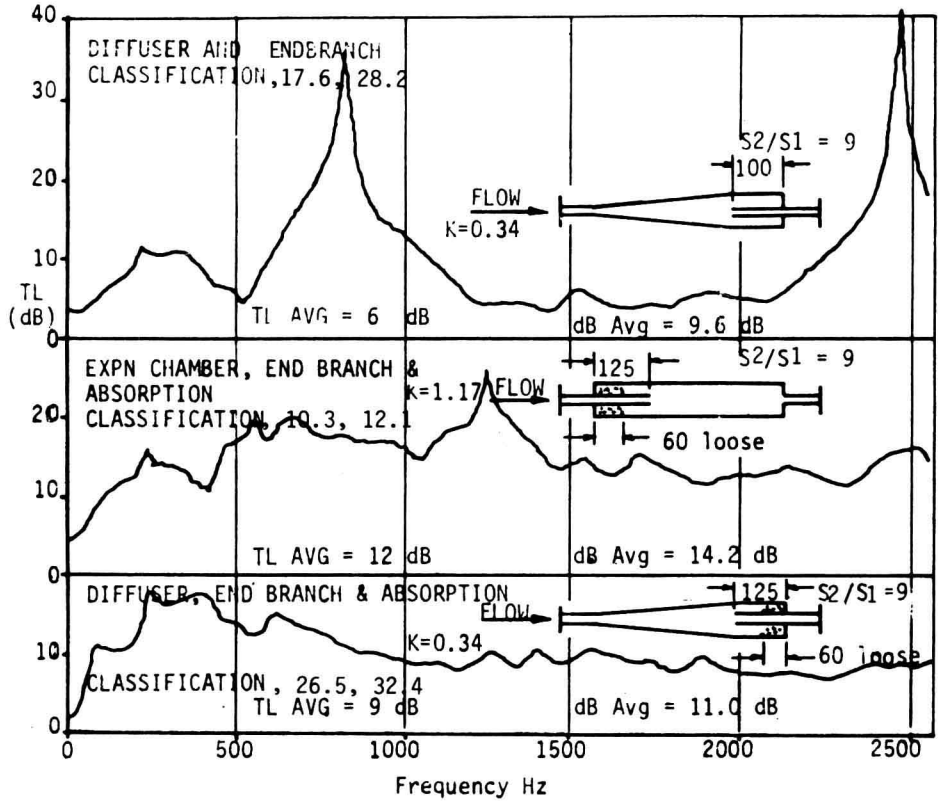

FIGURE 2 EXAMPLES OF EXPERIMENTAL CLASSIFICATION OF SILENCERS

4. APPLICATIONS IN SILENCER DESIGN

Figure 3 shows that plotting of the classifications against non-dimensional shape parameters can provide useful trend information.

Figure 4 shows an application to an expansion chamber entry to achieve an optimum silencing/back pressure classification. The sudden expansion type of entry has a moderate silencing effect, but causes severe back pressure. A complete diffusion type entry has almost no silencing effect and creates little back pressure. The graphs of Fig. 4 show that setting the parameter $(S1\ S3)/S2^2 = 2$ will give close to the optimum result for normal practical ranges of the expansion ratio.

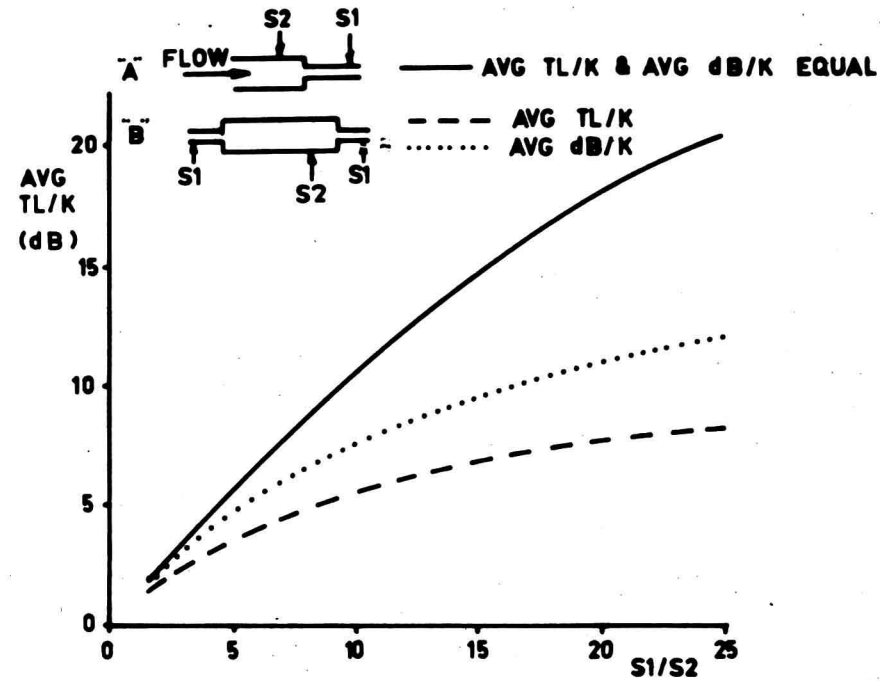

FIG.3. "A" CLASSIFICATION TREND WITH CONTRACTION RATIO
"B" CLASSIFICATION TREND WITH EXPANSION CHAMBER RATIO

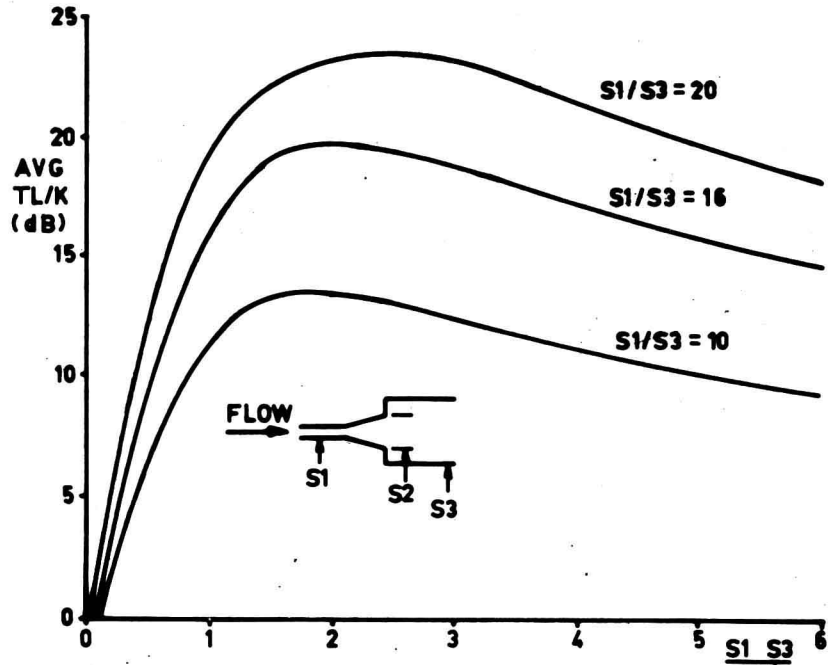

FIG.4. OPTIMISATION OF CLASSIFICATION WITH EXPANSION ENTRY DIFFUSER

5. FURTHER WORK REQUIRED

Back pressure considerations create the introduction of combinations of components and aerodynamic shapes which are impracticable to evaluate analytically. Many such shapes may be analysed by approximating with a finite difference computer program, but correct modelling of the interaction between components is not always obvious. Extensive experimental work will be needed therefore to provide designers with a useful collection of information.

Measurement of silencer transmission loss characteristics in the presence of fluid flow is not a simple matter. The noise generated by the flow masks the transmitted noise to an extent that causes problems even with computer processed signal analysis techniques and further work is needed to provide reliable silencing data under flow conditions.

The generation of flow noise by silencer components is also of interest. One particular component showed promising results with flow in one direction, but no instruments were needed when the flow was reversed. The generated noise was heard throughout the laboratory. (See ref. 4 for previous work on this topic).

Experimental determination of flow back pressure can also produce some surprises. The third silencer shown in Fig. 2 exhibited a significantly lower back pressure when flow was reversed. The influence of the projecting end branch was not predicted by any hand book data.

REFERENCES

1. Haynes, C.D. and Kell, R.L., 1964/3, 1965/2, 1065/12 (three reports) Motor Industry Research Association, "Engine Exhaust Silencing".
2. Knisler, L.E. and Frey, A.R., 1962, "Fundamentals of Acoustics", McGraw H-11 Book Co.
3. Streeter, V.L., 1971, "Fluid Mechanics", McGraw Hill Book Co.
4. Norfey, C.L., 1971, Journal of Sound and Vibration, Vol. 14, "Sound Transmission and Generation in Ducts with Flow".

BACK PRESSURE CONSIDERATIONS IN THE DESIGN OF DUCT SILENCERS AND CLASSIFICATION OF PERFORMANCE

ABSTRACT

This paper relates the acoustic performance of various duct silencer components to the back pressure effect on flow. It is limited to consideration of moderate flow velocities such that the simple incompressible flow relationships are reasonably valid. To assist selection of components in the design stages of a silencer, the paper looks at the possibilities of expressing the performance as a dimensionless value rating, "Transmission Loss (dB)/Pressure Drop Factor". Further consideration is given to inclusion of the tuneable characteristics of the components in the expression of this relationship.

TIME HISTORY ANALYSIS OF IMPACT NOISE IN THE TEXTILE INDUSTRY

K.R. ATKINSON and P.R. LAMB
CSIRO Division of Textile Industry,
P.O. Box 21, Belmont, Victoria 3216
Australia.

ABSTRACT Time domain analysis is an important tool in the study of impact noise. A technique for rapidly obtaining accurate time histories is described and demonstrated on a range of textile machinery.

INTRODUCTION

Machinery noise often arises from multiple impacts of loosely controlled moving parts. Individual impacts are not always audibly resolved and are difficult to quantify. However, a systematic engineering control program demands that the major impacts be identified and their relative contributions determined. This information can be provided by a high-resolution time history of the noise signal. A novel technique for producing such a time history on modern digital spectrum analysers is described.

METHOD AND APPARATUS

The microphone output signal of a sound level meter is squared using an integrated circuit multiplier and input to any digital spectrum analyser that has a time domain display. The noise from a large number of machine cycles is then averaged using an external trigger. If desired, only a part of the machine cycle can be examined using a post-trigger delay and a narrow time window.

The importance of the squarer is that it allows averaging over many machine cycles which is required because most impacts are not highly reproducible. The sound pressure cannot be usefully averaged because it corresponds to the wave amplitude and is both positive and negative. The squared signal corresponds to the sound intensity and can be averaged.

The spectrum analyser acts as a digital data storage device that enables averaging and smoothes the signal. The low-pass filters, which normally prevent aliasing during frequency analysis, automatically smooth the noise envelope by applying the optimum time constant for the chosen resolution. The sound level meter can be used to A-weight or octave-band filter the input signal.

The apparatus used in this study consisted of a Brüel and Kjaer 2607 measuring amplifier and 1/2" microphone, an Analogue Devices AD534J multiplier (frequency response to 50 kHz) and a Hewlett-Packard 5420A digital spectrum analyser (although a simple single channel analyser is sufficient). The trigger signal came from a photodetector detecting a reflective strip.

The area under the resulting time history curve is proportional to the sound energy radiated. In the following examples an arbitrary linear sound intensity scale is used and the area under the curve can be estimated graphically. In all cases the input signal has been A-weighted. The reduction in area that could be obtained by excluding a particular peak gives a prediction of the A-weighted noise reduction if that impact is eliminated.

The usefulness of the time history in source identification has been emphasised by others[1,2,3]. The advantages of the technique presented here are that only a simple addition to existing equipment is needed, the time resolution is high, and an accurate measure of the noise contribution of each impact is obtained.

CASE STUDIES OF TEXTILE MACHINERY

The technique has been applied to shuttle looms, gill boxes and a rectilinear comb. For all three types of machine, noise levels at operator positions in multi-machine installations vary from about 93 to 105 dBA.

Gill Boxes

A gill box (shown schematically in Fig. 1) is a machine used in wool processing to straighten and align fibres. The wool is carried between two pairs of rollers by two sets of metal "fallers" or combs. The fallers are propelled horizontally by pairs of screws and inserted and ejected by cams rigidly attached to the ends of the screws. The fallers carry the wool forward until the individual fibres are gripped by the delivery rollers and are pulled through the pins at about 5-12 times the rate of faller travel.

Noise is generated principally by impacts occurring during the insertion and ejection of fallers. Speeds range from about 500 to 2000 faller drops per minute (fdpm).

The time histories of a number of gill boxes were studied by running the machines with only one faller with triggering derived from a reflective strip on the faller. The relative importance of any drive noise is increased but such a uniform background signal only shows up as a base level on the time history curve.

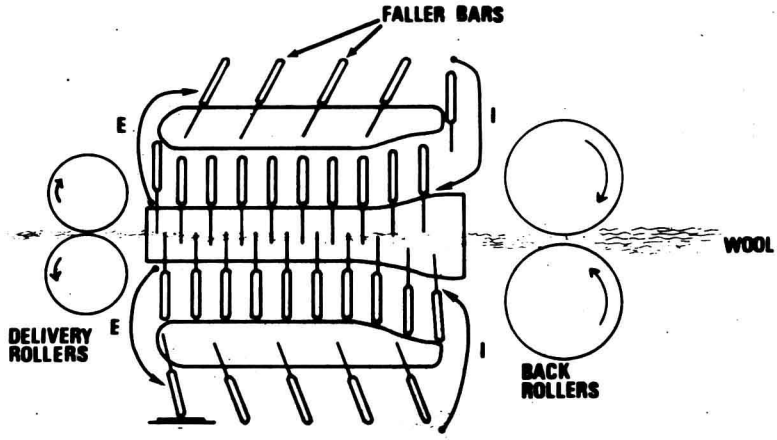

Figure 1 Schematic of gill box operation: I - insertion of fallers, E - ejection of fallers

The first example (Figs. 2 & 3) is from a low speed Prince-Smith & Stell machine (600 fdpm) with heavy fallers (750 g). Each insertion and ejection is seen to contain a peak associated with the cam/faller impact and one or more peaks as the faller enters the new path. In this example, the impact(s) as the faller entered the new screw during insertion was seen to be considerably louder than other peaks and therefore was tackled first. The faller slides were modified as shown in Fig. 4 by the addition of shock absorbers. These consisted of spring loaded leaves that frictionally dissipated the energy of the impacts as they were alternatively hit down and up by fallers from the top and bottom set. The subsequent time histories are shown as curves B in Figs. 2 & 3. The reduction in area, allowing for background noise, gave a predicted reduction in noise level of about 1.7 dBA. The measured reduction was 2 dBA.

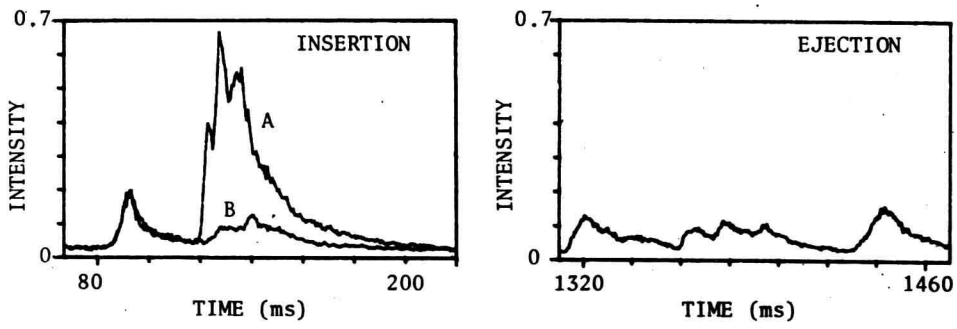

Figure 2 Time history of single faller - top set (100 averages) Insertion: (A) unmodified, (B) modified. Ejection: unmodified

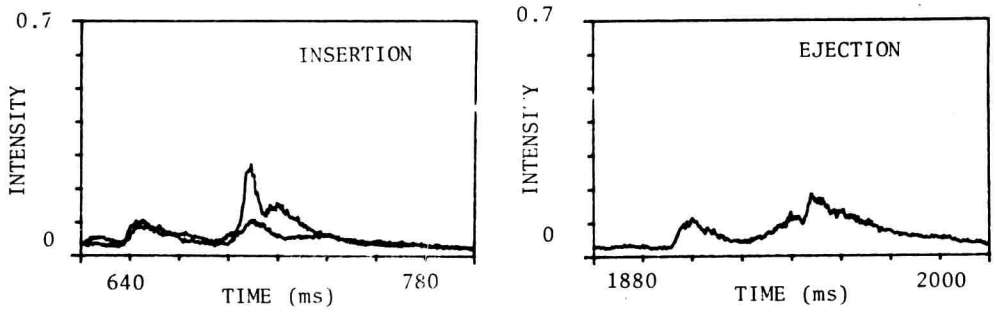

Figure 3 Time history of single faller - bottom set (100 averages). Insertion: (A) unmodified, (B) modified. Ejection: unmodified.

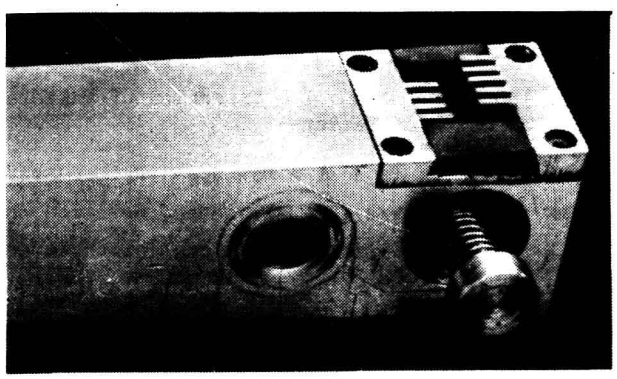

Figure 4

Modified faller slide showing friction brake

The second example is from a medium-speed Ingolstadt machine (1000 fdpm) employing light fallers (300g). The time histories of the top set of fallers before and after modification are shown in Figs. 5 & 6. The various impacts were studied using high-speed film and confirmed by modifying components and noting the effect on the time history[4]. Progress in quietening the machine was very slow until the time history was available. For example, cushioning on the slide as in the previous example made little difference to the largest peak as it was caused primarily by the faller impacting the drive screws before landing on the slide. It was also found that the last peak during ejection arose due to the faller bouncing. The major modifications made were to replace the metal conductors that guide the fallers during insertion and ejection by longer ones of different shape made of Hytrel® polyester elastomer, and to cushion the slide impacts with elastomeric slides of an altered shape. The metal cams and screws remained but the altered paths and firmer control of the bar reduced the amount of noise radiated. The reduction in area of the time history gave a predicted 7.2 dBA drop in noise level and a 6 dBA difference was measured using a full set of top fallers. *(® Du Pont)*

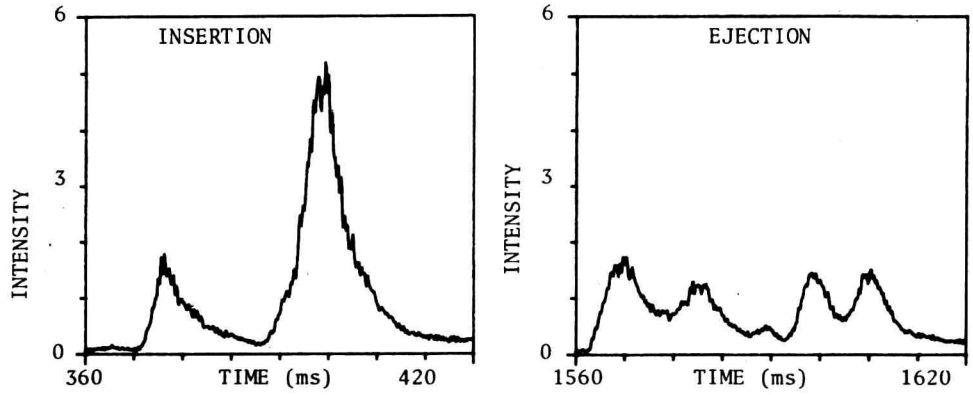

Figure 5 Time history of single faller - unmodified top set (100 averages).

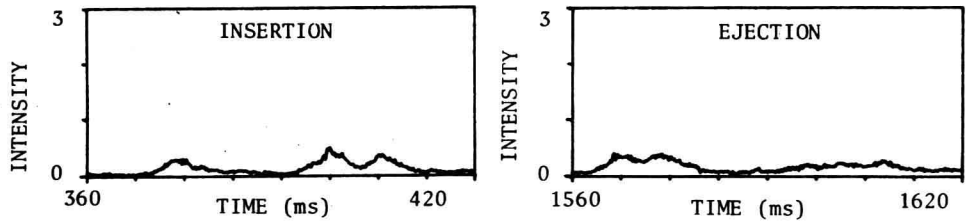

Figure 6 Time history of single faller - modified top set (100 averages).

The modifications have not been extensively tested for wear resistance but they do emphasize how small amounts of cushioning can give large reductions in impact noise[5].

Combs

Rectilinear combs are used in wool processing to remove foreign matter, tangles and short fibres, as well as to align the fibres. A typical modern comb, a Schlumberger PB27L, was studied. The time history of the complete cycle is shown in Fig. 7a. The number and size of the peaks showed the importance of impacts caused by the reciprocating motion of the machine.

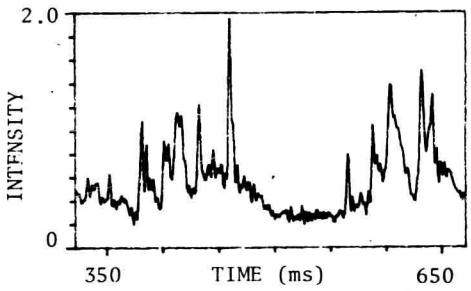

Figure 7a Comb time history Unmodified

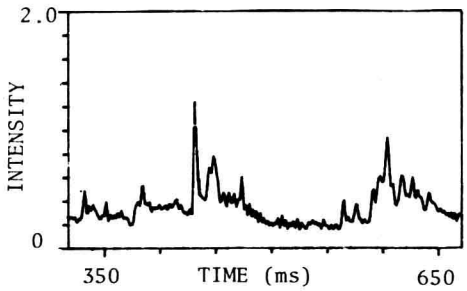

Figure 7b Comb time history Modified

It was difficult to identify the peaks from their position in the cycle. Therefore, various components were disconnected or removed and the effect on the time history was examined. Two components were located as important impact noise sources. The reciprocating feed comb that conveys the wool forward was hitting its mating part, the grid plate. A 1.5mm clearance was introduced which, although it is not the usual machine setting, has no effect on performance. The second component was the cam-driven shovel plate that moves forward once per cycle to hold the fibre beard in place whilst some of it is drawn off. The rapid acceleration as the direction of motion of the shovel plate was reversed produced a torque that rotated the light metal plate, which then bounced against the neighbouring metal surfaces. The torque was greatly reduced, as shown in Fig. 8, by moving the pivot point into the line of motion of the centre of mass.

The time history after the two modifications is shown in Fig. 7b. The major peaks have been removed and the noise level is much more uniform, suggesting that drive noise may now dominate. The reduction in area under the curve gave a predicted noise reduction of 2.2 dBA. The measured reduction was about 2.5 dBA.

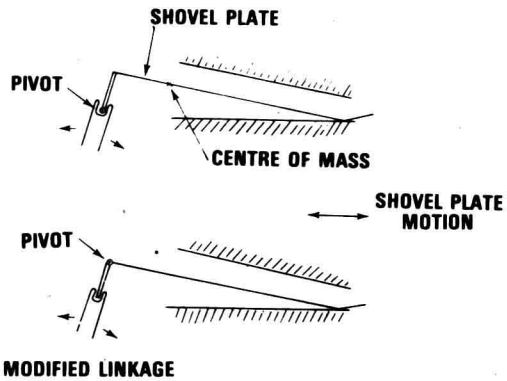

Figure 8

Schematic diagram of original and modified shovel plate linkage

Looms

In shuttle looms cloth is woven using a projectile (the shuttle) that is alternatively thrown (picked) and caught (checked). The drive mechanism is shown in Fig. 9. The shuttle is propelled by a picking stick, driven by a cam, and trails a yarn from one side of the loom to the other.

Preliminary investigations of a number of looms have been made and the relative importance of different impacts has been found to vary

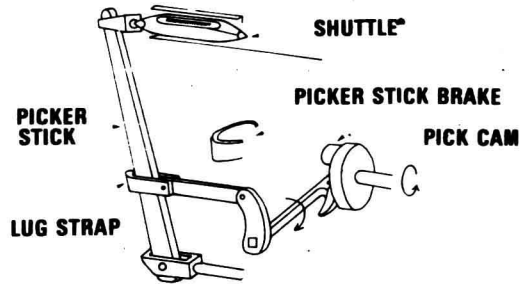

Figure 9

Schematic of shuttle drive mechanism

considerably. In one case, a Picanol loom, a single impact was found to dominate. Figure 10 shows the time history of both the left and right hand pick. The major impact is the braking of the picker stick against a number of stops. (The plot suggests a slight asymmetry in the loom and the long tails on the peaks are probably due to the small live room).

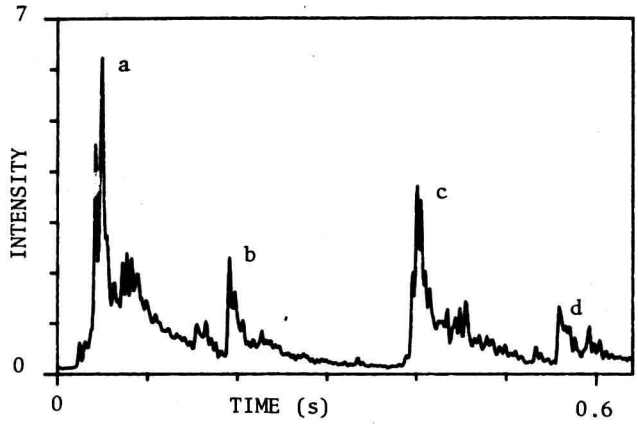

Figure 10

Time history of a Picanol loom (20 averages). Peaks: (a,c) picker stick braked; (b,d) shuttle checked

Luenenschloss[6] has reported a 2.2 dB reduction using a modified brake. The time history here suggests a larger reduction is possible.

Superposition of sound pressures traces on a CRT display as done by Eckert et al[7] will normally show the presence of a large number of peaks. However, the relative contributions are difficult to quantify. The technique presented here allows rapid quantification and is ideal for comparisons over time or between machines. For example, the time history, shown in Fig. 11, of two cycles of a Dobcross loom indicated that one pick cam was out of adjustment. Correct adjustment eliminated peak (b) and reduced the area of peak (c) and gave a 1 to 1.5 dBA reduction.

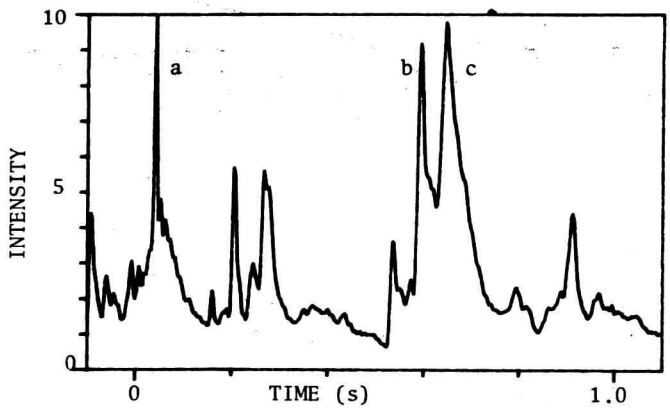

Figure 11

Time history of a Dobcross loom (100 averages). Peaks: (a,c) picker stick braked; (b) faulty pick cam adjustment

CONCLUSION

For multi-impact machinery noise, time history analysis can greatly speed the location and treatment of the major noise producing impacts. Suitable high-resolution time histories can be rapidly obtained by using a squarer coupled to a modern digital spectrum analyser.

REFERENCES

1. Baade, P.K., 'Identification of Noise Sources', Tutorial Papers of International Conference on Noise Control Engineering, M.J. Crocker, ed., Washington, 1972, pp 98-114.
2. Cudworth, A.L., 'Cutting out Noise from the Whole Cloth : Noise Control in the Textile Industry', Noise Control Engineering, 1, 1, 24-31 (1973).
3. Emerson, P.D., Bailey, J.R., and Hart, F.D., 'Manual of Textile Industry Noise Control', North Carolina State University, Raleigh, 1978.
4. Atkinson, K.R., and Lamb, P.R., 'Time History Analysis of Multi-Impact Noise', Noise Control Engineering, submitted for publication.
5. Richards, E.J., 'Impact Noise from Industrial Machinery : Some General Laws Regarding its Magnitude', Proceeding of International Conference on Noise Control Engineering, W.W. Lang, ed., San Francisco, 1978, pp 83-114.
6. Luenenschloss, J. "Gerauschmessung und Entwicklung einer Messmethodik zur Lokalisierung von Gerauschquellen am Beispiel einer einschutzigen Webmaschine', Typ President CM-C/SB. Bericht zur Forschungsaufgabe fur Picanol, Institut fur Textiltechnik, T.H. Aachen, February 1974.
7. Eckert, W.L., Booth, E.T., Bailey, J.R., and Emerson, P.D., 'Fly Shuttle Loom Noise', Mechanical Engineering, 99, 4, 40-43 (1977).

A METHOD FOR IDENTIFICATION OF NOISE SOURCES OF HIGH SPEED TRAINS

F.-R. Grosche and H. Stiewitt
Deutsche Forschungs- und Versuchsanstalt für Luft- und Raumfahrt e.V.
3400 Göttingen, Bunsenstr. 10, W-Germany

Abstract

A technique to locate sound sources by means of a large concave mirror is described. The mirror forms - in analogy to optics - an image of the investigated source field in the vicinity of its focal plane where one or several microphones are positioned. The spatial resolution of the system is limited mainly by refraction of the sound waves at the edge of the mirror. Two versions of the acoustic mirror system, for wind tunnel tests and for full scale measurements of vehicles passing by the mirror, are discussed in detail.

1. INTRODUCTION

Highly directional microphones allow to identify individual sound sources, to distinguish between different source regions and to determine the spatial intensity distribution of the source field. They may therefore be considered as a promising tool, complementary to other techniques, to investigate in detail the sound generating mechanisms of high speed trains, to check the relative importance of aerodynamic noise compared to wheel/rail interaction noise at very high velocities, and to establish the effectiveness of noise suppression devices influencing only parts of the source field while other sound sources of comparable strength are present.

Several directional microphone systems for sound source location have been developed to study flow noise problems, particularly jet noise, jet engine noise and air frame noise. Two of these systems, the phased microphone array [1]and the concave mirror [2, 3] were also recently applied to investigate the sound sources of high speed trains. The present paper gives a short description of the acoustic mirror telescope and its adaption to the special task of evaluating the noise sources of a train from the transient sound signals received when the vehicle passes the measuring system.

2. THE MEASURING TECHNIQUE

The Figure 1 illustrates the principle of the acoustic mirror telescope for sound source location and gives some geometrical dimensions of the system used in our tests. The concave mirror shown on the left hand side is a piece of the ellipsoid of revolution indicated by the dashed line. It has two focal points which are marked by small circles. A microphone is positioned in

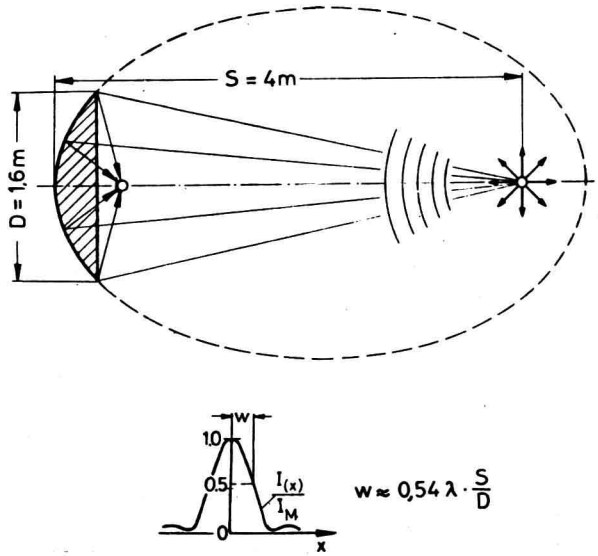

Fig. 1

Acoustic mirror microphone system for sound source location

the focal point close to the mirror. Sound waves emanating from a source in the other focal point are focused upon the microphone by reflexion at the elliptical mirror surface. Thus the sound intensity produced by this source is greatly enhanced at the mirror microphone as compared to its free field value. Sound waves radiated from other locations are concentrated by the mirror upon other image points in front of it, the mirror acts as an imaging system in analogy to optics. The elliptical contour of the mirror was selected instead of the spherical or parabolic shape because it produces the best image in the vicinity of its focal points. A parabolic mirror would be the optimum if the distance to the sources were infinite. Obviously, the spatial sound source distribution in a plane perpendicular to the mirror axis can be surveyed by traversing the mirror microphone unit, since the sound pressure level measured at the microphone is related directly to the sound source intensity at the position of the focal point.

The spatial resolution of the acoustic mirror microphone system is limited mainly by diffraction of the sound waves at the edge of the mirror since the wave lengths within the frequency region of interest are only one or two orders of magnitude smaller than the mirror diameter. The same effects are therefore observed as in the case of light waves passing through a small circular aperture. These effects can be approximately described by the theory of Fraunhofer diffraction.

If the point source of sound shown in Fig. 1 is shifted from the focal point by a distance x in the plane normal to the mirror axis, the sound intensity at the mirror microphone varies according to the diffraction pattern sketched in the lower part of Fig. 1. The distance between first minimum and center

of the diffraction pattern can be estimated readily from the well known equation for the angle α_{min} of the first minimum of radiation in the case of a circular aperture,

$$\sin \alpha_{min} = 1.22 \frac{\lambda}{D} . \qquad (1)$$

Thus, the sound intensity at the mirror microphone becomes a minimum when the sound source is shifted relative to the position of the mirror by

$$x_{min} = S \cdot \tan \alpha_{min} \approx S \cdot \sin \alpha_{min} \approx 1.22 \cdot \frac{S}{D} . \qquad (2)$$

The half-width W' of the diffraction pattern is indicated in the lower part of Fig. 1. For example, with S = 4 m and D = 1.6 m according to Fig. 1, the half-width of the diffraction image of a point source of sound at a sound frequency f = 4 kHz is $W \approx 11.5$ cm. The location of a single sound source can be determined even more accurately from the position of the maximum of its diffraction pattern, in general the error is less than $\pm$ 0.1 W.

Since the concave mirror concentrates the sound waves emanating from a point source upon the mirror mircophone and its close vicinity, the sound intensity I_M at the microphone is significantly higher than the intensity I_F of the acoustic free field of this source at the same position. The ratio I_M/I_F defines the gain factor G of the mirror microphone system

$$G = 10 \log \frac{I_M}{I_F} = L_M - L_F \ (dB). \qquad (3)$$

L_M and L_M are the corresponding sound pressure levels.
The gain factor varies with frequency in a similar way as the spatial resolution of the mirror. If the size of the diffraction pattern of the point source decreases, the sound intensity I_M within the pattern will increase. Since the diameter of the diffraction pattern is $\sim\lambda$, its area is $\sim \lambda^2$ and therefore the gain factor G increases with 6 dB/octave over a wide frequency range.
The gain factor of the mirror system sketched in Fig. 1, which was used in our measurements, varies from 14 dB to approximately 32 dB within the frequency range 1 kHz $\leq$ f $\leq$ 8 kHz.

3. WIND TUNNEL TESTS

Acoustic wind tunnel tests with a 1 : 20 scale model of an electric locomotive were performed using the acoustic mirror shown in Fig. 1. The model was mounted on a ground plate in the open test section of a low-speed wind tunnel which has a square nozzle of 3 x 3 m² exit area. The acoustic mirror was

situated outside of the open test section at 4 m distance from the model so that the focus of the mirror could be traversed across the model. The mirror axis was oriented approximately normal to the centerline of the test section. The source distribution of flow noise at the model locomotive was measured in several horizontal and vertical planes at wind velocities $40\ m/s \leq U_\infty \leq 60\ m/s$. Problems related to refraction and scattering of the sound waves crossing the turbulent shear layer of the wind tunnel while travelling from the model to the mirror are discussed in detail in Ref. [3].

Fig. 2 and Fig. 3 present typical results of the tests. The sound intensity I

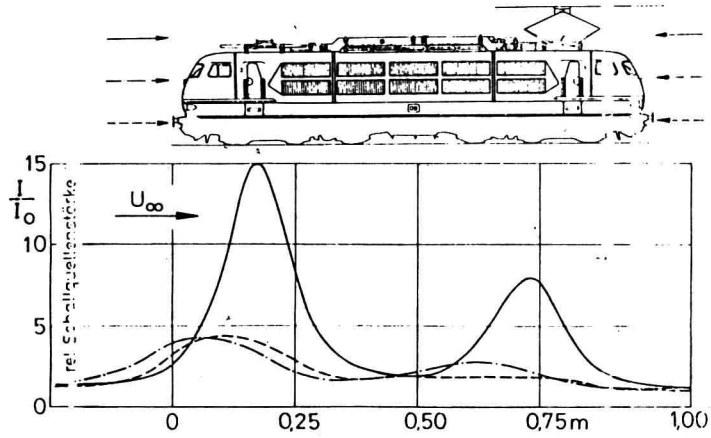

Figure 2
Model with pantographs

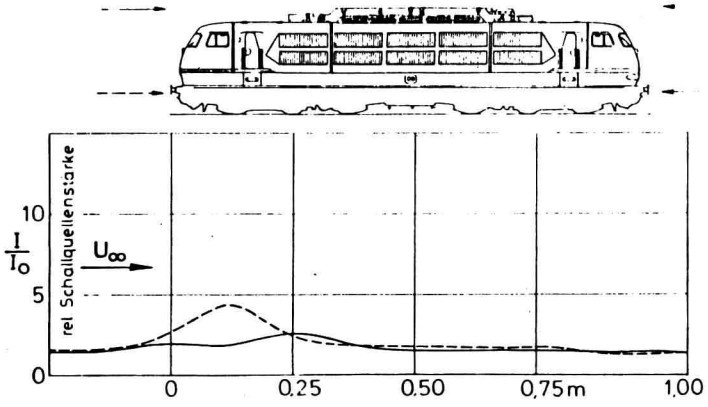

Figure 3
Model without pantographs

Figures 2 and 3 Distributions of sound source intensity at a wind tunnel model of the electric locomotive 103 measured along the horizontal traverses indicated in the upper parts of the figures. U_∞ = 40 m/s; 8 kHz 1/3 octave band.

measured by the mirror microphone is essentially proportional to the local acoustic source strength. It is normalized here rather arbitrarily by the tunnel background noise I_0 and is plotted as function of the position of the mirror focus at the model. The solid, dashed and dashed-dotted distributions pertain to the horizontal traverses indicated in the upper parts of Fig. 2 and Fig. 3 by the same symbols. Fig. 2 shows the sound source distributions measured with the forward pantograph collapsed and the rear pantograph in raised position. Strong sources of flow noise are present at the positions of both pantographs for the traverse just above the roof (solid line), while only weak maxima of sound radiation can be observed in both the lower traverses close to the front of the locomotive.

The source distributions of Fig. 3 were obtained with both pantographs removed. No significant sound sources are detected in the plane of the roof at this model condition, the distribution for the lowest traverse (dashed line) remains essentially unchanged.

Fig. 2 and Fig. 3 present data measured in the 8 kHz 1/3 octave band at wind velocity U_∞ = 40 m/s, but the results were quite similar at other frequencies and flow velocities. In all cases the pantographs turned out to be the dominant sources of flow noise of the model investigated. This result was verified by full scale tests with the mirror telescope described in the next section.

4. ACOUSTIC MIRROR SYSTEM FOR FULL SCALE TESTING

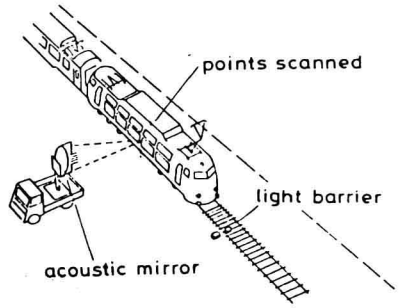

Figure 4
Test set-up for sound source location of a train passing-by.

The original version of the acoustic mirror with one microphone as shown in Fig. 1 was developed for wind tunnel tests and static tests where the microphone focus can be traversed over the model in all directions without time restrictions. In full scale tests with a fast train passing by the mirror as illustrated by Fig. 4, each run would render the sound source distribution along the train for just one vertical position. A large number of runs would be required to obtain a complete survey of the acoustic source field at the train surface.

The mirror system was therefore adapted to the task of measuring the longitudinal sound source distribution simultaneously at several vertical positions by mounting 6 additional microphones in front of the mirror, 3 above and 3 below the original mirror microphone. Fig. 5 presents the complete measuring system. The 7 microphones are focused on the points at the train indicated in Fig. 5, microphone No. 1 receiving the sound radiated from the wheel-region and microphone No. 7 being aimed at the vertical position of the middle of the raised pantograph. Thus, 7 horizontal traverses of the sound source distribution at the train are obtained at each run.

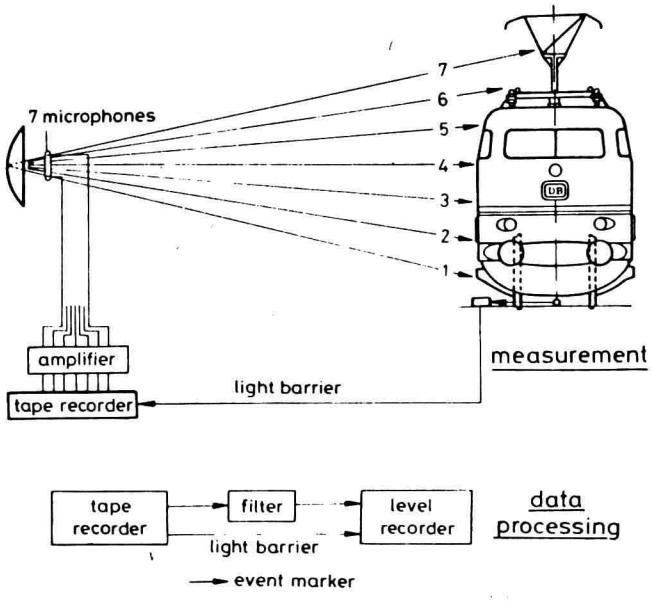

Figure 5
Mirror microphone arrangement with 7 microphones for simultaneous measurement of acoustic source strength at different vertical positions.

The signals of the 7 mirror microphones are amplified and recorded on magnetic tape, see Fig. 5. A light barrier is mounted above the rails which produces an electric pulse every time a wheel crosses the light path. The signal of the light barrier is also fed into the tape recorder thus allowing the microphone signals to be related to the position along the train. Before the measurements, the mirror system was adjusted and calibrated using a small loudspeaker as a point source of sound.

Results of tests with a high speed train are given in Ref. [4], some characteristic examples are shown in the following figures. Figure 6 presents source distributions measured by microphone No. 1 (of Fig. 5) at the vertical position of the axles within the 8 kHz and 4 kHz octave bands. The train is sketched in the center part of the figure, the exact positions of the axles in relation to the measured source distributions are marked by short vertical lines. The sound radiation of each individual axle of the carriages appears

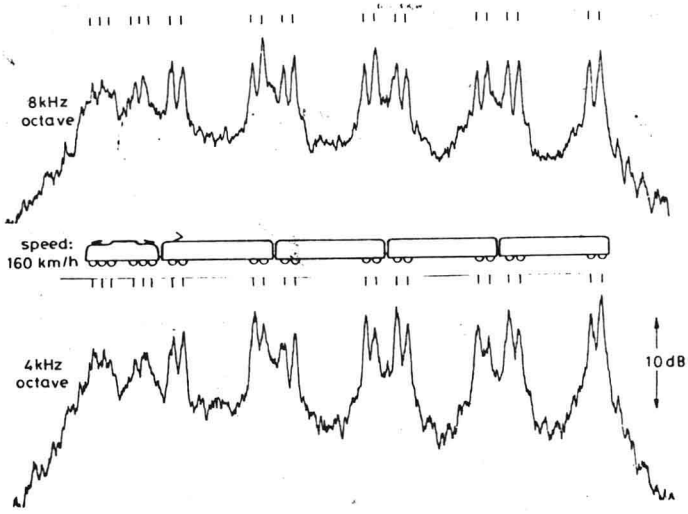

Figure 6 Sound source distributions of wheel/rail interaction noise measured in the plane of the axles (vertical station 1 of Fig. 5). Train speed: 160 km/h.

ı the source distributions as a very distinct peak.

Figure 7 shows - at a smaller scale - the source distributions along the ıme train at all the 7 vertical positions indicated in the sketch at the right ınd side. The lower boundaries of the hatched areas indicate the sound pressure vels measured simultaneously by an omnidirectional microphone located at same distance from the track as the acoustic mirror.

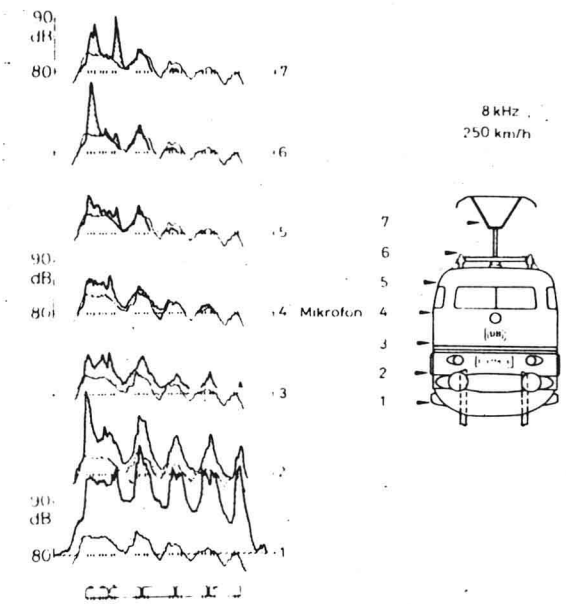

Figure 7 Sound source distributions along the train measured at the vertical stations 1 - 7. Train speed: 250 km/h 8 kHz octave band.

Some significant aerodynamic sound sources show up in the traces of vertical ations 6 and 7 in addition to the dominant wheel/rail interaction noise sources station 1. These aerodynamic sources could be identified as the forward, llapsed pantograph of the locomotive and the raised pantograph of the first rriage.

Another pronounced peak of the sound radiation occurs just in front of the forward bogie of the locomotive at vertical station 2. This peak indicates aerodynamic noise generation by the bumper region of the locomotive.

It was found from comparison with measurements at other train velocities U, that the intensity of these sources increases approximately with $U^{6.8\pm0.9}$ while the wheel/rail interaction noise increases with $U^{3.5\pm0.7}$.

These results of the full scale tests agree quite well with theoretical considerations and with the results of the wind tunnel experiments discussed in section 3.

ACKNOWLEDGEMENT

The support of this investigation by the German Ministry for Research and Technology (BMFT), "Deutsche Eisenbahn Consulting" (DEC) and "Deutsche Bundesbahn" is gratefully acknowledged.

REFERENCES

[1] Billingsley, J.; Kinns, R,: The acoustic telescope.
Journ. of Sound and Vibr. 48 (1976), pp. 485 - 510.

[2] Grosche, F.-R.: Distribution of sound source intensities in subsonic and supersonic jets.
AGARD CP-131 (1974), Paper 4

[3] Grosche, F.-R., Stiewitt, H., Binder, B., Acoustic wind-tunnel measurements with a highly directional microphone.
AIAA Journ., Vol. 15 (1977), pp. 1590-1596.

[4] Stiewitt, H., Grosche, F.-R., On aerodynamic noise generation by high speed trains.
Paper to be presented at the 10th International Congress on Acoustics (ICA), Sidney, 9-16 July, 1980.

内 部 交 流

P 90/9

第 10 届国际声学会议

(英 2-3/7076-4)

A 00120